

AFIT/DS/ENY/97-07

Reorientations of Flexible Spacecraft
Using
Momentum Exchange Devices

DISSERTATION
Kevin Anthony Ford
Major, United States Air Force

AFIT/DS/ENY/97-07

19970929 060

Approved for public release; distribution unlimited

The views expressed in this dissertation are those of the author and do not necessarily reflect the official policy or position of the Department of Defense or the United States Government.

AFIT/DS/ENY/97-07

Reorientations of Flexible Spacecraft
Using
Momentum Exchange Devices

DISSERTATION

Presented to the Faculty of the School of Engineering
of the Air Force Institute of Technology
Air University
In Partial Fulfillment of the
Requirements for the Degree of
Doctor of Philosophy

Kevin Anthony Ford, B.S., M.S., M.S.
Major, United States Air Force

September, 1997

Approved for public release; distribution unlimited

Reorientations of Flexible Spacecraft
Using
Momentum Exchange Devices

Kevin Anthony Ford, B.S., M.S., M.S.

Major, United States Air Force

Approved:

<u>Christopher D. Hall</u>	<u>5 Sep 97</u>
Dr. Christopher D. Hall Research Advisor	Date
<u>Bradley S. Liebst</u>	<u>5 Sep 97</u>
Dr. Bradley S. Liebst Committee Member	Date
<u>William P. Baker</u>	<u>5 Sep 97</u>
Dr. William P. Baker Committee Member	Date
<u>Dennis W. Quinn</u>	<u>5 SEP 97</u>
Dr. Dennis W. Quinn Dean's Representative	Date

Robert A. Calico, Jr. 9 Sept 97

Dr. Robert A. Calico, Jr.
Dean, Graduate School of Engineering

Acknowledgements

I cannot thank my advisor, Dr. Chris Hall, enough for the time and effort that he has put in to providing me with a first rate education. His talents as a professor and engineer come from an exceptional blend of technical, verbal, and interpersonal skills, along with an unbelievable work ethic. His generosity in sharing his talents with me are greatly appreciated.

Dr. Brad Liebst and Dr. William Baker both provided me with an excellent foundation through formal coursework, as well as hours and hours of enlightening counsel on this project. Both are experts in their fields and both provided superb guidance. They were perfect choices for committee members.

With regard to the success I have enjoyed throughout my career, however, the greatest thanks must go to my wonderful wife, Kelly. Her encouragement, support, and patience are unparalleled. The sacrifices she makes cannot be overstated. I also thank my parents, Barbara and Clayton, for providing a loving and positive environment in which to enter the world, not only for me, but for my five outstanding sisters and brothers as well. Finally, I would like to express my appreciation to my children, Anthony and Heidi, for so generously sharing CPU time with me at home, forgiving my occasional absence from their lives, and bravely enduring the Air Force lifestyle. Their sacrifices are appreciated.

Kevin Anthony Ford

Table of Contents

	Page
Acknowledgements	iii
List of Figures	vii
List of Tables	ix
Abstract	x
1. Introduction	1
1.1 Background	1
1.2 Research Overview	5
1.3 Outline of the Dissertation	6
2. Review of the Literature	8
2.1 Momentum Exchange Devices	8
2.1.1 Momentum Wheels	8
2.1.2 Control Moment Gyroscopes	9
2.2 Spacecraft Reorientations	11
2.3 Flexible Bodies	12
3. Momentum Exchange Devices	15
3.1 Gimbaled Momentum Wheel Kinematics	16
3.2 Equations of Motion	20
3.2.1 System Momenta	20
3.2.2 Gimbal Angles	21
3.2.3 Spin Axis Angular Momentum	22
3.2.4 Gimbal Axis Angular Momentum	24
3.2.5 Kinematics	27

	Page
3.2.6	GMW Equation Summary 28
3.2.7	Momentum Wheel Equation Summary 29
3.2.8	Control Moment Gyro Equation Summary 30
3.3	System Energy 31
3.4	Summary 35
4.	Euler-Bernoulli Appendages 36
4.1	Equations of Motion via the Lagrangian 36
4.2	System Energy 38
4.3	The Assumed Modes Method 44
4.4	Equation Summary for a Spacecraft with GMWs and Euler- Bernoulli Appendages 48
4.5	Summary 50
5.	Spacecraft Reorientations 51
5.1	Reorientations Using a Momentum Exchange Cluster 51
5.2	A Lyapunov Feedback Control Law 54
5.3	The CMG Singularity Problem 60
5.3.1	The Singularity-Robust Steering Law 60
5.3.2	The Singular Value Decomposition 62
5.3.3	Singular Direction Avoidance 63
5.3.4	The Singularity Avoidance Parameter 67
5.4	Maneuver Examples 69
5.4.1	Singular Direction Avoidance Example 69
5.4.2	Effect of the Singularity Avoidance Parameter 72
5.5	The Stationary Platform Maneuver 75
5.5.1	Stationary Condition for the GMW 75
5.5.2	Stationary Condition for the Momentum Wheel 78
5.5.3	Stationary Condition for the Control Moment Gyro 79

	Page
5.6 Lyapunov Control with Stationary Platform Weighting . . .	82
5.7 Summary	85
6. Simulation Results	86
6.1 Reorientations of a Small Flexible Satellite	86
6.1.1 The Small Satellite Model	86
6.1.2 Assumed Mode Shapes	87
6.1.3 Momentum Wheels	88
6.1.4 Control Moment Gyros	97
6.2 Reorientations of a Flexible Hubble Space Telescope	102
6.3 Summary	106
7. Summary and Conclusions	110
Appendix A. Definitions, Kinematics, and Fundamentals	113
A.1 Notation	113
A.2 Transformation Matrices	114
A.3 Eigenaxis Rotations	116
A.4 Quaternions	118
A.5 Rigid Body Equations of Motion	119
Appendix B. Simultaneous Eigenaxis and Stationary Platform Rotations .	122
Appendix C. Singularity Attraction Using Pseudoinverse Steering	124
Appendix D. Orthogonal CMG Cluster Envelope	128
Bibliography	131
Vita	135

List of Figures

Figure		Page
1.	A Gimbaled Momentum Wheel	16
2.	A Body with Multiple Gimbaled Momentum Wheels	16
3.	A Spacecraft with an Euler-Bernoulli Appendage	38
4.	Torque Output Near a Singularity for the SDA and SR Steering Laws	71
5.	Torque Produced and Torque Desired for the Singularity Avoidance Parameter Example	73
6.	Reorientation Parameters for SDA and SR Control Laws	74
7.	A CMG Stationary Platform Surface ($F = 1/2$)	80
8.	Cantilevered Beam Mode Shapes	89
9.	Reorientation Parameters for Stationary Platform and Direct Maneu- vers Using Momentum Wheels	91
10.	Cluster Norms for the Stationary Platform Maneuver and Direct Ma- neuver Using MWs	92
11.	Appendage Excitations for Stationary Platform and Direct Maneuvers Using MWs	93
12.	Reorientation Parameters for Lyapunov Maneuver With and Without Stationary Platform Weighting Using MWs	95
13.	Appendage Excitations for Lyapunov Maneuver With and Without Stationary Platform Weighting Using MWs	96
14.	Reorientation Parameters for Stationary Platform and Direct Maneu- vers Using CMGs	99
15.	Cluster Norms and Singular Values for the Stationary Platform and Direct Maneuvers Using CMGs	100
16.	Reorientation Parameters for Four CMG Control Laws	103
17.	Modal Responses for Four CMG Control Laws	104
18.	Singular Values and Potential Energy for Four CMG Control Laws	105
19.	Hubble Reorientation Parameters for Lyapunov Maneuver With and Without Stationary Platform Weighting	107

Figure		Page
20.	Hubble Appendage Excitations for Lyapunov Maneuver With and Without Stationary Platform Weighting	108
21.	Gimbal Angle Flow for Pseudoinverse Steering Law	127
22.	External Momentum Envelope for a Three CMG Orthogonal Cluster	130

List of Tables

Table		Page
1.	Spacecraft Physical Data for Singularity Avoidance Example	69
2.	SDA Example Simulation Data	70
3.	Singularity Avoidance Parameter Comparison Data	72
4.	Physical Data for the Small Flexible Satellite	87
5.	Cluster Data for the Small Satellite with Momentum Wheels	90
6.	Cluster Data for Small Satellite with CMGs	98
7.	Flexible Hubble Space Telescope Physical Data	106
8.	Hubble Space Telescope CMG Cluster Data	109

Abstract

We study rest-to-rest reorientations of flexible spacecraft using momentum exchange devices. A new and concise form of the equations of motion for a rigid body containing a cluster of gimballed momentum wheels is developed using the Euler-Newton approach. Special restrictions of the gimballed momentum wheel equations yield equations of motion for the momentum wheel cluster and the control moment gyroscope cluster.

Though control laws for reorienting rigid bodies using momentum wheels and control moment gyros were previously available, the oscillatory nature of a body containing a momentum cluster presents a challenge for a spacecraft with flexible appendages. In addition, reorientations which call for high angular accelerations naturally tend to excite oscillations of the appendages. A mathematical model of a free spacecraft with Euler-Bernoulli appendages is developed using the Lagrangian approach. Using the assumed modes method, a complete set of vector nonlinear differential equations is developed which describes the dynamics of a spacecraft with flexible appendages and a cluster of gimballed momentum wheels. This model is useful in comparing the merits of candidate spacecraft reorientations.

Special attention is paid to singularity problems in control moment gyro clusters. The singularity-robust control law commonly used to avoid singular cluster configurations can cause abrupt changes in torque output. An improved law based on the singular value decomposition is developed which avoids torque output commands in the nearly singular direction.

The stationary platform maneuver, a maneuver along the set of equilibrium solutions of a zero angular velocity spacecraft, is extended to the control moment gyro cluster. For a cluster of momentum wheels, the set of equilibria is a hyper-ellipsoid in rotor momenta space. The set of equilibria for a control moment gyro cluster is a unique surface in gimbal angle space. A control law which reorients the spacecraft while remaining close to this surface is developed using a Lyapunov method.

Reorientations of Flexible Spacecraft
Using
Momentum Exchange Devices

1. Introduction

1.1 Background

The spacecraft of tomorrow are no doubt still beyond even the most vivid imaginations. The missions of future spacecraft will likely require that they become more efficient and versatile. While the designs of today seem to be meeting our immediate needs, the maneuverability and attitude control requirements of future craft will likely increase.

The attitude control of spacecraft to date has been largely a problem of maintaining orientation and stability. One notable exception is the Hubble Space Telescope, which must be reoriented on command to a very precise orientation in inertial space and maintained there for a period of time. While the telescope's reaction wheel control system has proven worthy of the required task, the time required of such reorientations is measured in large fractions of an hour. It is certainly possible that future missions might require such reorientations in seconds.

We should also anticipate more variation in the sizes of future spacecraft, ranging from microsats to spacestations. A manned space station would likely be more efficient with increased size. Perhaps one day, a commercial station might exist which would permit companies to add on a module to an already existing configuration. Depending on the mission, the company might have a requirement for their module or equipment to periodically attain and then maintain a certain orientation in space (earthward or sunward for example). This requirement translates to a need for maneuverability. Some scheme to provide a maneuver torque to the structure must be adopted. Of course, even to maintain a stationary orientation in space requires a method to counteract the ubiquitous environmental torques due to aerodynamics, gravity gradient, and radiation pressure.

Two common devices for applying control torques today are external thrusters and magnetic dipoles. Both have drawbacks and limitations. External thrusters need some type of expendable, chemical fuel for operation. Launching fuel into space is costly. Thrusters have the additional fault of expelling propellants. This may create problems for sensitive sensor equipment. This drawback apparently ruled out external thrusters for use on the Hubble Space Telescope. Just as importantly, once the thruster configuration is established, there are now limitations on where new modules may be placed, as the thruster exhaust must be avoided.

Magnetic torquers are popular as they operate electrically (a replenishable supply of energy in space). Magnetic torquers take advantage of the earth's magnetic field and can provide a sustained external torque to the platform, thereby changing the system's angular momentum markedly over a period of time. The magnitude of the torque which can be achieved, however, is generally inadequate for effecting any sort of rapid reorientation. Additionally, the strength and direction of the magnetic field varies with orbital position. Magnetic torquers would be useless on spacecraft operating out of the influence of a magnetic field, such as interplanetary spacecraft.

One solution to these problems is the use of appropriately mounted internal rotors (flywheels) to store angular momentum. This angular momentum can then be transferred to the vehicle structure to effect a desired angular velocity, and subsequently a reorientation. The mechanization of these wheels varies, and the two of particular interest here are the momentum wheel and the control moment gyro.

The momentum wheel is mounted along a fixed axis in the platform. Angular momentum is then exchanged between the body and the rotor by applying a torque to the rotor via an electric motor. The dynamics involve only a relative change in speed between the rotor and spacecraft. It is common to mount at least three momentum wheels in an orthogonal arrangement to permit exchange of angular momentum about any axis in the body. The rate of momentum exchange with the spacecraft (the output torque) is restricted by the rate at which the wheel spin speeds can be changed.

The control moment gyro (CMG), conversely, operates at a constant rotor speed. The exchange in momentum is generated by varying the spin axis orientation with respect to the spacecraft. The dynamics of the gyroscopic effects can lead to rather complicated responses, requiring complicated algorithms to compute the required input for a desired response. Also, whereas momentum wheels maintain their design orientation, CMGs can achieve certain orientations which allow no torque capability in a particular direction, resulting in a singularity in the control law. This condition must be guarded against. The rate of momentum exchange with the spacecraft in the case of the CMG is dependent on the gimbal angle rate.

The reorientation problem is one of determining the current orientation and angular velocity in inertial space, determining the desired orientation and angular velocity at some future time (the final state conditions), and finding the best path to take in reaching the desired final state conditions. There are an infinite number of paths which can be followed, but certainly some are better than others. Paths which might be convenient for reorientations have been the subject of many studies. Some of these paths are obvious, whereas others are not.

The eigenaxis rotation is the most direct path between two orientations. For any rotation, there exists an axis (the eigenaxis) which remains fixed in space. If the rotation matrix is known, the eigenaxis can be computed. Furthermore, the angle of rotation about the eigenaxis is also easily computed. Reorientation is simply a matter of accelerating to a constant angular velocity about the eigenaxis, maintaining the velocity, and decelerating to the new orientation.

Optimal control theory suggests that, assuming we had the capability to provide a given torque about any axis, the minimum time reorientation would be the result of bang-bang control. That is, accelerate at maximum torque about the eigenaxis until halfway to the desired orientation, and then decelerate at maximum torque into the new orientation. However, it is unlikely that any real control system could provide the maximum torque in the eigenaxis direction. Moreover, if the eigenaxis is other than the direction of a principal moment of inertia, a torque perpendicular to the rotation will be required to overcome gyroscopic effects.

Another path might be dictated by the mechanization of the momentum wheel or CMGs. Supposing that the angular momentum at the beginning of the maneuver is contained solely in the wheels, then the vehicle's total angular momentum is determined and is fixed in space. For a desired final orientation, the necessary angular momentum relative to the body can be calculated. We might suspect that by adjusting the momentum in the momentum wheels to the required final values, the desired final orientation would be achieved. Achieving the proper cluster momentum in the body frame, however, is necessary but not sufficient to ensure the desired final orientation.

The variation of the wheel speeds in a linear fashion was investigated by Schultz [46] and was referred to as the direct path. If in fact the body angular velocity can be reduced to zero at the final orientation, then the direct path will achieve the objective (to within a rotation about the angular momentum vector). Unfortunately, for a specific set of final condition wheel speeds, the same total angular momentum vector can be achieved with an infinite number of body rates. The direct method does not necessarily keep body rates low, and most likely will *not* achieve the final orientation with zero body rates.

Oscillatory motion of the body is a common phenomenon associated with spacecraft containing rotors. This motion presents a serious problem to flexible spacecraft, as it can easily excite flexible modes of vibration causing loss of mission effectiveness or even structural damage. A control law which keeps angular velocities under control is required for these types of structures.

A technique investigated by Hall [20] proved promising in the reorientation of flexible space structures by keeping body rates low throughout the maneuver. They were termed "stationary platform maneuvers" by Hall, because they consist of following paths in rotor momenta space which are the equilibrium solutions for a stationary platform. Of course, while maneuvering, the platform is not stationary, but by remaining close to these branches of equilibria, the dynamic effects of the body are minimized and the spacecraft tends to arrive at the final orientation with low body angular velocity.

The purpose of this research is to investigate and compare various reorientation schemes of flexible space structures using momentum exchange devices such as momentum

wheels and control moment gyros. Insight into the utility of particular maneuvers should be gained by comparing time required for the maneuvers, control use required for the maneuvers, the possibility of achieving the desired final state conditions, oscillations of flexible appendages during the maneuvers, and the residual oscillations at termination.

1.2 Research Overview

The objective of this research is to develop improved control laws for momentum exchange devices imbedded in flexible spacecraft. Since the available background literature on control moment gyros is limited, we develop herein a concise vectorial form of the equations of motion for a body with a cluster of gimballed momentum wheels. The gimballed momentum wheel is a generalization of the momentum wheel and of the control moment gyro – essentially a variable speed single gimbal control moment gyro. This new development allows for easy specialization to momentum wheels or control moment gyros if desired.

Next, control laws which reorient the spacecraft are investigated. The stationary platform maneuver developed by Hall [18] shows great promise for application to flexible spacecraft due to its nature of keeping angular velocities low during a maneuver. We examine the maneuver's extension to the gimballed momentum wheel and the control moment gyro. We show that, because a momentum cluster, regardless of type, possesses a cluster momentum whose rate of change is actually the control torque, the concept is valid for all momentum exchange devices.

A drawback of the stationary platform maneuver is that kinematics are not accounted for, and the final orientation is only correct to within a rotation about the angular momentum vector. A method is sought to effect a reorientation to the target attitude while maintaining the stationary platform condition. The Lyapunov approach is used to produce a correction to the cluster momentum rate which keeps the cluster arbitrarily close to the stationary platform condition.

The control moment gyro cluster has several characteristics which make its use in attitude control a challenge. While momentum may be exchanged rapidly with the spacecraft,

the amount of momentum which may be exchanged is finite. Control moment gyro clusters also admit singular configurations which allow torque output only in a plane. Torque commands normal to this plane near the singular condition can cause unreasonably high gimbal rate commands. A singularity-robust control law developed by Oh and Vadali [42] avoids these singular conditions, but can cause abrupt changes in torque direction near the singularity. A new singular direction avoidance law is developed herein. This modification to the singularity-robust law is based on the singular value decomposition and smooths the gimbal rates while only altering the output torque in the singular direction.

In order to evaluate the effectiveness of the new control laws, a mathematical model of a flexible spacecraft is developed. Equations of motion for a free flying spacecraft with Euler-Bernoulli appendages (allowed flexure only in a plane) are developed using the Lagrangian approach. The assumed modes method is used to reduce the infinite degrees of freedom to a finite number suitable for numerical solution. The equations of motion for the flexible model can be coupled directly to the spacecraft/gimbaled momentum wheel equations for numerical evaluation.

1.3 Outline of the Dissertation

In Chapter 2 we review the literature relevant to this research. Specifically, some of the relevant works on the use of momentum wheels and control moment gyros in the control of space vehicles are summarized. A review of literature relevant to reorientations and the flexible modeling of space structures is also presented.

The unique qualities of momentum wheels and control moment gyroscopes are addressed in Chapter 3. We develop the equations of motion for the gimbaled momentum wheel, a generalization combining the qualities of the momentum wheel and the control moment gyroscope. This chapter includes some original work regarding the kinematics of the orthogonal CMG cluster. The equations are developed in vector form, with spin axis and gimbal axis torques as the control inputs. A compact expression for the kinetic energy of the system is also given.

In Chapter 4, the equations of motion for a body with flexible appendages are developed using the Lagrangian approach. The set of equations developed are mixed partial and ordinary differential equations. They are then discretized using the assumed modes method, and a finite set of ordinary differential equations are produced. This set is then integrated with the equations of Chapter 3 to produce a mathematical model of a flexible spacecraft with a cluster of gimbale momentum wheels as the attitude control device.

Methods of achieving reorientations of the body are discussed in Chapter 5. We begin with a general development which takes the "black box" approach, assuming that the momentum of the cluster relative to the spacecraft can be controlled as desired. A general Lyapunov feedback control law using the cluster momentum as the control input is derived. We then relate the control law to the special cases of momentum wheels and control moment gyros.

Some special consideration is given to the CMG singularity problem in Chapter 5, and a new approach to avoiding the singularity is presented. We conclude the chapter with a discussion of the stationary platform condition.

The numerical results of the study are presented in Chapter 6. The qualitative and quantitative results of several proposed control laws are presented. A summary and conclusions of the dissertation research are in Chapter 7.

2. Review of the Literature

In this chapter, we review relevant literature in the disciplines which form the cornerstone of this research. Many contributions have been made which provide an excellent foundation for the study. To the best of our knowledge, the application of momentum storage devices to the control of flexible structures has not been consolidated into a single research effort.

2.1 Momentum Exchange Devices

2.1.1 Momentum Wheels. The development of equations of motion for a momentum wheel imbedded in a rigid body has been approached in a number of ways. Any general body to which is attached an axisymmetric spinning body is classified as a *gyrostat*. The axisymmetric portion of the gyrostat is a momentum wheel. In the case where the momentum wheels spin axis is aligned with a principal axis, the system is called an *axial gyrostat*, and a closed-form solution for the angular momentum in terms of Jacobi's elliptic functions has been given (see Cochran *et al.* [12] for references).

Hughes [23] provided an excellent development of the equations of motion for a rigid body containing a single wheel in terms of the absolute angular momentum of the system and the absolute angular momentum of the wheel. Hall [18] extended the development to a system of multiple wheels and derived a torque control law which maintains his so-called *stationary platform maneuver*. Hall [20] also reduced the equations of motion from the normal $N + 3$ first order differential equations (for an N -rotor gyrostat) to one equation involving a Hamiltonian by applying the method of averaging for the case of small spinup torques. Hall [18] and Hall and Rand [19] used this averaging approach to show that the Hamiltonian approach can provide insight into the qualitative nature of the dynamics during spinup of the rotors.

Schultz [46] investigated and compared rest-to-rest reorientations of rigid bodies using a cluster of momentum wheels. His investigation included maneuvers along the stationary platform condition developed by Hall as well as maneuvers resulting from linear variation of the momentum wheels from initial to the required final values (constant torque applied to each wheel). He found that intermediate angular velocities, as well as final angular veloci-

ties and attitude errors were significantly smaller using the stationary platform maneuver. These results motivate the investigation of this control law for flexible space structures.

The gyrostat with flexible appendages has been investigated mostly in the context of stability of motion. Likins *et al.* [30] and Mingori *et al.* [37] were both concerned with the limit cycles possible for dual-spin spacecraft whose sections contain nonlinear flexible elements. Their approach was based primarily on the energy sink approach, but was reinforced by comparison with the results of numerical integration. Stabb and Schlack [50] developed a model which consisted of a gyrostat with an attached torsionally flexible appendage. They developed the equations of motion for the system, but the primary thrust was on the application of the Krylov-Bogoliubov-Mitropolsky (KBM) method to aid in analyzing the motion of the system for small perturbations from the undeformed state. Mazzoleni *et al.* [33] integrated the work of Stabb [50] and Hall [19] via a double averaging approach to develop a single equation which allows the projection of solutions onto a bifurcation diagram relating the rotor angular momentum to the system Hamiltonian.

Actual application of momentum wheel control to a spacecraft is described by Creamer *et al.* [14] in the case of the Clementine spacecraft. Control laws were developed to maneuver the spacecraft around the eigenaxis using a bang-coast-bang profile. They simplified development of the control laws by assuming that the nonlinear dynamics were negligible. The computed open-loop momentum wheel input torques for the maneuver were sent to a feedback control law for implementation of the actual maneuver, however. Flexible structural modes were not considered.

2.1.2 Control Moment Gyroscopes. The torque amplification phenomenon associated with single gimbal control moment gyros make them an appealing alternative to momentum wheels, but the theory for CMGs is not quite as mature. There apparently are no texts which address the full nonlinear dynamics of the CMG. Jacot and Liska [24] were among the first to see the usefulness of the CMG for space vehicle attitude control. Though they attempted a careful development utilizing a conservation of momentum approach, they omitted the inertia about the gimbal axis from the very first equation. They also linearized early in the development.

O'Connor and Morine [41] expounded on the merits of various CMG configurations for space vehicles and compared the utility of CMG control laws. They dismissed torque as a command input to the single-gimbal CMG as unusable due to the appreciable friction on the gimbal bearings. Instead they recommended a gimbal rate (feedback) control law.

Singularities were discussed in an early work by Margulies and Aubrun [32]. They showed that for a cluster of n CMGs, there exist for any direction in space 2^n combinations of gimbal angles for which the system cannot produce any torque in that direction. In addition, they demonstrated that for n CMGs in a cluster, there is an $n - 3$ parameter family of *null motions* which produce no output torque. As such, these null motions can be combined with torque-producing motions without affecting the dynamics of the system.

A useful development of the complete equations of motion (including the gimbal inertia terms) was given in Oh and Vadali [42]. They presented some candidate feedback control laws and claimed that, with the gimbal inertias included, the control laws must provide gimbal acceleration commands (instead of gimbal rate commands). They also gave some considerations for avoiding singularities in the case of a redundant set of CMGs. Hoelscher and Vadali [22] further considered open-loop and feedback control laws which not only minimized a mix of control effort and maneuver time, but also avoided singular CMG configurations. Vadali and Krishnan [52] narrowed the focus exclusively to avoiding these singularities by parameterizing gimbal rates as polynomial functions of time and optimizing the parameters with respect to a singularity avoidance objective function. Going one step further, Vadali *et al.* [53] developed a method for determining a family of initial gimbal angles which would avoid singularities during a maneuver. Bedrossian *et al.* [3, 4] developed a way of instituting the addition of null-motion into the control algorithm to avoid singularities. Paradiso [43] developed a computer algorithm which was capable of globally avoiding singular states in a feed-forward steering law.

An application of a highly linearized axis-decoupled CMG steering law for the space station was presented by Singh and Bossart [48] and another by Bishop *et al.* [7]. Neither of these studies extrapolate their capability to a control scheme for large angle reorientations or high angular velocities.

2.2 *Spacecraft Reorientations*

Perhaps the best compendium of notation and methods for dealing with reorientations of spacecraft is the text by Junkins and Turner [26]. Included are methods for optimizing the reorientations based on several different types of cost functions, along with some considerations for flexible modes of vibration. Carrington and Junkins [10] developed a solution for the nonlinear spacecraft slew maneuver by assuming a polynomial feedback form. Kinematics were formulated in terms of Euler parameters (also known as *quaternions*).

One of the early works on feedback control for reorientations was written by Wie and Barba [55]. They proposed three distinct quaternion feedback laws capable of general three-axis reorientations. Wie *et al.* [57] devised a quaternion feedback regulator to perform eigenaxis rotations (which they considered “optimal”) and included the control torque required to decouple the gyroscopic coupling torques. Wie and Lu [56] further developed this nonlinear feedback controller to perform eigenaxis rotations under slew rate and control torque constraints. Cristi *et al.* [15] provided a quaternion feedback regulator which is evidently globally stable and needs no knowledge of the spacecraft inertia matrix, an excellent property for control of a modular space station. Long [31] developed an equivalent axis coordinate frame for rest-to-rest reorientations which transforms the nonlinear spacecraft control problem into a linear problem.

Understandably, the problem of optimum time reorientations has also received considerable attention. A survey of contributions in this area was provided by Scrivener and Thompson [47]. An extremely important contribution was made by Bilimoria and Wie [6] when they demonstrated that with specified control constraints in all three axes, the eigenaxis rotation is in general not time optimal. The optimal control is bang-bang in all three axes and results in a significant nutational component. The task is only to find the switching functions for each axis. Byers and Vadali [8] applied these ideas to the development of a method for computing solutions for the time-optimal control switch times in the reorientation of a rigid spacecraft. They intentionally omitted the gyroscopic coupling terms from the dynamical equations. Vadali *et al.* [51] used a parameter optimization scheme to develop an open-loop control law for the reorientation of a particular ground-

based test article. The control law was then utilized in a feedback controller. Theoretical and experimental results were then compared with apparently excellent agreement.

We should point out that studies in the robotics field have a great deal in common with this idea of internal momentum exchange devices to effect reorientation of the primary body. Many works have borrowed the singularity robust inverse presented by Nakamura [39] as a method of avoiding singularities in control laws. An intriguing paper detailing a strategy for planar reorientation of a system of pinned bodies using only internal controls is provided by Reyhanoglu and McClamroch [45].

2.3 Flexible Bodies

An entire text devoted to the dynamics and control of flexible space structures was prepared by Junkins and Kim [25]. Their treatment of flexible structure models and the application of the Lagrangian approach for generation of the equations of motion are particularly noteworthy. A text by Craig [13] also provided an overview of various methods useful in modeling a flexible body, along with limitations of the finite-dimensional representations of the body which must be employed for numerical evaluation of the problem. Many of the papers concerned with the problem of flexible appendages attached to a satellite were summarized by Modi [38].

An early attempt at constructing the equations of motion for a flexible spacecraft was given by Grote *et al.* [17]. The equations were constructed for a model consisting of rigid bodies attached with springs and dampers. It was assumed that the motion of the central rigid body is prescribed, and the flexible appendages effect a deviation from this nominal motion. Keat [27] described an analogous method applicable when the flexibility is modeled by generalized coordinates.

Most studies investigating reorientation maneuvers with flexible appendages attack the problem with simplifying assumptions. Barbieri and Ozguner [2] were able to construct a minimum-time control law to slew an undamped, one-mode model of a flexible structure using the single-axis bang-bang control with multiple switchings. The single flexible mode was suppressed at the final orientation. Byers *et al.* [9] used smoothed bang-bang control

inputs to achieve a near-minimum time planar reorientation of a fixed rigid hub with four identical flexible appendages. The control inputs were simply smoothed approximations to the optimal bang-bang inputs for a rigid body. Small antisymmetric deformations of the appendages were assumed.

The three-dimensional case was pursued by Vadali *et al.* [54] using a parameter optimization approach as a flexible extrapolation to [51]. The only consideration given here to the flexible modes was in the smoothing of the control inputs using a multiplier function during the initial and final phases of a maneuver. Bell and Junkins [5] took the same approach but used controllably sharp spline switches to reduce flexible excitations. A momentum exchange feedback control concept was investigated by Li and Bainum [28], but was restricted to a pair of symmetric appendages affixed to a rigid hub. The control torques included not only feedback of the rigid body motion, but also the time rate of change of momentum resulting from the flexible motion.

An early introduction to the use of hybrid coordinates in the design of attitude control systems was given by Likins and Fleischer [29]. They were primarily interested in the stability of an attitude controller with the flexible modes included. Barbera and Likins [1] presented a method for testing the stability of a system with an arbitrary discretized appendage, and closed form stability criteria were developed for a very restricted model. Meirovitch and Calico [34] compared three essentially different methods for investigating the stability of flexible spacecraft. The more specific problem of attitude stability in dual-spin systems bearing flexible members was addressed by Gale and Likins [16] as well as Cherchas and Hughes [11]. Not all work has been theoretical in nature. A summary of some experimental investigations into the control of flexible structures was given by Sparks and Juang [49].

Though the aforementioned works provide a firm foundation for this dissertation research, the study of momentum exchange devices imbedded in a general three-dimensional flexible spacecraft remains largely unexplored. We attempt to retain the general nonlinear and 3-D nature of the problem by avoiding such simplifications as symmetric appendages, an inertially-fixed center of mass, or the discarding of inertia terms associated with the

momentum devices. We now turn to the development of a new set of equations of motion for a rigid spacecraft containing a momentum exchange cluster.

3. Momentum Exchange Devices

Two types of momentum exchange devices receive most of the attention in the literature. The *momentum wheel* (MW) is a variable speed flywheel mounted on an axis fixed in the body. Momentum exchange is effected by changing the speed of the wheel relative to the body using an electric motor. A cluster of at least three MWs with non-coplanar axes can be used to exchange momentum with the body about any axis.

The second type of momentum exchange device is the *control moment gyroscope* (CMG). The flywheel of a typical CMG spins at a constant speed and a gimbal arrangement allows variation of the spin axis in the body reference frame. A double gimbal arrangement can permit the spin axis of the CMG to assume any direction in the body. The single gimbal CMG (SGCMG) allows reorientation of the spin axis only in a plane which is perpendicular to the gimbal axis. The advantage of the SGCMG is the well-known torque amplification property. Essentially, a rate about the gimbal axis can produce an output torque orthogonal to both the gimbal and spin axes which is much greater than the gimbal axis torque. A reference to the CMG in this dissertation implies the single gimbal variety.

A *gimbaled momentum wheel* (GMW) is a generalization of the momentum wheel and single gimbal control moment gyroscope. The GMW allows for variation in wheel speed and reorientation about a gimbal axis (see Figure 1). A new form of the equations of motion for the GMW is developed using a momentum approach. The development leads to a system of $6 + 3N$ ordinary differential equations for the system angular momentum, system linear momentum, the angular momenta of the GMWs about the gimbal axes, the angular momenta of the GMWs about the spin axes, and the gimbal angles. Once the equations of motion for the GMW are available, specialization to the momentum wheel and CMG follows naturally. When linear momentum is assumed to be zero (and constant) the equations of motion for the momentum wheel case reduce to a $3 + N$ order set, whereas the CMG case reduces to a $3 + 2N$ order set. Notation and a review of the basic concepts relevant to the subsequent development can be found in Appendix A.

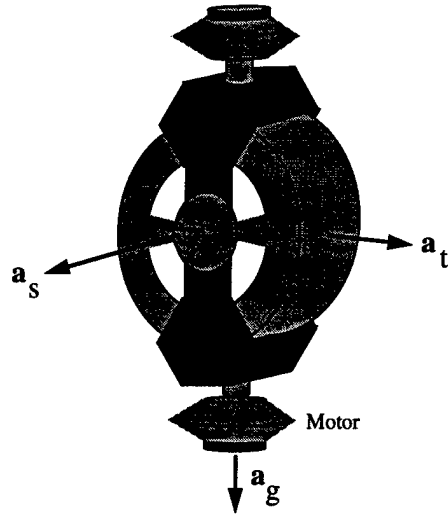


Figure 1 A Gimbaled Momentum Wheel

3.1 Gimbaled Momentum Wheel Kinematics

Consider a rigid body in which N gimbaled momentum wheels are imbedded (Figure 2). Each GMW is composed of a flywheel mounted in a gimbal frame and incorporates the variable speed of a momentum wheel and the gimbal arrangement of a typical single gimbal CMG. The GMWs are designated W_1, W_2, \dots, W_N and the rigid platform is identi-

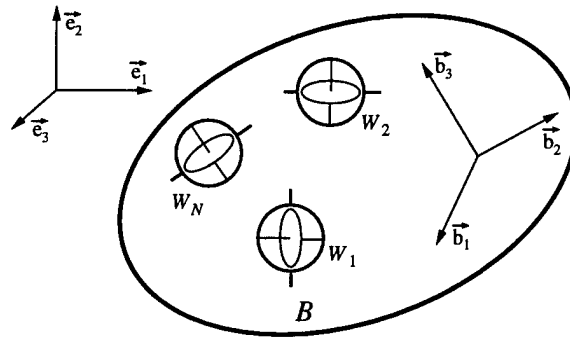


Figure 2 A Body with Multiple Gimbaled Momentum Wheels

fied as B . The platform is in general not symmetric. A reference frame, \mathcal{F}_b , is established in the body which has basis $(\vec{b}_1, \vec{b}_2, \vec{b}_3)$. The body is free to translate and rotate with respect to the inertially fixed reference frame, \mathcal{F}_i , with basis $(\vec{e}_1, \vec{e}_2, \vec{e}_3)$.

The wheels spin about their individual axes of symmetry which are expressed as the unit vectors $\vec{\mathbf{a}}_{s1}, \vec{\mathbf{a}}_{s2}, \dots, \vec{\mathbf{a}}_{sN}$. The directions of the spin axis unit vectors vary with the gimbal angles. The gimbal axes are always orthogonal to the spin axes and are denoted by the unit vectors $\vec{\mathbf{a}}_{g1}, \vec{\mathbf{a}}_{g2}, \dots, \vec{\mathbf{a}}_{gN}$. A third set of unit vectors given by $\vec{\mathbf{a}}_{t1}, \vec{\mathbf{a}}_{t2}, \dots, \vec{\mathbf{a}}_{tN}$ (subscript representing *transverse*), where $\vec{\mathbf{a}}_{tj} = \vec{\mathbf{a}}_{sj} \times \vec{\mathbf{a}}_{gj}$, will prove useful in the derivation.

We define a matrix \mathbf{A}_s such that the columns of \mathbf{A}_s are the column matrices \mathbf{a}_{sj} ($j = 1 \dots N$) which specify the orientations of the spin axes of the wheels, W_j ($j = 1 \dots N$), in the vehicle body frame \mathcal{F}_b . That is

$$\mathbf{A}_s = \begin{bmatrix} \mathbf{a}_{s1} & \mathbf{a}_{s2} & \cdots & \mathbf{a}_{sN} \end{bmatrix} \quad (1)$$

The matrices \mathbf{A}_g and \mathbf{A}_t are defined similarly. Whereas \mathbf{A}_g is a constant matrix, the matrices \mathbf{A}_s and \mathbf{A}_t depend on the gimbal angles.

The moment of inertia for the spacecraft is assumed constant except for the change caused by variation in the gimbal angles. It is also assumed that the center of mass of the spacecraft is fixed in the body and does not vary with gimbal angles. The inertia dyadic $\vec{\mathbf{I}}$ is formed from the body inertia dyadic plus the parallel axis contributions of the wheels. It is given by

$$\vec{\mathbf{I}} = \vec{\mathbf{I}}_B + \sum_{j=1}^N m_j (\vec{\mathbf{r}}_j \cdot \vec{\mathbf{r}}_j \vec{\mathbf{1}} - \vec{\mathbf{r}}_j \vec{\mathbf{r}}_j) \quad (2)$$

where m_j is the mass and $\vec{\mathbf{r}}_j$ the fixed location of the center of mass of the j -th GMW.

We define the terms I_{sj} , I_{gj} , and I_{tj} to be the total spin axis inertia, the total gimbal axis inertia, and the total transverse axis inertia of the j -th GMW (including the gimbal frame). The total spin axis inertia of the GMW is the sum of the gimbal frame inertia and wheel inertia. We split it into the terms I_{swj} and I_{sgj} so that

$$I_{sj} = I_{swj} + I_{sgj} \quad (3)$$

We form \mathbf{I}_{sw} as a diagonal matrix composed of the spin axis moments of inertia of the GMW wheels:

$$\mathbf{I}_{sw} = \text{diag}(I_{sw1}, I_{sw2}, \dots, I_{swN}) \quad (4)$$

Four other $N \times N$ inertia matrices, \mathbf{I}_s , \mathbf{I}_g , and \mathbf{I}_t , and \mathbf{I}_{sg} are defined in a similar manner.

The linear momentum of the system is given by

$$\vec{\mathbf{p}} = m\vec{\mathbf{v}} + \vec{\boldsymbol{\omega}} \times \vec{\mathbf{c}} \quad (5)$$

where $\vec{\mathbf{v}}$ is the velocity of the origin of \mathcal{F}_b and $\vec{\mathbf{c}}$ is the first mass moment of the body/GMW system about the origin of \mathcal{F}_b . The angular velocity of the body (and body reference frame) with respect to inertial space is $\vec{\boldsymbol{\omega}}$. We write Equation (5) in the body coordinate frame as

$$\mathbf{p} = m\mathbf{v} + \boldsymbol{\omega}^\times \mathbf{c} \quad (6)$$

where we use the cross notation defined by Equation (340).

The system angular momentum can be expressed as

$$\vec{\mathbf{h}} = \vec{\mathbf{I}} \cdot \vec{\boldsymbol{\omega}} + \vec{\mathbf{c}} \times \vec{\mathbf{v}} + \sum_{j=1}^N \vec{\mathbf{h}}_{aj} \quad (7)$$

where $\vec{\mathbf{h}}_{aj}$ is the *absolute* angular momentum of the j -th GMW about its own center of mass. Instead of grouping the GMW contributions to the angular momentum by GMW (as did Oh and Vadali [42]), we decompose the GMW contributions to angular momentum into components in the spin, gimbal, and transverse directions. This is expressed as (using body frame components)

$$\mathbf{h} = \mathbf{I}\boldsymbol{\omega} + \mathbf{c}^\times \mathbf{v} + \mathbf{A}_s \mathbf{h}_{sa} + \mathbf{A}_g \mathbf{h}_{ga} + \mathbf{A}_t \mathbf{h}_{ta} \quad (8)$$

The new terms \mathbf{h}_{sa} , \mathbf{h}_{ga} , and \mathbf{h}_{ta} are $N \times 1$ column matrices which represent the components of absolute angular momentum of the GMWs about their spin axes, gimbal axes, and spin axes respectively. From Equation (8), we see that if we know the gimbal angles (and therefore the $3 \times N$ basis matrices) along with \mathbf{h} , \mathbf{h}_{sa} , \mathbf{h}_{ga} , \mathbf{h}_{ta} , and \mathbf{v} , then we can compute the current body angular velocity $\boldsymbol{\omega}$.

One term in Equation (8) deserves special attention. The angular momentum of a GMW about its spin axis is a combination of angular momentum due to the flywheel itself,

plus a contribution due to the gimbal frame. We simply split \mathbf{h}_{sa} into two terms as

$$\mathbf{h}_{sa} = \mathbf{h}_{swa} + \mathbf{h}_{sga} \quad (9)$$

where \mathbf{h}_{swa} is the $N \times 1$ column matrix of absolute angular momenta of the wheels about their spin axes, and \mathbf{h}_{sga} is the $N \times 1$ column matrix of absolute angular momenta of the gimbal frames about the GMW spin axes.

The absolute angular momentum components may be expressed in terms of the platform angular velocity and *relative* angular momenta. The relationships are

$$\mathbf{h}_{swa} = \mathbf{I}_{sw} \mathbf{A}_s^T \boldsymbol{\omega} + \mathbf{h}_{swr} \quad (10)$$

$$\mathbf{h}_{sga} = \mathbf{I}_{sg} \mathbf{A}_s^T \boldsymbol{\omega} + \mathbf{h}_{sgr} \quad (11)$$

$$\mathbf{h}_{ga} = \mathbf{I}_g \mathbf{A}_g^T \boldsymbol{\omega} + \mathbf{h}_{gr} \quad (12)$$

$$\mathbf{h}_{ta} = \mathbf{I}_t \mathbf{A}_t^T \boldsymbol{\omega} + \mathbf{h}_{tr} \quad (13)$$

In the case of mechanical gimbals, the motion of the GMW gimbal is constrained to rotation about the gimbal axis, so there can be no motion of the GMW relative to the platform in the transverse direction, nor can the gimbal rotate relative to the platform about the spin axis. Therefore

$$\mathbf{h}_{tr} = \mathbf{h}_{sgr} = \mathbf{0} \quad (14)$$

which implies that we can rewrite Equation (8) as

$$\mathbf{h} = (\mathbf{I} + \mathbf{A}_t \mathbf{I}_t \mathbf{A}_t^T + \mathbf{A}_s \mathbf{I}_{sg} \mathbf{A}_s^T) \boldsymbol{\omega} + \mathbf{c}^\times \mathbf{v} + \mathbf{A}_s \mathbf{h}_{swa} + \mathbf{A}_g \mathbf{h}_{ga} \quad (15)$$

Note that the inertia-like matrix multiplying $\boldsymbol{\omega}$ in Equation (15) is not necessarily constant.

The definitions of this section allow for a concise expression of the equations of motion, which we now address.

3.2 Equations of Motion

In this section, we develop the equations of motion for a rigid body with GMWs in terms of the system linear and angular momenta, as well as the angular momenta components of each GMW about the spin and gimbal axes. Because the orientation of the GMW is important (as it gives the direction of the spin momentum vector), an equation of motion is also developed for the gimbal angle. A summary of the GMW equations and specializations to the momentum wheel and CMG cases are also presented.

3.2.1 System Momenta. The absolute time derivative of any vector \vec{x} in \mathcal{F}_i is related to the time derivative of that vector in \mathcal{F}_b by

$$\left. \frac{d\vec{x}}{dt} \right|_i = \left(\left. \frac{d\vec{x}}{dt} + \vec{\omega} \times \vec{x} \right) \right|_b \quad (16)$$

The equation of motion relating linear momentum to the total external force is

$$\dot{\vec{p}} = \vec{f}_e \quad (17)$$

Therefore, the differential equation for linear momentum in the body reference frame is given by

$$\dot{\vec{p}} = -\boldsymbol{\omega}^\times \vec{p} + \vec{f}_e \quad (18)$$

The absolute time derivative of angular momentum (in \mathcal{F}_i) can be shown to be

$$\dot{\vec{h}} = -\vec{v} \times \vec{p} + \vec{g}_e \quad (19)$$

so that we can write the differential equation for the total angular momentum in body coordinates as

$$\dot{\vec{h}} = -\boldsymbol{\omega}^\times \vec{h} - \vec{v}^\times \vec{p} + \vec{g}_e \quad (20)$$

3.2.2 *Gimbal Angles.* We note from Equation (12) that the relative angular momentum of the GMW about the gimbal axis is

$$\mathbf{h}_{gr} = \mathbf{h}_{ga} - \mathbf{I}_g \mathbf{A}_g^T \boldsymbol{\omega} = \mathbf{I}_g \boldsymbol{\omega}_{gr} \quad (21)$$

so that we find the gimbal angle rate from the expression

$$\dot{\boldsymbol{\delta}} = \boldsymbol{\omega}_{gr} = \mathbf{I}_g^{-1} \mathbf{h}_{ga} - \mathbf{A}_g^T \boldsymbol{\omega} \quad (22)$$

which must be integrated to produce the gimbal angles. The gimbal angles are required to compute the matrices \mathbf{A}_s and \mathbf{A}_t . We assign the gimbal angles to be zero when the spin axes point in a set of arbitrary directions given by $\mathbf{a}_{s1_0}, \mathbf{a}_{s2_0}, \dots, \mathbf{a}_{sN_0}$.

The gimbal axis direction and gimbal angle for a particular GMW defines a rotation matrix relating the components of the the zero gimbal angle unit vectors (\mathbf{a}_{s0} , \mathbf{a}_{t0} , and \mathbf{a}_g) to the components of the current unit vectors (\mathbf{a}_s , \mathbf{a}_t , and \mathbf{a}_g). For an eigenaxis rotation (in this case about \mathbf{a}_g) through an eigenangle given by δ , we can express the 3×3 rotation matrix relating components in the two frames as

$$\mathbf{C} = \cos \delta \mathbf{1} + (1 - \cos \delta) \mathbf{a}_g \mathbf{a}_g^T - \sin \delta \mathbf{a}_g^\times \quad (23)$$

Thus, the spin axis unit vector for the j -th GMW is given by

$$\mathbf{a}_{sj} = \mathbf{C}_j^T \mathbf{a}_{sj_0} = \cos \delta_j \mathbf{a}_{sj_0} + (1 - \cos \delta_j) \mathbf{a}_{gj} \mathbf{a}_{gj}^T \mathbf{a}_{sj_0} + \sin \delta_j \mathbf{a}_{gj}^\times \mathbf{a}_{sj_0} \quad (24)$$

Since the gimbal axis is perpendicular to the spin axis ($\mathbf{a}_{gj}^T \mathbf{a}_{sj_0} = 0$), and if we assume that the gimbal axis is fixed in the body frame, then we can further reduce Equation (24) to

$$\mathbf{a}_{sj} = \cos \delta_j \mathbf{a}_{sj_0} - \sin \delta_j \mathbf{a}_{tj_0} \quad (25)$$

In a similar manner, we can show that the j -th transverse unit vector is given by

$$\mathbf{a}_{tj} = \cos \delta_j \mathbf{a}_{tj_0} + \sin \delta_j \mathbf{a}_{sj_0} \quad (26)$$

We define some new terms to aid in the numerical computation of the $3 \times N$ matrices \mathbf{A}_s and \mathbf{A}_t . From the $N \times 1$ matrix, $\boldsymbol{\delta}$, of gimbal angles, we compute the $N \times N$ matrices Δ^c and Δ^s where

$$\Delta^c = \text{diag}(\cos \boldsymbol{\delta}) \quad (27)$$

$$\Delta^s = \text{diag}(\sin \boldsymbol{\delta}) \quad (28)$$

and $\cos \boldsymbol{\delta}$ and $\sin \boldsymbol{\delta}$ are column matrices of the cosines and sines taken term by term of the column matrix $\boldsymbol{\delta}$.

By defining the matrices \mathbf{A}_{s0} and \mathbf{A}_{t0} as the values of \mathbf{A}_s and \mathbf{A}_t when the gimbal angles are all zero, then we compute \mathbf{A}_s and \mathbf{A}_t as functions of gimbal angles from the expressions

$$\mathbf{A}_s = \mathbf{A}_{s0}\Delta^c - \mathbf{A}_{t0}\Delta^s \quad (29)$$

$$\mathbf{A}_t = \mathbf{A}_{t0}\Delta^c + \mathbf{A}_{s0}\Delta^s \quad (30)$$

For single-gimbal GMWs, $\mathbf{A}_g = \mathbf{A}_{g0}$ is fixed, so $\dot{\mathbf{A}}_g = \mathbf{0}$. The rates of change of \mathbf{A}_s and \mathbf{A}_t , however, can be shown to be

$$\dot{\mathbf{A}}_s = -\mathbf{A}_t \text{diag}(\dot{\boldsymbol{\delta}}) \quad (31)$$

$$\dot{\mathbf{A}}_t = \mathbf{A}_s \text{diag}(\dot{\boldsymbol{\delta}}) \quad (32)$$

3.2.3 Spin Axis Angular Momentum. We now investigate the equations of motion for \mathbf{h}_{swa} and \mathbf{h}_{ga} since these terms are affected by the spin axis torque and gimbal torque respectively. Toward this end, we will for the time drop the subscript, j , referring to the j -th GMW, and consider only a single GMW. We begin by defining a scalar component of the torque applied to the spinning wheel as

$$g_w = \vec{\mathbf{a}}_s \cdot \vec{\mathbf{g}}_{bw} \quad (33)$$

where \vec{a}_s is a unit *vector* in the spin direction (independent of the reference frame). The term \vec{g}_{bw} is the total torque vector applied by the body/gimbal system on the spinning wheel, and in general includes components orthogonal to the spin axis.

The component of the absolute angular momentum of the wheel about the GMW center of mass in the \vec{a}_s direction is

$$h_{swa} = \vec{a}_s \cdot \vec{h}_{wa} \quad (34)$$

Note that we have included only the wheel momentum in the definition, since we will be applying a spin axis torque to the wheel only. (The total angular momentum of the GMW is $\vec{h}_a = \vec{h}_{wa} + \vec{h}_{ga}$ where \vec{h}_{ga} is the gimbal frame momentum about the spin axis.) For each GMW, then, we have

$$\dot{h}_{swa} = \dot{\vec{a}}_s \cdot \vec{h}_{wa} + \vec{a}_s \cdot \dot{\vec{h}}_{wa} \quad (35)$$

Since $\dot{\vec{h}}_{wa} = \vec{g}_{bw}$, Equation (35) becomes

$$\dot{h}_{swa} = \dot{\vec{a}}_s \cdot \vec{h}_{wa} + g_w \quad (36)$$

Because \vec{a}_s is fixed in the gimbal reference frame, which has angular velocity $\vec{\omega} + \delta\vec{a}_g$, we have

$$\dot{\vec{a}}_s = (\vec{\omega} + \delta\vec{a}_g) \times \vec{a}_s \quad (37)$$

Since the wheel is axisymmetric, the inertia dyadic can be expressed as

$$\vec{I}_w = I_{tw}\vec{1} + (I_{sw} - I_{tw})\vec{a}_s\vec{a}_s \quad (38)$$

where I_{tw} and I_{sw} represent the wheel transverse axis inertia and spin axis inertia respectively, and $\vec{h}_{wa} = \vec{I}_w \cdot \vec{\omega}_{wa}$ (where $\vec{\omega}_{wa}$ is the absolute angular velocity of the wheel with respect to inertial space), then Equation (36) becomes

$$\dot{h}_{swa} = ((\vec{\omega} + \delta\vec{a}_g) \times \vec{a}_s) \cdot (I_{tw}\vec{1} + (I_{sw} - I_{tw})\vec{a}_s\vec{a}_s) \cdot \vec{\omega}_{wa} + g_w \quad (39)$$

The total angular velocity of the wheel is made up of the body angular velocity, plus relative velocities in the spin axis direction $\vec{\omega}_{swr}$ and gimbal axis direction $\vec{\omega}_{gwr}$. So we use

$$\vec{\omega}_{wa} = \vec{\omega}_{swr} + \vec{\omega}_{gwr} + \vec{\omega} = \omega_{swr} \vec{a}_s + \dot{\delta} \vec{a}_g + \vec{\omega} \quad (40)$$

and also make use of the fact that $\vec{a}_s \cdot \vec{a}_g = \vec{a}_s \cdot \vec{a}_t = 0$ whereas $\vec{a}_g \cdot \vec{a}_g = 1$ to recast Equation (39) as

$$\dot{h}_{swa} = (\vec{\omega} \times \vec{a}_s - \dot{\delta} \vec{a}_t) \cdot (I_{tw} \dot{\delta} \vec{a}_g + I_{tw} \vec{\omega} + \omega_{swr} I_{sw} \vec{a}_s + (I_{sw} - I_{tw}) \vec{a}_s \vec{a}_s \cdot \vec{\omega}) + g_w \quad (41)$$

Eliminating terms based on orthogonality arguments, we obtain

$$\dot{h}_{swa} = (I_{tw} \dot{\delta} (\vec{\omega} \times \vec{a}_s) \cdot \vec{a}_g) - \dot{\delta} \vec{a}_t \cdot (I_{tw} \vec{\omega}) + g_w \quad (42)$$

whereupon we use the vector identity $(\vec{\omega} \times \vec{a}_s) \cdot \vec{a}_g = \vec{\omega} \cdot (\vec{a}_s \times \vec{a}_g) = \vec{\omega} \cdot \vec{a}_t$, giving the result

$$\dot{h}_{swa} = g_w \quad (43)$$

for the single GMW. This simply states that the rate of change of the absolute angular momentum component in the spin axis direction is equal to the torque transmitted to the wheel in that direction. The simplicity of this expression is a result of the axisymmetry of the wheel, and is identical to the symmetry axis equation of motion for an axisymmetric rigid body. Since we have N GMWs, we form the $N \times 1$ column matrix $\dot{\mathbf{h}}_{swa}$ for all N GMWs and write

$$\dot{\mathbf{h}}_{swa} = \mathbf{g}_w \quad (44)$$

The simplicity of this matrix differential equation motivates a similar approach to deriving the equations of motion for the GMWs about their gimbal axes.

3.2.4 Gimbal Axis Angular Momentum. We now engage in a similar development for the column matrix of gimbal axes momenta. To this end, we define the gimbal axis torque for a single GMW as

$$g_g = \vec{a}_g \cdot \vec{\mathbf{g}}_{bgmw} \quad (45)$$

where $\vec{\mathbf{g}}_{\text{b gmw}}$ is the torque applied by the body to the GMW. This includes the gimbal frame, since we are interested in the change in angular momentum of the spinning wheel plus gimbals. Since

$$h_{ga} = \vec{\mathbf{a}}_g \cdot \vec{\mathbf{h}}_{\text{gmw}} \quad (46)$$

we proceed along the lines of the previous development to arrive at

$$\dot{h}_{ga} = \dot{\vec{\mathbf{a}}}_g \cdot \vec{\mathbf{h}}_{\text{gmw}} + g_g \quad (47)$$

where in this case $\dot{\vec{\mathbf{a}}}_g = \vec{\omega} \times \vec{\mathbf{a}}_g$ as long as $\vec{\mathbf{a}}_g$ is fixed in the body frame.

Applying a vector identity, we get

$$\dot{h}_{ga} = (\vec{\omega} \times \vec{\mathbf{a}}_g) \cdot \vec{\mathbf{h}}_{\text{gmw}} + g_g = \vec{\omega} \cdot (\vec{\mathbf{a}}_g \times \vec{\mathbf{h}}_{\text{gmw}}) + g_g \quad (48)$$

The momentum in this case is more complicated, as we must include the gimbal frame. We separate the wheel momentum from the gimbal as

$$\vec{\mathbf{h}}_{\text{gmw}} = \vec{\mathbf{I}}_w \cdot \vec{\omega}_{wa} + \vec{\mathbf{I}}_g \cdot \vec{\omega}_{ga} \quad (49)$$

where $\vec{\mathbf{I}}_w$ is given by Equation (38) and $\vec{\omega}_{wa}$ by Equation (40), whereas $\vec{\omega}_{ga}$ only contains the terms

$$\vec{\omega}_{ga} = \vec{\omega}_{gr} + \vec{\omega} = \delta \vec{\mathbf{a}}_g + \vec{\omega} \quad (50)$$

This yields the apparently involved expression

$$\dot{h}_{ga} = \vec{\omega} \cdot (\vec{\mathbf{a}}_g \times (\vec{\mathbf{I}}_w \cdot (\omega_{swr} \vec{\mathbf{a}}_s + \delta \vec{\mathbf{a}}_g + \vec{\omega}) + \vec{\mathbf{I}}_g \cdot (\delta \vec{\mathbf{a}}_g + \vec{\omega}))) + g_g \quad (51)$$

which we subsequently simplify.

For simplicity, we break the complicated expression on the right hand side of Equation (51) into two parts and consider first the term $\vec{\omega} \cdot (\vec{\mathbf{a}}_g \times (\vec{\mathbf{I}}_w \cdot (\omega_{swr} \vec{\mathbf{a}}_s + \delta \vec{\mathbf{a}}_g + \vec{\omega})))$. We substitute for the wheel inertia dyadic to get

$$\vec{\omega} \cdot (\vec{\mathbf{a}}_g \times (I_{tw} \vec{\mathbf{I}} + (I_{sw} - I_{tw}) \vec{\mathbf{a}}_s \vec{\mathbf{a}}_s) \cdot (\omega_{swr} \vec{\mathbf{a}}_s + \delta \vec{\mathbf{a}}_g + \vec{\omega}))$$

$$\begin{aligned}
&= \vec{\omega} \cdot (\vec{\mathbf{a}}_g \times (I_{tw}(\omega_{swr}\vec{\mathbf{a}}_s + \vec{\omega}) + (\omega_{swr}(I_{sw} - I_{tw})\vec{\mathbf{a}}_s + (I_{sw} - I_{tw})\vec{\mathbf{a}}_s\vec{\mathbf{a}}_s \cdot \vec{\omega}))) \\
&= \vec{\omega} \cdot (I_{tw}(\omega_{swr}\vec{\mathbf{a}}_g \times \vec{\mathbf{a}}_s + \vec{\mathbf{a}}_g \times \vec{\omega}) + (\omega_{swr}(I_{sw} - I_{tw})\vec{\mathbf{a}}_g \times \vec{\mathbf{a}}_s + (I_{sw} - I_{tw})\vec{\mathbf{a}}_g \times \vec{\mathbf{a}}_s\vec{\mathbf{a}}_s \cdot \vec{\omega})) \\
&= \vec{\omega} \cdot (I_{tw}(-\omega_{swr}\vec{\mathbf{a}}_t) + (-\omega_{swr}(I_{sw} - I_{tw})\vec{\mathbf{a}}_t - (I_{sw} - I_{tw})\vec{\mathbf{a}}_t\vec{\mathbf{a}}_s \cdot \vec{\omega})) \\
&= -\omega_{swr}I_{sw}\vec{\omega} \cdot \vec{\mathbf{a}}_t - (I_{sw} - I_{tw})\vec{\omega} \cdot \vec{\mathbf{a}}_t\vec{\mathbf{a}}_s \cdot \vec{\omega} \tag{52}
\end{aligned}$$

Now we consider the second part of the large expression in Equation (51), namely $\vec{\omega} \cdot (\vec{\mathbf{a}}_g \times (\vec{\mathbf{I}}_g \cdot (\dot{\delta}\vec{\mathbf{a}}_g + \vec{\omega})))$. We make the reasonable assumption that the spin, gimbal, and transverse axes for the GMW are principal axes. This allows the gimbal inertia dyadic to be expressed in the form

$$\vec{\mathbf{I}}_g = I_{sg}\vec{\mathbf{a}}_s\vec{\mathbf{a}}_s + I_{gg}\vec{\mathbf{a}}_g\vec{\mathbf{a}}_g + I_{tg}\vec{\mathbf{a}}_t\vec{\mathbf{a}}_t \tag{53}$$

where the scalar coefficients are the gimbal frame inertias about the spin axis, gimbal axis, and transverse axis respectively, and which are in general unique. So we reduce the term as follows:

$$\begin{aligned}
&\vec{\omega} \cdot (\vec{\mathbf{a}}_g \times ((I_{sg}\vec{\mathbf{a}}_s\vec{\mathbf{a}}_s + I_{gg}\vec{\mathbf{a}}_g\vec{\mathbf{a}}_g + I_{tg}\vec{\mathbf{a}}_t\vec{\mathbf{a}}_t) \cdot (\dot{\delta}\vec{\mathbf{a}}_g + \vec{\omega}))) \\
&= \vec{\omega} \cdot (I_{sg}\vec{\mathbf{a}}_g \times \vec{\mathbf{a}}_s\vec{\mathbf{a}}_s + I_{tg}\vec{\mathbf{a}}_g \times \vec{\mathbf{a}}_t\vec{\mathbf{a}}_t) \cdot \vec{\omega} \\
&= \vec{\omega} \cdot (-I_{sg}\vec{\mathbf{a}}_t\vec{\mathbf{a}}_s + I_{tg}\vec{\mathbf{a}}_s\vec{\mathbf{a}}_t) \cdot \vec{\omega} \tag{54}
\end{aligned}$$

We make use of the fact that $\vec{\omega} \cdot \vec{\mathbf{a}}_s\vec{\mathbf{a}}_t \cdot \vec{\omega} = (\vec{\omega} \cdot \vec{\mathbf{a}}_s)(\vec{\mathbf{a}}_t \cdot \vec{\omega}) = \vec{\omega} \cdot \vec{\mathbf{a}}_t\vec{\mathbf{a}}_s \cdot \vec{\omega}$ so that we finally arrive at

$$\dot{h}_{ga} = (I_{tw} + I_{tg} - I_{sw} - I_{sg})\vec{\omega} \cdot \vec{\mathbf{a}}_s\vec{\mathbf{a}}_t \cdot \vec{\omega} - I_{sw}\omega_{swr}\vec{\omega} \cdot \vec{\mathbf{a}}_t + g_g \tag{55}$$

Note that $I_{tw} + I_{tg}$ is the inertia of the wheel plus gimbal about the transverse axis, whereas $I_{sw} + I_{sg}$ is the inertia of wheel plus gimbal about the spin axis so that the entire scalar coefficient is a constant. In the case where the GMW package is spherically symmetric, then the coefficient of the first term in Equation (55) reduces to zero and the term disappears completely. In the body axis reference frame, Equation (55) is expressed as

$$\dot{h}_{ga} = (I_t - I_s)\mathbf{a}_s^T \boldsymbol{\omega} \mathbf{a}_t^T \boldsymbol{\omega} - I_{sw}\omega_{swr}\mathbf{a}_t^T \boldsymbol{\omega} + g_g \tag{56}$$

Equation (10) for a single GMW would be

$$h_{swa} = I_{sw} \mathbf{a}_s^T \boldsymbol{\omega} + I_{sw} \omega_{swr} \quad (57)$$

and we use this to cast \dot{h}_{ga} as

$$\dot{h}_{ga} = ((I_t - I_{sg}) \mathbf{a}_s^T \boldsymbol{\omega} - h_{swa}) \mathbf{a}_t^T \boldsymbol{\omega} + g_g \quad (58)$$

Equation (58) can be put in a convenient form for the entire $N \times 1$ matrix of absolute gimbal direction angular momenta,

$$\dot{\mathbf{h}}_{ga} = ((\mathbf{I}_t - \mathbf{I}_{sg}) \mathbf{A}_s^T \boldsymbol{\omega} - \mathbf{h}_{swa}) \star (\mathbf{A}_t^T \boldsymbol{\omega}) + \mathbf{g}_g \quad (59)$$

where the operator \star represents term by term multiplication of the two adjacent $N \times 1$ column matrices. The \star operation could be carried out alternatively as

$$\mathbf{u} \star \mathbf{v} = \text{diag}(\mathbf{u})\mathbf{v} = \text{diag}(\mathbf{v})\mathbf{u} \quad (60)$$

Equation (59) provides the last N equations needed to describe the dynamics of the rigid body/GMW system.

3.2.5 Kinematics. The dynamical equations must be appended with a set of equations to describe the kinematics. We use quaternions, so that the four equations

$$\dot{\mathbf{q}} = \frac{1}{2} \mathbf{G}(\mathbf{q}) \boldsymbol{\omega} \quad (61)$$

where

$$\mathbf{G}(\mathbf{q}) = \begin{bmatrix} -q_1 & -q_2 & -q_3 \\ q_0 & -q_3 & q_2 \\ q_3 & q_0 & -q_1 \\ -q_2 & q_1 & q_0 \end{bmatrix} \quad (62)$$

are added to describe completely the dynamics and kinematics of a maneuver. See Appendix A for the definition and a discussion of quaternions.

3.2.6 GMW Equation Summary. We summarize the equations as $3N + 10$ nonlinear ordinary differential equations as follows

$$\dot{\mathbf{h}} = -\boldsymbol{\omega}^\times \mathbf{h} - \mathbf{v}^\times \mathbf{p} + \mathbf{g}_e \quad (63)$$

$$\dot{\mathbf{p}} = -\boldsymbol{\omega}^\times \mathbf{p} + \mathbf{f}_e \quad (64)$$

$$\dot{\mathbf{h}}_{swa} = \mathbf{g}_w \quad (65)$$

$$\dot{\mathbf{h}}_{ga} = ((\mathbf{I}_t - \mathbf{I}_{sg})\mathbf{A}_s^T \boldsymbol{\omega} - \mathbf{h}_{swa}) \star (\mathbf{A}_t^T \boldsymbol{\omega}) + \mathbf{g}_g \quad (66)$$

$$\dot{\boldsymbol{\delta}} = \mathbf{I}_g^{-1} \mathbf{h}_{ga} - \mathbf{A}_g^T \boldsymbol{\omega} \quad (67)$$

$$\dot{\mathbf{q}} = \frac{1}{2} \mathbf{G}(\mathbf{q}) \boldsymbol{\omega} \quad (68)$$

where \mathbf{g}_e , \mathbf{g}_w , and \mathbf{g}_g represent the external torque, the spin axis torques, and the gimballed torques respectively. Also, the $3 \times N$ matrices

$$\mathbf{A}_s = \mathbf{A}_{s0} \boldsymbol{\Delta}^c - \mathbf{A}_{t0} \boldsymbol{\Delta}^s \quad (69)$$

$$\mathbf{A}_t = \mathbf{A}_{t0} \boldsymbol{\Delta}^c + \mathbf{A}_{s0} \boldsymbol{\Delta}^s \quad (70)$$

define the spin axis and transverse axis components in the body frame. To find the system velocities from the momenta, we note that they are related in matrix form as

$$\begin{bmatrix} \mathbf{h} \\ \mathbf{p} \\ \mathbf{h}_{ga} \\ \mathbf{h}_{swa} \end{bmatrix} = \begin{bmatrix} \mathbf{J} & \mathbf{c}^\times & \mathbf{A}_g \mathbf{I}_g & \mathbf{A}_s \mathbf{I}_{sw} \\ -\mathbf{c}^\times & m\mathbf{1} & \mathbf{0}^{(3 \times N)} & \mathbf{0}^{(3 \times N)} \\ \mathbf{I}_g \mathbf{A}_g^T & \mathbf{0}^{(N \times 3)} & \mathbf{I}_g & \mathbf{0}^{(N \times N)} \\ \mathbf{I}_{sw} \mathbf{A}_s^T & \mathbf{0}^{(N \times 3)} & \mathbf{0}^{(N \times N)} & \mathbf{I}_{sw} \end{bmatrix} \begin{bmatrix} \boldsymbol{\omega} \\ \mathbf{v} \\ \boldsymbol{\delta} \\ \boldsymbol{\omega}_{swr} \end{bmatrix} = \Phi_{gmw} \begin{bmatrix} \boldsymbol{\omega} \\ \mathbf{v} \\ \boldsymbol{\delta} \\ \boldsymbol{\omega}_{swr} \end{bmatrix} \quad (71)$$

where

$$\mathbf{J} = \mathbf{I} + \mathbf{A}_t \mathbf{I}_t \mathbf{A}_t^T + \mathbf{A}_s \mathbf{I}_s \mathbf{A}_s^T + \mathbf{A}_g \mathbf{I}_g \mathbf{A}_g^T \quad (72)$$

For a rigid spacecraft with GMWs, \mathbf{J} represents the inertia of the entire spacecraft.

It is also useful to define the system momentum and system velocity vectors as

$$\bar{\mathbf{p}}_{gmw} = \begin{bmatrix} \mathbf{h} \\ \mathbf{p} \\ \mathbf{h}_{ga} \\ \mathbf{h}_{swa} \end{bmatrix} \quad (73)$$

and

$$\bar{\mathbf{v}}_{gmw} = \begin{bmatrix} \boldsymbol{\omega} \\ \mathbf{v} \\ \dot{\boldsymbol{\delta}} \\ \boldsymbol{\omega}_{swr} \end{bmatrix} \quad (74)$$

respectively, resulting in the concise equation

$$\bar{\mathbf{p}}_{gmw} = \Phi_{gmw} \bar{\mathbf{v}}_{gmw} \quad (75)$$

In integrating Equations (63) through (68), it is necessary to solve the linear system, Equation (75), at each time step since the velocities $\bar{\mathbf{v}}_{gmw}$ appear in the right hand sides of the differential equations. Note that $\dot{\boldsymbol{\delta}}$ is available from the solution for system velocities.

The rigid spacecraft with gimbaled momentum wheels is a generalization of both the rigid spacecraft with momentum wheels, and with control moment gyros. In the next sections, we develop the equations of motion for these two special cases.

3.2.7 Momentum Wheel Equation Summary. We now consider the specific case in which the gimbal angles are constant (and can be set to zero without loss of generality). Gimbaled momentum wheels with fixed axes in the body are momentum wheels.

From Equation (67) with $\dot{\boldsymbol{\delta}} = \mathbf{0}$ we have the condition

$$\mathbf{h}_{ga} = \mathbf{I}_g \mathbf{A}_g^T \boldsymbol{\omega} \quad (76)$$

which may be substituted into Equation (15) to generate the set of equations

$$\dot{\mathbf{h}} = -\boldsymbol{\omega}^\times \mathbf{h} - \mathbf{v}^\times \mathbf{p} + \mathbf{g}_e \quad (77)$$

$$\dot{\mathbf{p}} = -\boldsymbol{\omega}^\times \mathbf{p} + \mathbf{f}_e \quad (78)$$

$$\dot{\mathbf{h}}_{swa} = \mathbf{g}_w \quad (79)$$

$$\dot{\mathbf{q}} = \frac{1}{2} \mathbf{G}(\mathbf{q}) \boldsymbol{\omega} \quad (80)$$

The relationship between momenta and velocities is

$$\begin{bmatrix} \mathbf{h} \\ \mathbf{p} \\ \mathbf{h}_{swa} \end{bmatrix} = \begin{bmatrix} \mathbf{J} & \mathbf{c}^\times & \mathbf{A}_s \mathbf{I}_{sw} \\ -\mathbf{c}^\times & m\mathbf{1} & \mathbf{0}^{(3 \times N)} \\ \mathbf{I}_{sw} \mathbf{A}_s^T & \mathbf{0}^{(N \times 3)} & \mathbf{I}_{sw} \end{bmatrix} \begin{bmatrix} \boldsymbol{\omega} \\ \mathbf{v} \\ \boldsymbol{\omega}_{swr} \end{bmatrix} \quad (81)$$

where

$$\begin{aligned} \mathbf{A}_s &= \mathbf{A}_{s0} \\ \mathbf{A}_t &= \mathbf{A}_{t0} \end{aligned} \quad (82)$$

These equations should be compared with the results of Section 3.5 in Hughes [23] for the single-rotor gyrostatt.

3.2.8 Control Moment Gyro Equation Summary. Consider also the case where the rotors spin at constant speeds relative to the body. Gimbaled momentum wheels with fixed spin speeds relative to the body are control moment gyros. In this case

$$\mathbf{h}_{swa} = \mathbf{I}_{sw} \mathbf{A}_s^T \boldsymbol{\omega} + \mathbf{h}_{swr} \quad (83)$$

where \mathbf{h}_{swr} is a constant and can be computed from

$$\mathbf{h}_{swr} = \mathbf{I}_{sw} \boldsymbol{\omega}_{swr} \quad (84)$$

The appropriate substitutions lead to the set of equations

$$\dot{\mathbf{h}} = -\boldsymbol{\omega}^\times \mathbf{h} - \mathbf{v}^\times \mathbf{p} + \mathbf{g}_e \quad (85)$$

$$\dot{\mathbf{p}} = -\boldsymbol{\omega}^\times \mathbf{p} + \mathbf{f}_e \quad (86)$$

$$\dot{\mathbf{h}}_{ga} = ((\mathbf{I}_t - \mathbf{I}_s) \mathbf{A}_s^T \boldsymbol{\omega} - \mathbf{h}_{swr}) \star (\mathbf{A}_t^T \boldsymbol{\omega}) + \mathbf{g}_g \quad (87)$$

$$\dot{\boldsymbol{\delta}} = \mathbf{I}_g^{-1} \mathbf{h}_{ga} - \mathbf{A}_g^T \boldsymbol{\omega} \quad (88)$$

$$\dot{\mathbf{q}} = \frac{1}{2} \mathbf{G}(\mathbf{q}) \boldsymbol{\omega} \quad (89)$$

and the momenta and states are related by the expression

$$\begin{bmatrix} \mathbf{h} \\ \mathbf{p} \\ \mathbf{h}_{ga} \end{bmatrix} = \begin{bmatrix} \mathbf{J} & \mathbf{c}^\times & \mathbf{A}_g \mathbf{I}_g \\ -\mathbf{c}^\times & m\mathbf{1} & \mathbf{0}^{(3 \times N)} \\ \mathbf{I}_g \mathbf{A}_g^T & \mathbf{0}^{(N \times 3)} & \mathbf{I}_g \end{bmatrix} \begin{bmatrix} \boldsymbol{\omega} \\ \mathbf{v} \\ \dot{\boldsymbol{\delta}} \end{bmatrix} + \begin{bmatrix} \mathbf{A}_s \mathbf{h}_{swr} \\ \mathbf{0}^{(3 \times 1)} \\ \mathbf{0}^{(N \times 1)} \end{bmatrix} \quad (90)$$

Equations (85) through (89) and (90) represent a new form of the equations of motion for a spacecraft with CMGs. The reader should compare them to the summation notation used by Oh and Vadali [42], wherein the rotation matrix for *each* CMG must be carried during the integration.

3.3 System Energy

The kinetic energy of a body containing GMWs consists of contributions from the rigid body itself, plus the kinetic energy of the N GMWs. For the rigid body, B , the kinetic energy is by definition

$$T_B = \frac{1}{2} \int_B (\vec{\mathbf{v}} + \vec{\boldsymbol{\omega}} \times \vec{\mathbf{r}}) \cdot (\vec{\mathbf{v}} + \vec{\boldsymbol{\omega}} \times \vec{\mathbf{r}}) dm \quad (91)$$

where $\vec{\mathbf{v}}$ is the velocity of an arbitrary reference point in the body with respect to inertial space and $\vec{\mathbf{r}}$ is the location of the differential mass element dm with respect to the same point. Expansion results in

$$T_B = \frac{1}{2} \vec{\mathbf{v}} \cdot \vec{\mathbf{v}} \int_B dm + \vec{\mathbf{v}} \cdot \vec{\boldsymbol{\omega}} \times \int_B \vec{\mathbf{r}} dm + \frac{1}{2} \vec{\boldsymbol{\omega}} \cdot \int_B -\vec{\mathbf{r}} \times (\vec{\mathbf{r}} \times \vec{\boldsymbol{\omega}}) dm$$

Using the familiar definitions of total mass m_B , first mass moment of inertia \vec{c}_B , and second mass moment of inertia \vec{I}_B , we put the kinetic energy of the rigid body in its familiar form

$$T_B = \frac{1}{2} m_B \vec{v} \cdot \vec{v} + \frac{1}{2} \vec{\omega} \cdot \vec{I}_B \cdot \vec{\omega} + \vec{v} \cdot \vec{\omega} \times \vec{c}_B \quad (92)$$

Note that if the reference point is inertially fixed so that $\vec{v} = \vec{0}$, or if the reference point is the mass center of the body so that $\vec{c}_B = \vec{0}$, then the last term disappears. We wish to keep the development general enough to allow a reference point not meeting either of these two conditions.

We now develop the kinetic energy for a single GMW. The total kinetic energy of the system may then be formed by summing the energy of the body and all GMWs. For each GMW, the kinetic energy is defined as

$$T_{\text{gmw}} = \frac{1}{2} \int_{\text{gmw}} (\vec{v} + \vec{\omega} \times \vec{r}) \cdot (\vec{v} + \vec{\omega} \times \vec{r}) dm$$

where to be consistent, we choose the reference point to be identical to the point used for the body. In order to simplify the derivation, we separate the kinetic energy of the GMW into that due to the gimbal frame, T_g , and that due to the wheel, T_w , so that $T_{\text{gmw}} = T_g + T_w$. We compute the contributions separately.

We assume that the center of mass of the GMW does not vary with gimbal angle. We further assume that the centers of mass of the wheel and gimbal frame coincide with that of the total GMW and are fixed. We denote the vector from the reference to the center of mass of the GMW as \vec{r}_G , and the vector from \vec{r}_G to \vec{r} as $\vec{\rho}$, so that

$$\vec{r} = \vec{r}_G + \vec{\rho} \quad (93)$$

For the wheel the kinetic energy is given by

$$T_w = \frac{1}{2} \int_w (\vec{v}_G + \vec{\omega}_{wa} \times \vec{\rho}) \cdot (\vec{v}_G + \vec{\omega}_{wa} \times \vec{\rho}) dm \quad (94)$$

where \vec{v}_G is the velocity of the GMW center of mass, that is $\vec{v}_G = \vec{v} + \vec{\omega} \times \vec{r}_G$. Substitution into the wheel kinetic energy expression gives

$$\begin{aligned} T_w = & \frac{1}{2} \int_w (\vec{v} \cdot \vec{v}) dm + \int_w (\vec{v} \cdot \vec{\omega} \times \vec{r}_G) dm + \int_w (\vec{v} \cdot \vec{\omega}_{wa} \times \vec{\rho}) dm \\ & + \int_w (\vec{\omega} \times \vec{r}_G) \cdot (\vec{\omega}_{wa} \times \vec{\rho}) dm + \frac{1}{2} \int_w (\vec{\omega} \times \vec{r}_G) \cdot (\vec{\omega} \times \vec{r}_G) dm \\ & + \frac{1}{2} \int_w (\vec{\omega}_{wa} \times \vec{\rho}) \cdot (\vec{\omega}_{wa} \times \vec{\rho}) dm \end{aligned}$$

Since $\int_w \vec{\rho} dm = \vec{0}$, the third and fourth terms in the above sum are identically zero.

We rewrite the above as

$$T_w = \frac{1}{2} m_w (\vec{v} \cdot \vec{v}) + \vec{v} \cdot (\vec{\omega} \times \vec{c}_w) + \frac{1}{2} \vec{\omega} \cdot \vec{I}_{w_{mass}} \cdot \vec{\omega} + \frac{1}{2} \vec{\omega}_{wa} \cdot \vec{I}_w \cdot \vec{\omega}_{wa} \quad (95)$$

where $\vec{I}_{w_{mass}}$ is the inertia dyadic of the wheel mass about the body reference point. It is the parallel axis contribution of the wheel. The term \vec{I}_w is the inertia dyadic of the wheel about its own center of mass.

A similar analysis on the gimbal frame leads to the gimbal frame kinetic energy

$$T_g = \frac{1}{2} m_g (\vec{v} \cdot \vec{v}) + \vec{v} \cdot (\vec{\omega} \times \vec{c}_g) + \frac{1}{2} \vec{\omega} \cdot \vec{I}_{g_{mass}} \cdot \vec{\omega} + \frac{1}{2} \vec{\omega}_{ga} \cdot \vec{I}_g \cdot \vec{\omega}_{ga} \quad (96)$$

The combined energy of the body in which is imbedded a single GMW is therefore

$$T = \frac{1}{2} m (\vec{v} \cdot \vec{v}) + \vec{v} \cdot (\vec{\omega} \times \vec{c}) + \frac{1}{2} \vec{\omega} \cdot \vec{I} \cdot \vec{\omega} + \frac{1}{2} \vec{\omega}_{ga} \cdot \vec{I}_g \cdot \vec{\omega}_{ga} + \frac{1}{2} \vec{\omega}_{wa} \cdot \vec{I}_w \cdot \vec{\omega}_{wa} \quad (97)$$

where $m = m_B + m_w + m_g$ and $\vec{c} = \vec{c}_B + \vec{c}_w + \vec{c}_g$. The inertia dyadic \vec{I} includes the parallel axis terms for the mass of the GMW as in Equation (2).

We now note that the absolute gimbal angular velocity is given by

$$\vec{\omega}_{ga} = \delta \vec{a}_g + \vec{\omega} \quad (98)$$

and that the wheel angular velocity given by

$$\vec{\omega}_{wa} = \omega_{swr} \vec{a}_s + \dot{\delta} \vec{a}_g + \vec{\omega} \quad (99)$$

We also substitute for the gimbal inertias and wheel inertias which are given by

$$\vec{I}_g = I_{sg} \vec{a}_s \vec{a}_s + I_{tg} \vec{a}_t \vec{a}_t + I_{gg} \vec{a}_g \vec{a}_g \quad (100)$$

and

$$\vec{I}_w = I_{tw} \vec{I} + (I_{sw} - I_{tw}) \vec{a}_s \vec{a}_s \quad (101)$$

After substitution of the above into Equation (97), we attain the energy in terms of the current reference axes as

$$\begin{aligned} T = & \frac{1}{2} m (\vec{v} \cdot \vec{v}) + \vec{v} \cdot (\vec{\omega} \times \vec{c}) + \frac{1}{2} \vec{\omega} \cdot \vec{I} \cdot \vec{\omega} \\ & + I_g \dot{\delta} \vec{a}_g \cdot \vec{\omega} + I_{sw} \omega_{swr} \vec{a}_s \cdot \vec{\omega} + \frac{1}{2} (I_g \dot{\delta}^2) + \frac{1}{2} (I_{sw} \omega_{swr}^2) + \frac{1}{2} \vec{\omega} \cdot \vec{I}_{gmw} \cdot \vec{\omega} \end{aligned} \quad (102)$$

where

$$\vec{I}_{gmw} = I_s \vec{a}_s \vec{a}_s + I_t \vec{a}_t \vec{a}_t + I_g \vec{a}_g \vec{a}_g \quad (103)$$

If we now include N GMWs, and choose a body-fixed coordinate frame, then the kinetic energy may be written in matrix notation as

$$\begin{aligned} T = & \frac{1}{2} m \mathbf{v}^T \mathbf{v} + \mathbf{v}^T \boldsymbol{\omega} \times \mathbf{c} + \frac{1}{2} \boldsymbol{\omega}^T \mathbf{I} \boldsymbol{\omega} + \frac{1}{2} \boldsymbol{\omega}^T (\mathbf{A}_s \mathbf{I}_s \mathbf{A}_s^T + \mathbf{A}_g \mathbf{I}_g \mathbf{A}_g^T + \mathbf{A}_t \mathbf{I}_t \mathbf{A}_t^T) \boldsymbol{\omega} \\ & + \dot{\delta}^T \mathbf{I}_g \mathbf{A}_g^T \boldsymbol{\omega} + \omega_{swr}^T \mathbf{I}_{sw} \mathbf{A}_s^T \boldsymbol{\omega} + \frac{1}{2} \dot{\delta}^T \mathbf{I}_g \dot{\delta} + \frac{1}{2} \omega_{swr}^T \mathbf{I}_{sw} \omega_{swr} \end{aligned} \quad (104)$$

Using the notation of Equations (71) to (74), the kinetic energy for the body/GMW system can be written in the concise form

$$T = \frac{1}{2} \bar{\mathbf{v}}_{gmw}^T \boldsymbol{\Phi}_{gmw} \bar{\mathbf{v}}_{gmw} \quad (105)$$

Since energy is in general being added to the system by external forces and moments, along with wheel and gimbal torques, we do not expect the energy of the system to remain constant. In fact, the rate of change of system energy must equal the rate of work done, which is given by

$$\dot{T} = \mathbf{f}_e^T \mathbf{v} + \mathbf{g}_e^T \boldsymbol{\omega} + \mathbf{g}_g^T \dot{\boldsymbol{\delta}} + \mathbf{g}_w^T \boldsymbol{\omega}_{swr} \quad (106)$$

This expression will prove useful in monitoring the numerical results when the control inputs are given. Note that Equation (106) can be integrated for the system energy, while system energy can also be computed from the system states. Defining

$$\bar{\mathbf{g}}_{gmw} = \begin{bmatrix} \mathbf{g}_e \\ \mathbf{f}_e \\ \mathbf{g}_g \\ \mathbf{g}_w \end{bmatrix} \quad (107)$$

then note that the system energy changes as

$$\dot{T} = \bar{\mathbf{g}}_{gmw}^T \bar{\mathbf{v}}_{gmw} \quad (108)$$

providing a concise vectorial form for the time rate of change of system energy.

3.4 Summary

This chapter provides the dynamical and kinematical relations for the rigid body system with a gimballed momentum wheel cluster, and the specialization of the equations to the momentum wheel cluster and the control moment gyro cluster. Later, we use these equations to develop laws to effect reorientation maneuvers.

Unfortunately, the truly rigid spacecraft does not exist. In fact, many spacecraft possess flexible members which must be considered during an attitude maneuver. In the next chapter, we develop a three-dimensional model to be used in the analysis of candidate control laws for flexible spacecraft.

4. Euler-Bernoulli Appendages

Using Hamilton's Principle, we develop the equations of motion for a rigid body to which is attached a number of flexible Euler-Bernoulli appendages. We first develop a model making no assumptions regarding the number of flexible modes, nor do we discretize the modes as in the methods outlined in the subsequent sections. The differential equations resulting from the derivation are considered *hybrid* equations due to the mix of non-spatial and spatial variables. The result is a mix of partial and ordinary differential equations. We then use the method of assumed modes to reduce the system to one with a finite number of degrees of freedom for purposes of computer simulation.

4.1 Equations of Motion via the Lagrangian

In this section, we present a set of equations which will be used to develop a mathematical model for the flexible spacecraft studied here. These equations are developed and presented in more detail by Junkins and Kim [25].

We begin by defining the Lagrangian L of a physical system as the difference between the system kinetic energy T and potential energy V , that is

$$L = T - V \tag{109}$$

The kinetic and potential energies are functions of the generalized coordinates q_i , ($i = 1, 2, \dots, N$) and the generalized velocities \dot{q}_i , ($i = 1, 2, \dots, N$). With the Lagrangian defined in this manner, an application of Hamilton's principle results in N equations (one equation for each coordinate) given by

$$\frac{d}{dt} \left(\frac{\partial L}{\partial \dot{q}_i} \right) - \frac{\partial L}{\partial q_i} = Q_i, \quad i = 1, 2, \dots, N \tag{110}$$

where Q_i denotes the generalized force corresponding to the i -th coordinate [36].

The extension of Hamilton's principle to include flexible members of the body was generalized by Junkins and Kim [25]. A particularly useful set of equations is developed when only one independent spatial variable, say x , is allowed for a particular beamlike

section, but which might admit a vector, \mathbf{w} , of generalized coordinates describing elastic motions relative to an undeformed body-fixed spatial position. The vector might, for example, include the elongation, u , and vertical displacement, v , of the beam, so that $\mathbf{w} = [u \ v]^T$.

The Lagrangian is divided into three terms such that

$$L = L_D + \int_{\Omega} \hat{L} d\Omega + L_B \quad (111)$$

where Ω is the spatial domain occupied by the undeformed flexible body. The discrete part of the Lagrangian (the rigid body terms) is L_D and is a function of \mathbf{q} and $\dot{\mathbf{q}}$, where we introduce the notation \mathbf{q} to represent the column vector $[q_1 \ q_2 \ \dots \ q_n]^T$. The term \hat{L} represents the Lagrangian density for that part of the Lagrangian distributed along a flexible member. If the variation in the Lagrangian is a one-dimensional function of x , then \hat{L} is a function of $\mathbf{w}(x)$, $\dot{\mathbf{w}}(x)$, $\mathbf{w}'(x)$, $\mathbf{w}''(x)$, \mathbf{q} , and $\dot{\mathbf{q}}$. The spatial domain Ω becomes $\Omega = \{x : 0 \leq x \leq l\}$. Overdots represent time differentiation and the primes designate spatial differentiation with respect to x . The last term, L_B , denotes the boundary terms portion of the Lagrangian and is a function of $\mathbf{w}(l)$, $\dot{\mathbf{w}}(l)$, $\mathbf{w}'(l)$, $\dot{\mathbf{w}}'(l)$, \mathbf{q} , and $\dot{\mathbf{q}}$ where $x = l$ at the boundary.

The hybrid coordinate differential equations and boundary condition equations are then given by

$$\frac{d}{dt} \left(\frac{\partial L}{\partial \dot{\mathbf{q}}} \right) - \frac{\partial L}{\partial \mathbf{q}} = \mathbf{Q} \quad (112)$$

$$\frac{d}{dt} \left(\frac{\partial \hat{L}}{\partial \dot{\mathbf{w}}} \right) - \frac{\partial \hat{L}}{\partial \mathbf{w}} + \frac{\partial}{\partial x} \left(\frac{\partial \hat{L}}{\partial \mathbf{w}'} \right) - \frac{\partial^2}{\partial x^2} \left(\frac{\partial \hat{L}}{\partial \mathbf{w}''} \right) = \hat{\mathbf{f}} \quad (113)$$

$$\left\{ \frac{\partial \hat{L}}{\partial \mathbf{w}'} - \frac{\partial}{\partial x} \left(\frac{\partial \hat{L}}{\partial \mathbf{w}''} \right) \right\}^T \delta \mathbf{w} \Big|_0^l + \left\{ \frac{\partial L_B}{\partial \mathbf{w}(l)} - \frac{d}{dt} \left(\frac{\partial L_B}{\partial \dot{\mathbf{w}}(l)} \right) \right\}^T \delta \mathbf{w}(l) + \mathbf{f}_1^T \delta \mathbf{w}(l) = 0 \quad (114)$$

$$\left\{ \frac{\partial \hat{L}}{\partial \mathbf{w}''} \right\}^T \delta \mathbf{w}' \Big|_0^l + \left\{ \frac{\partial L_B}{\partial \mathbf{w}'(l)} - \frac{d}{dt} \left(\frac{\partial L_B}{\partial \dot{\mathbf{w}}'(l)} \right) \right\}^T \delta \mathbf{w}'(l) + \mathbf{f}_2^T \delta \mathbf{w}'(l) = 0 \quad (115)$$

We have adopted a convention wherein $(\partial L / \partial \mathbf{q})$ is a column matrix. The generalized forces corresponding to the discrete coordinates \mathbf{q} are \mathbf{Q} . The generalized force density

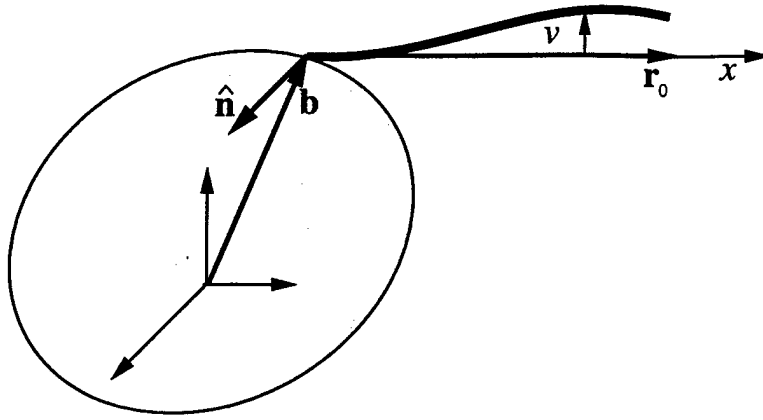


Figure 3 A Spacecraft with an Euler-Bernoulli Appendage

distributed along the spatial variable x is $\hat{\mathbf{f}}$, while \mathbf{f}_1 and \mathbf{f}_2 are the generalized forces associated with a virtual displacement and rotation (respectively) at the end of the appendage.

4.2 System Energy

We now develop the energy of a system to which we shall apply Hamilton's Principle. A diagram of a spacecraft with an Euler-Bernoulli beam is in Figure 3. The system consists of the main rigid body (which will ultimately contain a cluster of momentum exchange devices) and a flexible beam appendage. The beam is allowed to flex only in the plane which has normal component $\hat{\mathbf{n}}$. The attach point of the beam to the rigid body is described by body coordinates \mathbf{b} from the origin to the attach point. The vector along which the appendage is undeformed is given by \mathbf{r}_0 . We make a special but realistic assumption that $\hat{\mathbf{n}}^T \mathbf{r}_0 = 0$. For convenience, we define an axis, the x -axis, to have origin at the attach point and direction along \mathbf{r}_0 . The length of the beam is l .

The kinetic energy of the rigid body hub is given by

$$T_B = \frac{1}{2} m_B \mathbf{v}^T \mathbf{v} + \frac{1}{2} \boldsymbol{\omega}^T \mathbf{I}_B \boldsymbol{\omega} + \mathbf{v}^T \boldsymbol{\omega} \times \mathbf{c}_B \quad (116)$$

and we assume that the rigid body is not capable of storing potential energy.

A state of zero potential energy exists when the beam is in the undeformed state. We denote the deflection of the beam by $v(x, t)$. For an Euler-Bernoulli beam, the potential energy V is given solely as a function of the beam deflection:

$$V = \frac{1}{2} \int_0^l EI(v'')^2 dx \quad (117)$$

where E is the Young's modulus of the beam material and I is the moment of inertia of the beam's cross section about the centroidal axis. In general, E and I may depend on x .

We now develop the kinetic energy of the beam. We denote the position vector of a point on the beam by \mathbf{r} and assume that it is given by

$$\mathbf{r} = \mathbf{b} + \left(\frac{x}{l}\right) \mathbf{r}_0 + v \hat{\mathbf{n}} \times \left(\frac{\mathbf{r}_0}{l}\right) \quad (118)$$

Note that the translation along the x -axis due to curvature has been assumed negligible. The velocity of a point along the beam $\mathbf{v}_b(x)$ at position vector \mathbf{r} is closely approximated by

$$\mathbf{v}_b(x) = \mathbf{v} + \boldsymbol{\omega} \times \mathbf{r} + \dot{v} \hat{\mathbf{n}} \times \left(\frac{\mathbf{r}_0}{l}\right) \quad (119)$$

where \mathbf{v} and $\boldsymbol{\omega}$ are the linear and angular velocities of frame \mathcal{F}_b with respect to frame \mathcal{F}_i and we again neglect motion of the beam along the x -axis.

The kinetic energy of the beam is therefore

$$T_{beam} = \frac{1}{2} \int_0^l \left(\mathbf{v} + \boldsymbol{\omega} \times \mathbf{r} + \frac{\dot{v}}{l} \hat{\mathbf{n}} \times \mathbf{r}_0 \right)^T \left(\mathbf{v} + \boldsymbol{\omega} \times \mathbf{r} + \frac{\dot{v}}{l} \hat{\mathbf{n}} \times \mathbf{r}_0 \right) dm \quad (120)$$

where dm is the differential mass element along the beam. This expands to

$$\begin{aligned} T_{beam} &= \frac{1}{2} m_{beam} \mathbf{v}^T \mathbf{v} + \frac{1}{2} \int_0^l (\boldsymbol{\omega} \times \mathbf{r})^T (\boldsymbol{\omega} \times \mathbf{r}) dm + \frac{1}{2} \int_0^l \dot{v}(x)^2 dm \\ &\quad + \int_0^l \mathbf{v}^T \boldsymbol{\omega} \times \mathbf{r} dm + \int_0^l \frac{\dot{v}(x)}{l} \mathbf{v}^T \mathbf{r}_0 dm - \int_0^l \frac{\dot{v}(x)}{l} \mathbf{r}_0^T \hat{\mathbf{n}} \boldsymbol{\omega} \times \mathbf{r} dm \end{aligned} \quad (121)$$

in which the dependence of \dot{v} on x is reemphasized. Since

$$\frac{1}{2} \int_0^l \left(\boldsymbol{\omega}^\times \left(\mathbf{b} + \left(\frac{x}{l} \right) \mathbf{r}_0 \right) \right)^\top \left(\boldsymbol{\omega}^\times \left(\mathbf{b} + \left(\frac{x}{l} \right) \mathbf{r}_0 \right) \right) dm = \frac{1}{2} \boldsymbol{\omega}^\top \mathbf{I}_{b0} \boldsymbol{\omega} \quad (122)$$

where \mathbf{I}_{b0} is the inertia of the undeformed beam about the origin, then

$$\begin{aligned} \frac{1}{2} \int_0^l (\boldsymbol{\omega}^\times \mathbf{r})^\top (\boldsymbol{\omega}^\times \mathbf{r}) dm = \\ \frac{1}{2} \boldsymbol{\omega}^\top \mathbf{I}_{b0} \boldsymbol{\omega} + \mathbf{r}_0^\top \hat{\mathbf{n}}^\times \boldsymbol{\omega}^\times \boldsymbol{\omega}^\times \left\{ \mathbf{b} \int_0^l \frac{v}{l} dm + \mathbf{r}_0 \int_0^l \frac{vx}{l^2} dm + \hat{\mathbf{n}}^\times \mathbf{r}_0 \int_0^l \frac{v^2}{2l^2} dm \right\} \end{aligned} \quad (123)$$

which is a useful expansion of the second term in Equation (121).

In a similar manner, denoting the first moment of inertia of the undeformed beam about the origin as \mathbf{c}_{b0} , the third integral in Equation (121) may be written as

$$\int_0^l \mathbf{v}^\top \boldsymbol{\omega}^\times \mathbf{r} dm = m_{beam} \mathbf{v}^\top \boldsymbol{\omega}^\times \mathbf{c}_{b0} + \mathbf{v}^\top \boldsymbol{\omega}^\times \hat{\mathbf{n}}^\times \mathbf{r}_0 \int_0^l \frac{v}{l} dm \quad (124)$$

Finally, the last integral in Equation (121) may be written as

$$- \int_0^l \frac{\dot{v}(x)}{l} \mathbf{r}_0^\top \hat{\mathbf{n}}^\times \boldsymbol{\omega}^\times \mathbf{r} dm = - \mathbf{r}_0^\top \hat{\mathbf{n}}^\times \boldsymbol{\omega}^\times \left\{ \mathbf{b} \int_0^l \frac{\dot{v}}{l} dm + \mathbf{r}_0 \int_0^l \frac{x \dot{v}}{l^2} dm \right\} \quad (125)$$

where some simplification results from $\mathbf{r}_0^\top \hat{\mathbf{n}}^\times \boldsymbol{\omega}^\times \hat{\mathbf{n}}^\times \mathbf{r}_0 = 0$ (since $\mathbf{r}_0^\top \hat{\mathbf{n}} = 0$).

Therefore the kinetic energy of a single Euler-Bernoulli beam is

$$T_{beam} = \frac{1}{2} m_{beam} \mathbf{v}^\top \mathbf{v} + \frac{1}{2} \boldsymbol{\omega}^\top \mathbf{I}_{b0} \boldsymbol{\omega} + \mathbf{v}^\top \boldsymbol{\omega}^\times \mathbf{c}_{b0} + T_{flex} \quad (126)$$

The flexure term, T_{flex} , is zero when $v(x) = 0$ and $\dot{v}(x) = 0$, and is given by

$$\begin{aligned} T_{flex} = \rho \left\{ a_1 \int_0^l \frac{v}{l} dx + a_2 \int_0^l \frac{vx}{l^2} dx + a_3 \int_0^l \frac{v^2}{l^2} dx \right. \\ \left. + a_4 \int_0^l \frac{\dot{v}}{l} dx + a_5 \int_0^l \frac{\dot{v}x}{l^2} dx + \frac{1}{2} \int_0^l \dot{v}^2 dx \right\} \end{aligned} \quad (127)$$

where ρ is the mass per unit length of the beam. That is

$$dm = \rho dx \quad (128)$$

The coefficients in the terms of Equation (127) are given by

$$a_1 = \mathbf{r}_0^T \hat{\mathbf{n}}^\times \boldsymbol{\omega}^\times \boldsymbol{\omega}^\times \mathbf{b} + \mathbf{v}^T \boldsymbol{\omega}^\times \hat{\mathbf{n}}^\times \mathbf{r}_0 \quad (129)$$

$$a_2 = \mathbf{r}_0^T \hat{\mathbf{n}}^\times \boldsymbol{\omega}^\times \boldsymbol{\omega}^\times \mathbf{r}_0 \quad (130)$$

$$a_3 = (1/2) \mathbf{r}_0^T \hat{\mathbf{n}}^\times \boldsymbol{\omega}^\times \boldsymbol{\omega}^\times \hat{\mathbf{n}}^\times \mathbf{r}_0 \quad (131)$$

$$a_4 = \mathbf{v}^T \hat{\mathbf{n}}^\times \mathbf{r}_0 - \mathbf{r}_0^T \hat{\mathbf{n}}^\times \boldsymbol{\omega}^\times \mathbf{b} \quad (132)$$

$$a_5 = -\mathbf{r}_0^T \hat{\mathbf{n}}^\times \boldsymbol{\omega}^\times \mathbf{r}_0 \quad (133)$$

The above coefficients are all at most quadratic in the velocities. Since application of Hamilton's principle requires derivatives with respect to these velocities, we rewrite the above coefficients as

$$a_1 = \boldsymbol{\omega}^T \mathbf{r}_0^\times \hat{\mathbf{n}} \mathbf{b}^T \boldsymbol{\omega} - \boldsymbol{\omega}^T \boldsymbol{\omega} \mathbf{r}_0^T \hat{\mathbf{n}}^\times \mathbf{b} + \boldsymbol{\omega}^T (\mathbf{r}_0 \hat{\mathbf{n}}^T - \hat{\mathbf{n}} \mathbf{r}_0^T) \mathbf{v} \quad (134)$$

$$a_2 = \boldsymbol{\omega}^T \mathbf{r}_0^\times \hat{\mathbf{n}} \mathbf{r}_0^T \boldsymbol{\omega} \quad (135)$$

$$a_3 = (1/2) \boldsymbol{\omega}^T (\mathbf{r}_0 \mathbf{r}_0^T + \hat{\mathbf{n}} \mathbf{r}_0^T \mathbf{r}_0 \hat{\mathbf{n}}^T) \boldsymbol{\omega} \quad (136)$$

$$a_4 = \mathbf{v}^T \hat{\mathbf{n}}^\times \mathbf{r}_0 + \boldsymbol{\omega}^T \mathbf{b}^\times \hat{\mathbf{n}}^\times \mathbf{r}_0 \quad (137)$$

$$a_5 = \boldsymbol{\omega}^T \hat{\mathbf{n}} \mathbf{r}_0^T \mathbf{r}_0 \quad (138)$$

The total Lagrangian for the system is therefore

$$\begin{aligned} L = & \frac{1}{2} m_{sys} \mathbf{v}^T \mathbf{v} + \frac{1}{2} \boldsymbol{\omega}^T \mathbf{I}_{sys} \boldsymbol{\omega} - \mathbf{v}^T \mathbf{c}_{sys}^\times \boldsymbol{\omega} \\ & + \int_0^l \rho \left\{ a_1(\boldsymbol{\omega}, \mathbf{v}) \frac{v}{l} + a_2(\boldsymbol{\omega}) \frac{vx}{l^2} + a_3(\boldsymbol{\omega}) \frac{v^2}{l^2} + a_4(\boldsymbol{\omega}, \mathbf{v}) \frac{\dot{v}}{l} + a_5(\boldsymbol{\omega}) \frac{\dot{v}x}{l^2} + \frac{1}{2} \dot{v}^2 \right\} dx \\ & - \frac{1}{2} \int_0^l EI (v'')^2 dx \end{aligned} \quad (139)$$

Recalling Equation (111), we separate the Lagrangian into the terms

$$L_D = \frac{1}{2}m_{sys}\mathbf{v}^T\mathbf{v} + \frac{1}{2}\boldsymbol{\omega}^T\mathbf{I}_{sys}\boldsymbol{\omega} - \mathbf{v}^T\mathbf{c}_{sys}^\times\boldsymbol{\omega} \quad (140)$$

and

$$\hat{L} = \rho \left\{ a_1 \frac{v}{l} + a_2 \frac{vx}{l^2} + a_3 \frac{v^2}{l^2} + a_4 \frac{\dot{v}}{l} + a_5 \frac{\dot{v}x}{l^2} + \frac{1}{2}\dot{v}^2 \right\} - \frac{1}{2}EIv''^2 \quad (141)$$

Since there is no kinetic or potential energy contributed as a result of the deflection at the tip of the beam,

$$L_B = 0 \quad (142)$$

We now apply Equations (112) through (115) to generate the hybrid equations of motion for the system. Equation (112) must be replaced with its quasicordinate form, since in this case, the angular velocity $\boldsymbol{\omega}$ and the velocity of the origin \mathbf{v} are quasicordinates [36, 44]. Lagrange's equations for the discrete quasicordinates (when the Lagrangian is independent of spatial orientation and position) become [35]

$$\frac{d}{dt} \left(\frac{\partial L}{\partial \mathbf{v}} \right) + \boldsymbol{\omega}^\times \left(\frac{\partial L}{\partial \mathbf{v}} \right) = \mathbf{f}_e \quad (143)$$

$$\frac{d}{dt} \left(\frac{\partial L}{\partial \boldsymbol{\omega}} \right) + \boldsymbol{\omega}^\times \left(\frac{\partial L}{\partial \boldsymbol{\omega}} \right) + \mathbf{v}^\times \left(\frac{\partial L}{\partial \boldsymbol{\omega}} \right) = \mathbf{g}_e \quad (144)$$

It is worth comparing Equations (143) and (144) to Equations (381) and (382).

Introducing the notation

$$a_{i,\boldsymbol{\omega}} \equiv \frac{\partial a_i}{\partial \boldsymbol{\omega}} \quad (145)$$

$$a_{i,\mathbf{v}} \equiv \frac{\partial a_i}{\partial \mathbf{v}} \quad (146)$$

then

$$a_{1,\boldsymbol{\omega}} = (\mathbf{r}_0^\times \hat{\mathbf{n}}\mathbf{b}^T - \mathbf{b}\hat{\mathbf{n}}^T \mathbf{r}_0^\times)\boldsymbol{\omega} - 2\boldsymbol{\omega}\mathbf{r}_0^T \hat{\mathbf{n}}^\times \mathbf{b} + (\mathbf{r}_0\hat{\mathbf{n}}^T - \hat{\mathbf{n}}\mathbf{r}_0^T)\mathbf{v} \quad (147)$$

$$a_{2,\boldsymbol{\omega}} = (\mathbf{r}_0^\times \hat{\mathbf{n}}\mathbf{r}_0^T - \mathbf{r}_0\hat{\mathbf{n}}^T \mathbf{r}_0^\times)\boldsymbol{\omega} \quad (148)$$

$$a_{3,\boldsymbol{\omega}} = \mathbf{r}_0\mathbf{r}_0^T\boldsymbol{\omega} + \hat{\mathbf{n}}\mathbf{r}_0^T \mathbf{r}_0\hat{\mathbf{n}}^T\boldsymbol{\omega} \quad (149)$$

$$a_{4,\omega} = \mathbf{b}^\times \hat{\mathbf{n}}^\times \mathbf{r}_0 \quad (150)$$

$$a_{5,\omega} = \hat{\mathbf{n}} \mathbf{r}_0^\top \mathbf{r}_0 \quad (151)$$

$$a_{1,\mathbf{v}} = (\hat{\mathbf{n}} \mathbf{r}_0^\top - \mathbf{r}_0 \hat{\mathbf{n}}^\top) \boldsymbol{\omega} \quad (152)$$

$$a_{2,\mathbf{v}} = \mathbf{0} \quad (153)$$

$$a_{3,\mathbf{v}} = \mathbf{0} \quad (154)$$

$$a_{4,\mathbf{v}} = \hat{\mathbf{n}}^\times \mathbf{r}_0 \quad (155)$$

$$a_{5,\mathbf{v}} = \mathbf{0} \quad (156)$$

Assuming \mathbf{f}_1 , \mathbf{f}_2 , and $\hat{\mathbf{f}}$ of Equations (113) through (115) are zero, the hybrid equations of motion can be summarized as

$$\begin{aligned} & \frac{d}{dt} \left(m_{sys} \mathbf{v} - \mathbf{c}_{sys}^\times \boldsymbol{\omega} + \int_0^l \rho \left\{ \frac{a_{1,\mathbf{v}} v}{l} + \frac{a_{4,\mathbf{v}} \dot{v}}{l} \right\} dx \right) \\ & + \boldsymbol{\omega}^\times \left(m_{sys} \mathbf{v} - \mathbf{c}_{sys}^\times \boldsymbol{\omega} + \int_0^l \rho \left\{ \frac{a_{1,\mathbf{v}} v}{l} + \frac{a_{4,\mathbf{v}} \dot{v}}{l} \right\} dx \right) = \mathbf{f}_e \end{aligned} \quad (157)$$

$$\begin{aligned} & \frac{d}{dt} \left(\mathbf{I}_{sys} \boldsymbol{\omega} + \mathbf{c}_{sys}^\times \mathbf{v} + \int_0^l \rho \left\{ \frac{a_{1,\omega} v}{l} + \frac{a_{2,\omega} v x}{l^2} + \frac{a_{3,\omega} v^2}{l^2} + \frac{a_{4,\omega} \dot{v}}{l} + \frac{a_{5,\omega} \dot{v} x}{l^2} \right\} dx \right) \\ & + \boldsymbol{\omega}^\times \left(\mathbf{I}_{sys} \boldsymbol{\omega} + \mathbf{c}_{sys}^\times \mathbf{v} + \int_0^l \rho \left\{ \frac{a_{1,\omega} v}{l} + \frac{a_{2,\omega} v x}{l^2} + \frac{a_{3,\omega} v^2}{l^2} + \frac{a_{4,\omega} \dot{v}}{l} + \frac{a_{5,\omega} \dot{v} x}{l^2} \right\} dx \right) \\ & + \mathbf{v}^\times \left(m_{sys} \mathbf{v} - \mathbf{c}_{sys}^\times \boldsymbol{\omega} + \int_0^l \rho \left\{ \frac{a_{1,\mathbf{v}} v}{l} + \frac{a_{4,\mathbf{v}} \dot{v}}{l} \right\} dx \right) = \mathbf{g}_e \end{aligned} \quad (158)$$

$$\frac{d}{dt} \left(\frac{\rho a_4}{l} + \frac{\rho a_5 x}{l^2} + \rho \dot{v} \right) - \left(\frac{\rho a_1}{l} + \frac{\rho a_2 x}{l^2} + \frac{2\rho a_3 v}{l^2} \right) + \frac{\partial^2}{\partial x^2} (EI v'') = 0 \quad (159)$$

Since $v(0) = 0$ and $v'(0) = 0$, then Equations (114) and (115) reduce to

$$\frac{\partial}{\partial x} (EI v''(l)) = 0 \quad (160)$$

$$EI v''(l) = 0 \quad (161)$$

The above equations reduce to those of a rigid body when $v(x) = \dot{v}(x) = 0$. Also note that when $\boldsymbol{\omega} = \mathbf{v} = \mathbf{0}$, Equation (159) reduces to the familiar equation for a cantilevered

beam

$$\frac{d}{dt}(\rho\dot{v}) + \frac{\partial^2}{\partial x^2}(EIv'') = 0 \quad (162)$$

4.3 The Assumed Modes Method

We now apply the Method of Assumed Modes to the equations of motion [13]. We assume that the continuous variable $v(x, t)$ can be expressed as

$$v(x, t) = \sum_{i=1}^{\infty} \psi_i(x)\nu_i(t) \quad (163)$$

where ν_i retains the length dimension and ψ_i is dimensionless. If we retain m mode shapes, then (163) can be expressed in matrix form as

$$v(x, t) = \boldsymbol{\psi}^T \boldsymbol{\nu} \quad (164)$$

where $\boldsymbol{\psi}$ and $\boldsymbol{\nu}$ are the m -vectors formed by keeping only m modes.

We choose for ψ_i *comparison functions* [13] which meet the geometric and natural boundary conditions

$$\psi_i(0) = \psi_i'(0) = \psi_i''(l) = \psi_i'''(l) = 0 \quad (165)$$

A complete description of the assumed modes method and a description of comparison functions is in Craig [13].

To apply this method to our equations of motion, we introduce Equation (163) into Equation (127) and integrate out the spatial variable immediately. Note the simplification which results from Equation (163) in that, defining

$$v_i(x, t) \equiv \psi_i(x)\nu_i(t) \quad (166)$$

then

$$\dot{v}_i = \psi_i(x)\dot{\nu}_i(t) \quad (167)$$

and

$$v_i'' = \psi_i''(x)\nu_i(t) \quad (168)$$

The kinetic energy due to flexure becomes

$$T_{flex} = a_1 \mathbf{m}_1^T \boldsymbol{\nu} + a_2 \mathbf{m}_2^T \boldsymbol{\nu} + a_3 \boldsymbol{\nu}^T \mathbf{M}_3 \boldsymbol{\nu} + a_4 \mathbf{m}_1^T \dot{\boldsymbol{\nu}} + a_5 \mathbf{m}_2^T \dot{\boldsymbol{\nu}} + \frac{1}{2} \dot{\boldsymbol{\nu}}^T \mathbf{M}_3 \dot{\boldsymbol{\nu}} \quad (169)$$

where $\boldsymbol{\nu} = [\nu_1 \ \nu_2 \ \dots \ \nu_n]^T$ which we shall call the modal displacement vector and we define the components

$$\mathbf{m}_1 = \frac{1}{l} \int_0^l \rho \psi(x) dx \quad (170)$$

$$\mathbf{m}_2 = \frac{1}{l^2} \int_0^l \rho x \psi(x) dx \quad (171)$$

$$\mathbf{M}_3 = \frac{1}{l^2} \int_0^l \rho \psi(x) \psi(x)^T dx \quad (172)$$

We also define the stiffness matrix \mathbf{K} whose components are calculated from

$$\mathbf{K} = \int_0^l EI \psi''(x) \psi''(x)^T dx \quad (173)$$

so that the potential energy may be expressed as

$$V_{flex} = \frac{1}{2} \boldsymbol{\nu}^T \mathbf{K} \boldsymbol{\nu} \quad (174)$$

The new assumed modes Lagrangian is therefore given by

$$\begin{aligned} L_{asm} = & \frac{1}{2} m_{sys} \mathbf{v}^T \mathbf{v} + \frac{1}{2} \boldsymbol{\omega}^T \mathbf{I}_{sys} \boldsymbol{\omega} - \mathbf{v}^T \mathbf{c}_{sys}^x \boldsymbol{\omega} + a_1 \mathbf{m}_1^T \boldsymbol{\nu} + a_2 \mathbf{m}_2^T \boldsymbol{\nu} \\ & + a_3 \boldsymbol{\nu}^T \mathbf{M}_3 \boldsymbol{\nu} + a_4 \mathbf{m}_1^T \dot{\boldsymbol{\nu}} + a_5 \mathbf{m}_2^T \dot{\boldsymbol{\nu}} + \frac{l^2}{2} \dot{\boldsymbol{\nu}}^T \mathbf{M}_3 \dot{\boldsymbol{\nu}} - \frac{1}{2} \boldsymbol{\nu}^T \mathbf{K} \boldsymbol{\nu} \end{aligned} \quad (175)$$

Application of Hamilton's Principle to this Lagrangian yields a set of $6 + m$ equations of motion (containing only discrete coordinates) where m is the number of assumed modes. Of course, the above development is for only a single appendage with m assumed modes. Each additional appendage will add m more variables to the development. Continuing

$$\frac{\partial L_{asm}}{\partial \boldsymbol{\nu}} = a_1 \mathbf{m}_1 + a_2 \mathbf{m}_2 + 2a_3 \mathbf{M}_3 \boldsymbol{\nu} - \mathbf{K} \boldsymbol{\nu} \quad (176)$$

and

$$\frac{\partial L_{asm}}{\partial \dot{\boldsymbol{\nu}}} = a_4 \mathbf{m}_1 + a_5 \mathbf{m}_2 + l^2 \mathbf{M}_3 \dot{\boldsymbol{\nu}} \quad (177)$$

Once again, using the quasicoordinate form of Lagrange's Equations for $\boldsymbol{\omega}$ and \mathbf{v} , the $6 + m$ equations of motion for the system with one flexible appendage having m assumed modes are

$$\begin{aligned} \frac{d}{dt} \left(m_{sys} \mathbf{v} - \mathbf{c}_{sys}^{\times} \boldsymbol{\omega} + a_{1,v} \mathbf{m}_1^T \boldsymbol{\nu} + a_{4,v} \mathbf{m}_1^T \dot{\boldsymbol{\nu}} \right) \\ + \boldsymbol{\omega}^{\times} \left(m_{sys} \mathbf{v} - \mathbf{c}_{sys}^{\times} \boldsymbol{\omega} + a_{1,v} \mathbf{m}_1^T \boldsymbol{\nu} + a_{4,v} \mathbf{m}_1^T \dot{\boldsymbol{\nu}} \right) = \mathbf{f}_e \end{aligned} \quad (178)$$

$$\begin{aligned} \frac{d}{dt} \left(\mathbf{I}_{sys} \boldsymbol{\omega} + \mathbf{c}_{sys}^{\times} \mathbf{v} + a_{1,\omega} \mathbf{m}_1^T \boldsymbol{\nu} + a_{2,\omega} \mathbf{m}_2^T \boldsymbol{\nu} + a_{3,\omega} \boldsymbol{\nu}^T \mathbf{M}_3 \boldsymbol{\nu} + a_{4,\omega} \mathbf{m}_1^T \dot{\boldsymbol{\nu}} + a_{5,\omega} \mathbf{m}_2^T \dot{\boldsymbol{\nu}} \right) \\ + \boldsymbol{\omega}^{\times} \left(\mathbf{I}_{sys} \boldsymbol{\omega} + \mathbf{c}_{sys}^{\times} \mathbf{v} + a_{1,\omega} \mathbf{m}_1^T \boldsymbol{\nu} + a_{2,\omega} \mathbf{m}_2^T \boldsymbol{\nu} + a_{3,\omega} \boldsymbol{\nu}^T \mathbf{M}_3 \boldsymbol{\nu} + a_{4,\omega} \mathbf{m}_1^T \dot{\boldsymbol{\nu}} + a_{5,\omega} \mathbf{m}_2^T \dot{\boldsymbol{\nu}} \right) \\ + \mathbf{v}^{\times} \left(m_{sys} \mathbf{v} - \mathbf{c}_{sys}^{\times} \boldsymbol{\omega} + a_{1,v} \mathbf{m}_1^T \boldsymbol{\nu} + a_{4,v} \mathbf{m}_1^T \dot{\boldsymbol{\nu}} \right) = \mathbf{g}_e \end{aligned} \quad (179)$$

$$\frac{d}{dt} \left(a_4 \mathbf{m}_1 + a_5 \mathbf{m}_2 + l^2 \mathbf{M}_3 \dot{\boldsymbol{\nu}} \right) - (a_1 \mathbf{m}_1 + a_2 \mathbf{m}_2 + 2a_3 \mathbf{M}_3 \boldsymbol{\nu} - \mathbf{K} \boldsymbol{\nu}) = 0 \quad (180)$$

Equations (178) and (179) may be simplified by noting that

$$\frac{\partial L}{\partial \boldsymbol{\omega}} = \mathbf{h} \quad (181)$$

$$\frac{\partial L}{\partial \mathbf{v}} = \mathbf{p} \quad (182)$$

and by defining the generalized flexure momentum as

$$\mathbf{h}_\nu \equiv \frac{\partial L}{\partial \dot{\boldsymbol{\nu}}} = a_4 \mathbf{m}_1 + a_5 \mathbf{m}_2 + l^2 \mathbf{M}_3 \dot{\boldsymbol{\nu}} \quad (183)$$

As with Equation (71) of Chapter 3, we relate the momenta and velocities in a matrix form as

$$\bar{\mathbf{p}} = \begin{bmatrix} \mathbf{h} \\ \mathbf{p} \\ \mathbf{h}_\nu \end{bmatrix} = \Phi \bar{\mathbf{v}} = \begin{bmatrix} \Phi_{11} & \Phi_{12} & \Phi_{13} \\ \Phi_{21} & \Phi_{22} & \Phi_{23} \\ \Phi_{31} & \Phi_{32} & \Phi_{33} \end{bmatrix} \begin{bmatrix} \boldsymbol{\omega} \\ \mathbf{v} \\ \boldsymbol{\mu} \end{bmatrix} \quad (184)$$

where we have introduced the modal velocity

$$\boldsymbol{\mu} = \dot{\boldsymbol{\nu}} \quad (185)$$

and the elements of the symmetric positive definite matrix Φ are

$$\begin{aligned} \Phi_{11} = & \mathbf{I}_{sys} + (\mathbf{m}_1^T \boldsymbol{\nu})(\mathbf{r}_0^\times \hat{\mathbf{n}} \mathbf{b}^T - \mathbf{b} \hat{\mathbf{n}}^T \mathbf{r}_0^\times - 2(\mathbf{r}_0^T \hat{\mathbf{n}}^\times \mathbf{b}) \mathbf{1}) \\ & + (\mathbf{m}_2^T \boldsymbol{\nu})(\mathbf{r}_0^\times \hat{\mathbf{n}} \mathbf{r}_0^T - \mathbf{r}_0 \hat{\mathbf{n}}^T \mathbf{r}_0^\times) + (\boldsymbol{\nu} \mathbf{M}_3 \boldsymbol{\nu})(\hat{\mathbf{n}}^\times \mathbf{r}_0 \mathbf{r}_0^T \hat{\mathbf{n}}^\times + (\mathbf{r}_0^T \mathbf{r}_0) \mathbf{1}) \end{aligned} \quad (186)$$

$$\Phi_{12} = \mathbf{c}_{sys}^\times + (\mathbf{r}_0 \hat{\mathbf{n}}^T - \hat{\mathbf{n}} \mathbf{r}_0^T) \mathbf{m}_1^T \boldsymbol{\nu} \quad (187)$$

$$\Phi_{13} = \mathbf{b}^\times \hat{\mathbf{n}}^\times \mathbf{r}_0 \mathbf{m}_1^T + \hat{\mathbf{n}} \mathbf{r}_0^T \mathbf{r}_0 \mathbf{m}_2^T \quad (188)$$

$$\Phi_{21} = \Phi_{12}^T \quad (189)$$

$$\Phi_{22} = m_{sys} \mathbf{1} \quad (190)$$

$$\Phi_{23} = \hat{\mathbf{n}}^\times \mathbf{r}_0 \mathbf{m}_1^T \quad (191)$$

$$\Phi_{31} = \Phi_{13}^T \quad (192)$$

$$\Phi_{32} = \Phi_{23}^T \quad (193)$$

$$\Phi_{33} = l^2 \mathbf{M}_3 \quad (194)$$

It is interesting to note that Φ_{11} represents the second moment of inertia of the system in the deformed state whereas Φ_{12} represents the cross product form of the first moment in the deformed state.

The equations of motion for the assumed modes model with a single appendage therefore reduce to the fairly simple $6 + 2m$ order system of equations

$$\dot{\mathbf{h}} = -\boldsymbol{\omega}^\times \mathbf{h} - \mathbf{v}^\times \mathbf{p} \quad (195)$$

$$\dot{\mathbf{p}} = -\boldsymbol{\omega}^\times \mathbf{p} \quad (196)$$

$$\dot{\mathbf{h}}_\nu = a_1 \mathbf{m}_1 + a_2 \mathbf{m}_2 + 2a_3 \mathbf{M}_3 \boldsymbol{\nu} - \mathbf{K} \boldsymbol{\nu} \quad (197)$$

$$\dot{\boldsymbol{\nu}} = \boldsymbol{\mu} \quad (198)$$

Equation (184) must be solved at each time step, since the system velocities are required in the right hand sides of the equations of motion.

We can extrapolate the above development to additional appendages by noting that an additional appendage will result in additional terms in Equations (169) and (174). We must therefore adjust \mathbf{I}_{sys} , \mathbf{c}_{sys} , and m_{sys} to reflect the new values. The elements of Φ must include the additional terms due to the new appendage. An additional row and column must also be added to Φ to reflect the relationships between the additional vectors $\mathbf{h}_{\nu,i}$ and μ_i . Finally, we add $2m$ more differential equations reflecting Equations (197) and (198) for each appendage.

Computing the system energy for the body with Euler-Bernoulli appendages is relatively simple at this point, since the energy was required prior to formulation of the equations of motion. It is interesting to observe, however, that the system energy may be expressed in the relatively compact notation

$$T = \frac{1}{2} \bar{\mathbf{v}}^T \Phi \bar{\mathbf{v}} \quad (199)$$

or alternatively

$$T = \frac{1}{2} \bar{\mathbf{v}}^T \bar{\mathbf{p}} \quad (200)$$

4.4 Equation Summary for a Spacecraft with GMWs and Euler-Bernoulli Appendages

We now integrate the equations of motion for a spacecraft containing N GMWs and p flexible Euler-Bernoulli appendages. Equations (65) through (67) of Chapter 3 are not affected by the presence of external Euler-Bernoulli beams. The equations of motion for each gimballed momentum wheel are unaltered.

The Lagrangian density function given by Equation (141) is also unchanged if GMWs are added to the rigid body hub. Equations (159) and (180) are still valid, therefore, for the combined system of equations. Of course, the equations of motion for total linear and angular momentum for the entire flexible spacecraft model also remain unchanged. We therefore summarize the entire set of equations for the spacecraft containing GMWs and

flexible appendages as

$$\dot{\mathbf{h}} = -\boldsymbol{\omega}^\times \mathbf{h} - \mathbf{v}^\times \mathbf{p} + \mathbf{g}_e \quad (201)$$

$$\dot{\mathbf{p}} = -\boldsymbol{\omega}^\times \mathbf{p} + \mathbf{f}_e \quad (202)$$

$$\dot{\mathbf{h}}_{swa} = \mathbf{g}_w \quad (203)$$

$$\dot{\mathbf{h}}_{ga} = ((\mathbf{I}_t - \mathbf{I}_{sg})\mathbf{A}_s^\top \boldsymbol{\omega} - \mathbf{h}_{swa}) \star (\mathbf{A}_t^\top \boldsymbol{\omega}) + \mathbf{g}_g \quad (204)$$

$$\dot{\boldsymbol{\delta}} = \mathbf{I}_g^{-1} \mathbf{h}_{ga} - \mathbf{A}_g^\top \boldsymbol{\omega} \quad (205)$$

$$\dot{\mathbf{h}}_\nu = a_1 \mathbf{m}_1 + a_2 \mathbf{m}_2 + 2a_3 \mathbf{M}_3 \boldsymbol{\nu} - \mathbf{K} \boldsymbol{\nu} \quad (206)$$

$$\dot{\boldsymbol{\nu}} = \boldsymbol{\mu} \quad (207)$$

$$\dot{\mathbf{q}} = \frac{1}{2} \mathbf{G}(\mathbf{q}) \boldsymbol{\omega} \quad (208)$$

For a spacecraft containing N gimbaled momentum wheels and p appendages for which we assume m modes each, the set of first order nonlinear matrix differential equations is of order $10 + 3N + 2mp$. Note that a spacecraft with 3 GMWs and 3 flexible appendages will yield a set of 25 differential equations if we keep only the first mode of oscillation. As with the rigid body case, it is possible to express the relationship between momenta and velocities as

$$\begin{bmatrix} \mathbf{h} \\ \mathbf{p} \\ \mathbf{h}_{ga} \\ \mathbf{h}_{swa} \\ \mathbf{h}_\nu \end{bmatrix} = \boldsymbol{\Phi}_{sys} \begin{bmatrix} \boldsymbol{\omega} \\ \mathbf{v} \\ \dot{\boldsymbol{\delta}} \\ \boldsymbol{\omega}_{swr} \\ \boldsymbol{\mu} \end{bmatrix} \quad (209)$$

The coefficient matrix $\boldsymbol{\Phi}_{sys}$ is a function of $\boldsymbol{\delta}$ and $\boldsymbol{\nu}$. Equation (209) must be solved at each time step, since the velocities are needed in Equations (201) through (208).

The spacecraft with GMWs is a generalization of the spacecraft with momentum wheels, in which case the gimbal angles are always zero. Setting $\dot{\boldsymbol{\delta}} = \mathbf{0}$ leads to a set of $10 + N + 2mp$ equations. Similarly, for the CMG case, \mathbf{h}_{swr} is constant, and the equations of motion reduce to a set of order $10 + 2N + 2mp$.

With no external torques or forces acting on the spacecraft, then attitude control is accomplished solely by choice of the spin axis torques \mathbf{g}_w and gimbal axis torques \mathbf{g}_g . In the next chapter, we will turn to the task of choosing these control inputs to reorient the spacecraft while simultaneously seeking to minimize oscillations of the appendages.

4.5 Summary

The results of this chapter provide a mathematical 3-D flexible spacecraft model without restrictions on symmetry of appendages, mode shapes, or center of mass motion. The assumed modes method allows for the infinite dimensional nature of the flexible appendages to be truncated at a desired number of mode shapes. Any number of appendages may be modeled by these equations. The equations are integrated very smoothly with those of Chapter 3. We now turn to the development of control laws which provide a desired reorientation while keeping the appendage oscillations small.

5. *Spacecraft Reorientations*

We now turn to the task of finding control laws which reorient a spacecraft using momentum exchange devices. In general, the spacecraft may already possess significant angular momentum (stored in a cluster of momentum storage devices). We assume that the spacecraft initially has no angular velocity with respect to inertial space, and our goal is to take up a new orientation with the spacecraft again at rest. The problem is therefore a rest-to-rest maneuver, with the initial and final orientations specified. With no external torques, the total angular momentum of the spacecraft/cluster system remains fixed in inertial space. At the final orientation, therefore, the cluster momentum has a unique orientation in the body coordinate frame, a property not shared by *zero-momentum* spacecraft.

We begin this chapter by showing how the rate of change of cluster momentum is essentially the control input, regardless of the type of momentum exchange device. The relationship between cluster momentum rate and torque inputs is then discussed. A closed loop Lyapunov control law capable of reorienting the spacecraft is presented, with a momentum exchange cluster as the control device and where the control input is the rate of change of cluster momentum.

Next the problem of singularities for the control moment gyro cluster is addressed. The singularity-robust inverse is examined using the insight provided by the singular value decomposition, and an improved control law which avoids torque commands in the singular direction is introduced. Some examples demonstrating the improvement are presented.

We then discuss a class of maneuvers known as *stationary platform maneuvers* [20] which have the advantage of generally keeping angular velocities low during the reorientation. A modification to the Lyapunov control law allows for reorientations which remain arbitrarily close to the stationary platform condition.

5.1 *Reorientations Using a Momentum Exchange Cluster*

We begin by writing the general equations of motion for a spacecraft containing a momentum exchange cluster in a general form. This will show that the control input to

the spacecraft is essentially the rate of change of cluster momentum. We will then examine the possibilities of using specific control devices to effect the cluster momentum change.

The total angular momentum of a spacecraft about its mass center is

$$\mathbf{h} = \mathbf{J}\boldsymbol{\omega} + \mathbf{h}_c \quad (210)$$

where \mathbf{J} is an inertia-like matrix which will be defined in a suitable manner relevant to the momentum exchange device under consideration. We leave open the possibility of \mathbf{J} being variable. The cluster momentum \mathbf{h}_c includes the spin momentum of the GMWs relative to inertial space and the angular momentum associated with the GMW gimbal rate. For a GMW cluster, for example, we add a subscript to \mathbf{J} and \mathbf{J}_{gmw} takes the form

$$\mathbf{J}_{gmw} = \mathbf{I} + \mathbf{A}_t \mathbf{I}_t \mathbf{A}_t^T + \mathbf{A}_s \mathbf{I}_{sg} \mathbf{A}_s^T \quad (211)$$

and the cluster momentum is

$$\mathbf{h}_c = \mathbf{A}_s \mathbf{h}_{swa} + \mathbf{A}_g \mathbf{h}_{ga} \quad (212)$$

Assuming no external torques, the equation of motion for the spacecraft represented by Equation (210) is

$$\dot{\boldsymbol{\omega}} = \mathbf{J}^{-1}(-\boldsymbol{\omega}^\times(\mathbf{J}\boldsymbol{\omega} + \mathbf{h}_c) - \dot{\mathbf{J}}\boldsymbol{\omega} - \dot{\mathbf{h}}_c) \quad (213)$$

where $\dot{\mathbf{J}}$ is determined by the gimbal rates. Note that $\dot{\mathbf{J}} = \mathbf{0}$ for the momentum wheel case. The reorientation profile can be controlled as desired through the input term $\mathbf{J}^{-1}\dot{\mathbf{h}}_c$. There are, however, limitations on the types of maneuvers we may perform using the input $\dot{\mathbf{h}}_c$. A rotation, for example, about an arbitrary eigenaxis is not possible. See Appendix B for a discussion.

While $\dot{\mathbf{h}}_c$ can be viewed as the control input, it is actually changed by applying internal torques to the momentum exchange devices. The nature of these torques depends on the type of device. In the general case of the GMW, we have

$$\dot{\mathbf{h}}_c = \dot{\mathbf{A}}_s \mathbf{h}_{swa} + \mathbf{A}_s \dot{\mathbf{h}}_{swa} + \mathbf{A}_g \dot{\mathbf{h}}_{ga}$$

$$= -\mathbf{A}_t \text{diag}(\dot{\delta}) \mathbf{h}_{swa} + \mathbf{A}_s \dot{\mathbf{h}}_{swa} + \mathbf{A}_g \dot{\mathbf{h}}_{ga} \quad (214)$$

We have direct control over the last two terms of Equation (214) using the torque inputs \mathbf{g}_w and \mathbf{g}_g (see Equations (65) and (66)). Note, however, that the first term is dependent on the gimbal rates, which are *states* of the system. This term can dominate for the case of large \mathbf{h}_{swa} , and is indeed the term which provides the so-called torque amplification property of the single gimbal CMG.

For the momentum wheel case, we note that the second term on the right hand side of Equation (212) may be replaced with

$$\mathbf{A}_g \mathbf{h}_{ga} = \mathbf{A}_g \mathbf{h}_{gr} + \mathbf{A}_g \mathbf{I}_g \mathbf{A}_g^T \boldsymbol{\omega} \quad (215)$$

where $\mathbf{h}_{gr} = \mathbf{0}$ since the gimbal angles are fixed. It is convenient to lump the gimbal axis inertia into \mathbf{J} and define

$$\mathbf{J}_{mw} = \mathbf{I} + \mathbf{A}_t \mathbf{I}_t \mathbf{A}_t^T + \mathbf{A}_s \mathbf{I}_{sg} \mathbf{A}_s^T + \mathbf{A}_g \mathbf{I}_g \mathbf{A}_g^T \quad (216)$$

so that

$$\dot{\mathbf{h}}_c = \mathbf{A}_s \dot{\mathbf{h}}_{swa} = \mathbf{A}_s \mathbf{0} \mathbf{g}_w \quad (217)$$

Thus, a desired $\dot{\mathbf{h}}_c$ can be achieved by selecting \mathbf{g}_w to satisfy Equation (217). When $N = 3$ and the rotors are not coplanar, the solution for \mathbf{g}_w is unique. When $N > 3$, the solution for \mathbf{g}_w is underdetermined giving the possibility of an infinite number of solutions. It is common to choose a minimum norm solution for Equation (217). For $N = 2$, the torque output is confined to a plane, and when only one momentum wheel exists ($N = 1$), the torque output is confined to a line along the spin axis.

Similarly, for the CMG, the first term on the right hand side of Equation (212) may be written as

$$\mathbf{A}_s \mathbf{h}_{swa} = \mathbf{A}_s \mathbf{h}_{swr} + \mathbf{A}_s \mathbf{I}_{sw} \mathbf{A}_s^T \boldsymbol{\omega} \quad (218)$$

where \mathbf{h}_{swr} is constant.

Therefore, by defining

$$\mathbf{J}_{cm,g} = \mathbf{I} + \mathbf{A}_t \mathbf{I}_t \mathbf{A}_t^T + \mathbf{A}_s \mathbf{I}_s \mathbf{A}_s^T + \mathbf{A}_g \mathbf{I}_g \mathbf{A}_g^T \quad (219)$$

we have

$$\begin{aligned} \dot{\mathbf{h}}_c &= -\mathbf{A}_t \text{diag}(\dot{\boldsymbol{\delta}}) \mathbf{h}_{swr} + \mathbf{A}_g \dot{\mathbf{h}}_{gr} \\ &= -\mathbf{A}_t \text{diag}(\mathbf{h}_{swr}) \dot{\boldsymbol{\delta}} + \mathbf{A}_g \mathbf{I}_g \ddot{\boldsymbol{\delta}} \end{aligned} \quad (220)$$

This demonstrates that the torque generated by a cluster of CMGs has a component about the gimbal axes (due to gimbal acceleration) and a transverse torque output due to gimbal rates. The torque input \mathbf{g}_g can be computed given the desired $\ddot{\boldsymbol{\delta}}$.

An exact solution (for \mathbf{g}_g) to provide a desired $\dot{\mathbf{h}}_c$ is possible, but not desirable. The gimbal rates, $\dot{\boldsymbol{\delta}}$, and accelerations, $\ddot{\boldsymbol{\delta}}$, are not independent. For a typical CMG cluster, the objective is to take advantage of the control torque generated by the gimbal rates (the first term of Equation (220)). Since $\dot{\boldsymbol{\delta}}$ is actually a state of the system, we typically choose $\ddot{\boldsymbol{\delta}}$ to achieve a desired $\dot{\boldsymbol{\delta}}$ which provides the $\dot{\mathbf{h}}_c$ required by some control law. Choosing gimbal accelerations to instantaneously generate the torque demanded by a control law leads to unacceptable gimbal rates (and therefore torques) from the first term of Equation (220). Note that this is a compromise, since the torque produced by the initial gimbal acceleration will almost definitely provide an undesirable (if small) output torque.

5.2 A Lyapunov Feedback Control Law

In this section, we develop the stabilizing Lyapunov control law due to Oh and Vadali, but using the variables of the current development. We define a positive definite Lyapunov function

$$V = k_0 \mathbf{e}_1^T \mathbf{e}_1 + \frac{1}{2} \mathbf{e}_2^T \mathbf{J} \mathbf{e}_2 \quad (221)$$

where \mathbf{e}_1 is the attitude error, \mathbf{e}_2 is the angular velocity error, \mathbf{J} is positive definite, and k_0 is a positive scalar constant. Explicitly

$$\mathbf{e}_1 = \mathbf{q} - \mathbf{q}_f \quad (222)$$

$$\mathbf{e}_2 = \boldsymbol{\omega} - \boldsymbol{\omega}_f \quad (223)$$

where \mathbf{q} is the 4×1 quaternion vector and $\boldsymbol{\omega}$ is the 3×1 angular velocity vector. The constant terms \mathbf{q}_f and $\boldsymbol{\omega}_f$ are the desired final values for the reorientation maneuver. Though we intend to focus on rest-to-rest maneuvers, we carry $\boldsymbol{\omega}_f$ through the development for completeness.

The derivative of the Lyapunov function is

$$\dot{V} = 2k_0(\dot{\mathbf{q}} - \dot{\mathbf{q}}_f)^T(\mathbf{q} - \mathbf{q}_f) + (\boldsymbol{\omega} - \boldsymbol{\omega}_f)^T \mathbf{J}(\dot{\boldsymbol{\omega}} - \dot{\boldsymbol{\omega}}_f) + \frac{1}{2}(\boldsymbol{\omega} - \boldsymbol{\omega}_f)^T \dot{\mathbf{J}}(\boldsymbol{\omega} - \boldsymbol{\omega}_f) \quad (224)$$

The quaternion rates can be translated to angular velocities through the relations

$$\dot{\mathbf{q}} = \frac{1}{2} \mathbf{G}(\mathbf{q}) \boldsymbol{\omega} \quad (225)$$

$$\dot{\mathbf{q}}_f = \frac{1}{2} \mathbf{G}(\mathbf{q}_f) \boldsymbol{\omega}_f \quad (226)$$

Furthermore, we make use of the fact that

$$\mathbf{G}^T(\mathbf{q})\mathbf{q} = \mathbf{G}^T(\mathbf{q}_f)\mathbf{q}_f = \mathbf{0} \quad (227)$$

whereas

$$\mathbf{G}^T(\mathbf{q}_f)\mathbf{q} = -\mathbf{G}^T(\mathbf{q})\mathbf{q}_f \quad (228)$$

The above relations allow us to express the derivative of the Lyapunov function in the form

$$\dot{V} = -(\boldsymbol{\omega} - \boldsymbol{\omega}_f)^T \left(-k_0 \mathbf{G}^T(\mathbf{q}_f)\mathbf{q} + \mathbf{J}\dot{\boldsymbol{\omega}}_f - \mathbf{J}\dot{\boldsymbol{\omega}} + \frac{1}{2}\dot{\mathbf{J}}\boldsymbol{\omega}_f - \frac{1}{2}\dot{\mathbf{J}}\boldsymbol{\omega} \right) \quad (229)$$

We see that \dot{V} can be guaranteed negative semidefinite when we ensure that

$$-k_0 \mathbf{G}^T(\mathbf{q}_f) \mathbf{q} + \mathbf{J} \dot{\boldsymbol{\omega}}_f - \mathbf{J} \dot{\boldsymbol{\omega}} - \frac{1}{2} \dot{\mathbf{J}} \boldsymbol{\omega} + \frac{1}{2} \dot{\mathbf{J}} \boldsymbol{\omega}_f = \mathbf{K}_1 (\boldsymbol{\omega} - \boldsymbol{\omega}_f) \quad (230)$$

where \mathbf{K}_1 is a positive definite gain matrix, since then

$$\dot{V} = -(\boldsymbol{\omega} - \boldsymbol{\omega}_f)^T \mathbf{K}_1 (\boldsymbol{\omega} - \boldsymbol{\omega}_f) \quad (231)$$

Substitution of Equation (213) leads to the relationship

$$\dot{\mathbf{h}}_c = \mathbf{K}_1 (\boldsymbol{\omega} - \boldsymbol{\omega}_f) + k_0 \mathbf{G}^T(\mathbf{q}_f) \mathbf{q} - \mathbf{J} \dot{\boldsymbol{\omega}}_f - \boldsymbol{\omega}^\times (\mathbf{J} \boldsymbol{\omega} + \mathbf{h}_c) - \frac{1}{2} \dot{\mathbf{J}} (\boldsymbol{\omega} + \boldsymbol{\omega}_f) \quad (232)$$

In general, the magnitude of k_0 determines the speed of the reorientation, since it directly multiplies the quaternion error in deciding the magnitude of the required torque. It should be apparent from Equation (232) that choosing $k_0 = 0$ and $\mathbf{K}_1 \neq \mathbf{0}$ will simply drive $\boldsymbol{\omega} \rightarrow \mathbf{0}$ without any consideration for the quaternion error. Conversely, choosing $\mathbf{K}_1 = \mathbf{0}$ and $k_0 \neq 0$ will drive $\mathbf{q} \rightarrow \mathbf{q}_f$ without consideration of the desired target angular velocity, $\boldsymbol{\omega}_f$, generally causing an overshoot. The constant \mathbf{K}_1 should therefore be selected in consideration of the magnitude of k_0 . It can be shown that the system is critically damped in the linear range (near $\mathbf{q} = \mathbf{q}_f$) when the diagonals of \mathbf{K}_1 are chosen as [42]

$$K_{1,ii} = \sqrt{2J_{ii}k_0} \quad (233)$$

Since \mathbf{J} is variable, but closely approximated by \mathbf{I} when the GMW inertias are small relative to the spacecraft, the elements J_{ii} are closely approximated by the constant terms I_{ii} .

It is important to discuss the possibility of solutions other than $\boldsymbol{\omega} = \boldsymbol{\omega}_f$ and $\mathbf{q} = \mathbf{q}_f$ for which we might have $\dot{V} = 0$. Since \mathbf{K}_1 is a positive definite gain matrix, then $\dot{V} = 0$ implies $\boldsymbol{\omega} = \boldsymbol{\omega}_f$. This further implies that

$$\dot{\mathbf{h}}_c = k_0 \mathbf{G}^T(\mathbf{q}_f) \mathbf{q} - \mathbf{J} \dot{\boldsymbol{\omega}}_f - \boldsymbol{\omega}_f^\times (\mathbf{J} \boldsymbol{\omega}_f + \mathbf{h}_c) - \dot{\mathbf{J}} \boldsymbol{\omega}_f$$

Combining this with Equation (213) when $\boldsymbol{\omega} = \boldsymbol{\omega}_f$

$$\dot{\boldsymbol{\omega}}_f = \mathbf{J}^{-1}(-\boldsymbol{\omega}_f^\times(\mathbf{J}\boldsymbol{\omega}_f + \mathbf{h}_c) - \dot{\mathbf{J}}\boldsymbol{\omega}_f - \dot{\mathbf{h}}_c)$$

we have

$$\dot{\mathbf{h}}_c = k_0 \mathbf{G}^T(\mathbf{q}_f)\mathbf{q} + \dot{\mathbf{h}}_c$$

which is only possible when $\mathbf{q} = \mathbf{q}_f$ (or $\mathbf{q} = \mathbf{0}$, which violates the quaternion constraint). Therefore, the system is globally asymptotically stable when $\dot{\mathbf{h}}_c$ is chosen as in Equation (232). This cluster rate must ultimately be related to the input torques. In the momentum wheel case, we have $\dot{\mathbf{J}}_{mw} = \mathbf{0}$, and assuming we wish to accomplish a reorientation for which $\boldsymbol{\omega}_f = \mathbf{0}$ and $\dot{\boldsymbol{\omega}}_f = \mathbf{0}$, then Equation (232) simplifies to

$$\dot{\mathbf{h}}_c = \mathbf{K}_1\boldsymbol{\omega} + k_0 \mathbf{G}^T(\mathbf{q}_f)\mathbf{q} - \boldsymbol{\omega}^\times(\mathbf{J}\boldsymbol{\omega} + \mathbf{h}_c) \quad (234)$$

Generating the $\dot{\mathbf{h}}_c$ required by Equation (234) is relatively simple for the momentum wheel case. Equation (217) provides the relation for choosing the momentum wheel spin axis torques, \mathbf{g}_w . For the case of three non-coplanar momentum wheels (\mathbf{A}_{s0} non-singular), a unique solution for \mathbf{g}_w exists. For a redundant set of momentum wheels, an infinite number of solutions exists. It is common to choose the minimum norm solution for the torques given by

$$\mathbf{g}_w = \mathbf{A}_s^T(\mathbf{A}_s\mathbf{A}_s^T)^{-1}\dot{\mathbf{h}}_c \quad (235)$$

The case of the CMG cluster is not quite so simple. With changing gimbal angles, \mathbf{J}_{cmg} is not constant, and even after computing an $\dot{\mathbf{h}}_c$ to stabilize the system, Equation (220) causes complications in choosing the control input. First, we rearrange Equation (232) slightly to the form

$$\dot{\mathbf{h}}_c + \frac{1}{2}\dot{\mathbf{J}}_{cmg}(\boldsymbol{\omega} + \boldsymbol{\omega}_f) = \mathbf{K}_1(\boldsymbol{\omega} - \boldsymbol{\omega}_f) + k_0 \mathbf{G}^T(\mathbf{q}_f)\mathbf{q} - \mathbf{J}_{cmg}\dot{\boldsymbol{\omega}}_f - \boldsymbol{\omega}^\times(\mathbf{J}_{cmg}\boldsymbol{\omega} + \mathbf{h}_c) \quad (236)$$

so that all terms which are functions of gimbal rates and accelerations are on the left hand side. Then Equation (236) may be written as

$$\mathbf{B}\ddot{\boldsymbol{\delta}} + \mathbf{D}\dot{\boldsymbol{\delta}} = \mathbf{K}_1(\boldsymbol{\omega} - \boldsymbol{\omega}_f) + k_0\mathbf{G}^T(\mathbf{q}_f)\mathbf{q} - \mathbf{J}_{cmg}\dot{\boldsymbol{\omega}}_f - \boldsymbol{\omega}^\times(\mathbf{J}_{cmg}\boldsymbol{\omega} + \mathbf{h}_c) \quad (237)$$

where the $3 \times N$ matrix \mathbf{B} is simply (from Equation (220))

$$\mathbf{B} = \mathbf{A}_g\mathbf{I}_g \quad (238)$$

The $3 \times N$ \mathbf{D} matrix in Equation (237) is defined by

$$\mathbf{D}\dot{\boldsymbol{\delta}} = \frac{1}{2}\dot{\mathbf{J}}_{cmg}(\boldsymbol{\omega} + \boldsymbol{\omega}_f) - \mathbf{A}_t\text{diag}(\mathbf{h}_{swr})\dot{\boldsymbol{\delta}} \quad (239)$$

To compute \mathbf{D} , note that \mathbf{J}_{cmg} is a function of the gimbal rates, so that

$$\begin{aligned} \dot{\mathbf{J}}_{cmg} &= \mathbf{A}_s\text{diag}\dot{\mathbf{I}}_t\mathbf{A}_t^T + \mathbf{A}_t\text{diag}\dot{\mathbf{I}}_t\mathbf{A}_s^T - \mathbf{A}_t\text{diag}\dot{\mathbf{I}}_s\mathbf{A}_s^T - \mathbf{A}_s\text{diag}\dot{\mathbf{I}}_s\mathbf{A}_t^T \\ &= \mathbf{A}_s\text{diag}\dot{\boldsymbol{\delta}}(\mathbf{I}_t - \mathbf{I}_s)\mathbf{A}_t^T + \mathbf{A}_t\text{diag}\dot{\boldsymbol{\delta}}(\mathbf{I}_t - \mathbf{I}_s)\mathbf{A}_s^T \end{aligned} \quad (240)$$

It is possible, for example, to write the product of the first term on the right hand side of (240) with $\boldsymbol{\omega} + \boldsymbol{\omega}_f$ as

$$\begin{aligned} &\mathbf{A}_s\text{diag}\dot{\boldsymbol{\delta}}(\mathbf{I}_t - \mathbf{I}_s)\mathbf{A}_t^T(\boldsymbol{\omega} + \boldsymbol{\omega}_f) \\ &= \sum_{j=1}^N \mathbf{a}_{sj}\mathbf{a}_{tj}^T(\boldsymbol{\omega} + \boldsymbol{\omega}_f)(I_{tj} - I_{sj})\dot{\delta}_j \\ &= \left[\begin{array}{cccc} \mathbf{a}_{s1}\mathbf{a}_{t1}^T(\boldsymbol{\omega} + \boldsymbol{\omega}_f) & \mathbf{a}_{s2}\mathbf{a}_{t2}^T(\boldsymbol{\omega} + \boldsymbol{\omega}_f) & \cdots & \mathbf{a}_{sN}\mathbf{a}_{tN}^T(\boldsymbol{\omega} + \boldsymbol{\omega}_f) \end{array} \right] (\mathbf{I}_t - \mathbf{I}_s)\dot{\boldsymbol{\delta}} \end{aligned} \quad (241)$$

so that

$$\begin{aligned} \mathbf{D} &= -\mathbf{A}_t\text{diag}(\mathbf{h}_{swr}) \\ &\quad + \frac{1}{2} \left[\begin{array}{cccc} (\mathbf{a}_{s1}\mathbf{a}_{t1}^T + \mathbf{a}_{t1}\mathbf{a}_{s1}^T)(\boldsymbol{\omega} + \boldsymbol{\omega}_f) & (\mathbf{a}_{s2}\mathbf{a}_{t2}^T + \mathbf{a}_{t2}\mathbf{a}_{s2}^T)(\boldsymbol{\omega} + \boldsymbol{\omega}_f) & \cdots & \\ \cdots & (\mathbf{a}_{sN}\mathbf{a}_{tN}^T + \mathbf{a}_{tN}\mathbf{a}_{sN}^T)(\boldsymbol{\omega} + \boldsymbol{\omega}_f) & & \end{array} \right] (\mathbf{I}_t - \mathbf{I}_s) \end{aligned} \quad (242)$$

In general, because \mathbf{h}_{swr} is large, the contributions to \mathbf{D} from the first term of Equation (242) are of much greater magnitude than those of the second term (especially for small $\boldsymbol{\omega} + \boldsymbol{\omega}_f$ or when $\mathbf{I}_t \approx \mathbf{I}_s$).

The system is stable when Equation (237) is satisfied. Of course, $\dot{\boldsymbol{\delta}}$ is actually determined by the integration of $\ddot{\boldsymbol{\delta}}$ and is therefore a state of the system. The advantage of single gimbal control moment gyros, however, lies in the torque amplification resulting from the gimbal rates. Fortunately, $\mathbf{B}\ddot{\boldsymbol{\delta}}$ is generally many orders of magnitude smaller than $\mathbf{D}\dot{\boldsymbol{\delta}}$ (for high spin rate control moment gyros). Normally, we seek to drive the gimbals so that

$$\mathbf{D}\dot{\boldsymbol{\delta}} = \mathbf{K}_1(\boldsymbol{\omega} - \boldsymbol{\omega}_f) + k_0\mathbf{G}^T(\mathbf{q}_f)\mathbf{q} - \mathbf{J}_{cmg}\dot{\boldsymbol{\omega}}_f - \boldsymbol{\omega}^\times(\mathbf{J}_{cmg}\boldsymbol{\omega} + \mathbf{h}_c) \quad (243)$$

as closely as possible, while simply tolerating the resulting torque generated by the gimbal accelerations. That is, we assume $\mathbf{B}\ddot{\boldsymbol{\delta}}$ is negligible in Equation (237). A solution to Equation (243) gives the desired gimbal rates, which we denote as $\dot{\boldsymbol{\delta}}_{des}$. Oh and Vadali showed that by then choosing

$$\ddot{\boldsymbol{\delta}} = \mathbf{K}_\delta(\dot{\boldsymbol{\delta}}_{des} - \dot{\boldsymbol{\delta}}) \quad (244)$$

where \mathbf{K}_δ is positive definite, we can keep $\dot{\boldsymbol{\delta}}$ close to that required to satisfy Equation (243), ensuring that we are taking advantage of the torques generated from the gimbal rates.

Knowledge of the desired gimbal accelerations allows computation of the required gimbal axis torques (assuming that we can compute or measure $\dot{\boldsymbol{\omega}}$), since from Equation (87)

$$\mathbf{g}_g = \mathbf{I}_g\ddot{\boldsymbol{\delta}} + \mathbf{I}_g\mathbf{A}_g^T\dot{\boldsymbol{\omega}} - ((\mathbf{I}_t - \mathbf{I}_s)\mathbf{A}_s^T\boldsymbol{\omega} - \mathbf{h}_{swr} \star (\mathbf{A}_t^T\boldsymbol{\omega})) \quad (245)$$

As in the case of momentum wheels, a redundant set of CMGs leads to an underdetermined problem. Denoting the right hand side of Equation (243) as \mathbf{l}_r , then we seek a solution to the problem

$$\dot{\boldsymbol{\delta}}_{des} = \mathbf{D}^\dagger\mathbf{l}_r \quad (246)$$

The superscript \dagger is used in Equation (244) to indicate that when \mathbf{D} is not invertible then a suitable pseudoinverse should be used. This occurs when \mathbf{D} is not square. It may also

occur when the gimbals are in a singular configuration. We turn now to a discussion of the CMG singularity problem.

5.3 The CMG Singularity Problem

A singularity is encountered when there exists some direction in the body in which the cluster is not capable of producing torque. This occurs for a particular direction in the body frame when the spin axes of all CMGs in the cluster are either maximally or minimally projected in that direction. In this condition, all of the transverse axes of the CMGs are perpendicular to this direction. Thus, the elements of \mathbf{A}_t are coplanar, and \mathbf{D} is rank 2. We could also say that the range of the transformation from gimbal rates to output torque of the cluster is two-dimensional (planar). Operating near these singularities can result in unreasonably high gimbal rate commands and undesirable system response.

Of course, nothing physically significant actually happens at a singularity. There is no gimbal lock phenomenon or other adverse effect associated with these configurations. There is, however, a problem if one wishes to generate a torque in the singular direction. If the required torque is orthogonal to the singular direction, there is no reason to avoid the singularity during the reorientation profile. Based on the elegant results of the *singular value decomposition* (SVD), we are able to steer through some singularities, resulting in a much smoother reorientation. An excellent presentation of the principles of the SVD and its relationship to the typical pseudoinverse techniques was given by Junkins and Kim [25]. We begin with an analysis of the singularity-robust steering law before showing how it is modified into a singular direction avoidance law.

5.3.1 The Singularity-Robust Steering Law. For a system of three CMGs (with non-coplanar gimbal axes), and a non-singular matrix \mathbf{D} , Equation (243) can be solved for the desired gimbal rates as

$$\delta_{\text{des}} = \mathbf{D}^{-1}\mathbf{l}_r \quad (247)$$

When there are more than three CMGs in the cluster, then the solution for $\dot{\boldsymbol{\delta}}_{\text{des}}$ is under-determined, and a minimum 2-norm solution can be calculated from

$$\dot{\boldsymbol{\delta}}_{\text{des}} = \mathbf{D}^T(\mathbf{D}\mathbf{D}^T)^{-1}\mathbf{l}_r \quad (248)$$

Equation (248) gives the minimum norm solution for the gimbals rates for a desired torque, \mathbf{l}_r ¹. Equation (248) fails when \mathbf{D} drops below rank three, because $\mathbf{D}\mathbf{D}^T$ becomes singular. When \mathbf{D} is *nearly* singular, the inverse leads to unreasonably large gimbals angle rates.

A modification to Equation (248) prevents the gimbals rates from becoming excessive at or near a singularity [39]. The steering law is modified to

$$\dot{\boldsymbol{\delta}}_{\text{des}} = \mathbf{D}^T(\mathbf{D}\mathbf{D}^T + \alpha\mathbf{1})^{-1}\mathbf{l}_r \quad (249)$$

where $\mathbf{1}$ is the 3×3 identity matrix, and α is a scalar parameter which is negligible when $\mathbf{D}\mathbf{D}^T$ is non-singular, but increases as a singularity is approached. Oh and Vadali proposed, for example, letting

$$\alpha = \alpha_o e^{-\det(\mathbf{D}\mathbf{D}^T)} \quad (250)$$

where α_o is some small constant. This ensures that a solution for the gimbals rates always exists. Equation (249) is commonly referred to as the *singularity-robust* (SR) steering law.

Near or at a singularity, the computed gimbals rates do not produce the required torque. We are forced to accept some deviation, as it may be impossible to produce the desired torque with finite gimbals rates. In some cases, however, the required torque might be possible if it lies in the range of \mathbf{D} , even though \mathbf{D} is singular. The SR steering law will produce an errant torque, even when the desired torque is achievable. The singular value decomposition allows for an examination of the structure of the SR steering law and provides some insight which allows for an improvement in the steering law near or at a singularity.

¹The minimum norm solution is often criticized in the literature (see, for example [4, 43]) for actually contributing to the singularity problem. This phenomenon was not observed during this dissertation research, and a discussion of it is in Appendix C.

5.3.2 *The Singular Value Decomposition.* In general, any $m \times n$ matrix can be decomposed into the product of three special matrices:

$$\mathbf{D} = \mathbf{USV}^T \quad (251)$$

where \mathbf{U} is an $m \times m$ unitary matrix, \mathbf{V} is an $n \times n$ unitary matrix, and \mathbf{S} is an $m \times n$ matrix which is diagonal. If \mathbf{S} has more columns than rows (i.e. $m < n$), then the last $n - m$ columns are zeros. The diagonal elements of \mathbf{S} are known as the *singular values*. By convention, all singular values are positive and ordered so that

$$S_{11} \geq S_{22} \geq \dots \geq S_{mm} \geq 0 \quad (252)$$

Note that expressing \mathbf{D} in this form makes it easy to compute \mathbf{D}^{-1} , since in the case where \mathbf{D} is square,

$$\mathbf{D}^{-1} = \mathbf{VS}^{-1}\mathbf{U}^T \quad (253)$$

and \mathbf{S} is an easily inverted diagonal matrix. When $m < n$, then the matrix $\mathbf{D}^T(\mathbf{DD}^T)^{-1}$ can be calculated from the elements of the singular value decomposition by discarding the last $n - m$ zero columns of \mathbf{S} and \mathbf{V} , inverting the new $m \times m$ square matrix \mathbf{S} , and forming

$$\mathbf{D}^\dagger = \mathbf{V}_t \mathbf{S}_t^{-1} \mathbf{U}^T \quad (254)$$

where \mathbf{V}_t and \mathbf{S}_t are the truncated matrices.

Equation (254) gives the minimum norm solution to the undetermined case and works well for the CMG problem when $\text{rank}(\mathbf{D}) = 3$. When $\text{rank}(\mathbf{D})$ falls below 3, however, \mathbf{S}_t^{-1} does not exist because $S_{33} = 0$. The purpose of Equation (249) is to ensure that an inverse exists when $S_{33} \rightarrow 0$.

We ask how adding the singularity avoidance parameters to the underdetermined steering equation given by Equation (249) affects the singular value parameters. We proceed as follows:

$$\mathbf{D}^T(\mathbf{DD}^T + \alpha\mathbf{1})^{-1} = \mathbf{VS}^T\mathbf{U}^T(\mathbf{USS}^T\mathbf{U}^T + \alpha\mathbf{UU}^T)^{-1}$$

$$\begin{aligned}
&= \mathbf{V}\mathbf{S}^T(\mathbf{S}\mathbf{S}^T + \alpha\mathbf{1})^{-1}\mathbf{U}^T \\
&= \mathbf{V}_i\mathbf{S}_i(\mathbf{S}_i^2 + \alpha\mathbf{1})^{-1}\mathbf{U}^T
\end{aligned} \tag{255}$$

Note that both \mathbf{S}_i and $\mathbf{S}_i^2 + \alpha\mathbf{1}$ are diagonal matrices, so that

$$\mathbf{S}^T(\mathbf{S}\mathbf{S}^T + \alpha\mathbf{1})^{-1} = \text{diag} \left(\frac{S_{11}}{S_{11}^2 + \alpha}, \frac{S_{22}}{S_{22}^2 + \alpha}, \dots, \frac{S_{mm}}{S_{mm}^2 + \alpha} \right) \tag{256}$$

$$\equiv \mathbf{S}_{\text{SR}}^\dagger \tag{257}$$

This nature of the SR law in terms of singular values was observed by Bedrossian *et al.* [4], but was not used to improve the steering law.

Looking back at Equation (250), it is interesting to note that since

$$\mathbf{D}\mathbf{D}^T = \mathbf{U}\mathbf{S}^T\mathbf{S}\mathbf{U}^T \tag{258}$$

then

$$\begin{aligned}
\det(\mathbf{D}\mathbf{D}^T) &= \det(\mathbf{U}) \cdot \det(\mathbf{S}^T\mathbf{S}) \cdot \det(\mathbf{U}^T) \\
&= \det(\mathbf{S}^T\mathbf{S}) \\
&= \prod_{i=1}^m S_{ii}^2
\end{aligned} \tag{259}$$

so that the exponent term in the singularity avoidance parameter is a function of all of the singular values. Below, we propose a singularity avoidance parameter that depends only on S_{33} , the critical singular value for this problem.

5.3.3 Singular Direction Avoidance. For a transformation matrix, such as \mathbf{D} , which is a continuous function of several variables, the singular values are continuous functions as well. Since \mathbf{D} maps the $N \times 1$ vector of gimbal rates into the 3×1 vector of output torques, \mathbf{D} is rank 3 for non-singular gimbal angles. If a singularity is encountered, then \mathbf{D} falls to rank 2, with $S_{33} = 0$. The singular value decomposition provides some useful information through the unitary matrices \mathbf{U} and \mathbf{V} . With \mathbf{D} a $3 \times N$ matrix, the last $N - 3$ columns of \mathbf{V} span the null space of \mathbf{D} . These columns form a basis for the

gimbal *null motions* of the cluster, those gimbal rates which produce no output torque for a given configuration. The third column of \mathbf{V} always represents the direction mapped through the smallest singular value. When $S_{33} = 0$, the third column of \mathbf{V} is also in the null space of \mathbf{D} .

The columns of \mathbf{U} form the basis for the range of \mathbf{D} when \mathbf{D} is rank 3. However, when \mathbf{D} falls to rank 2, only the first two columns of \mathbf{U} span the range of \mathbf{D} , whereas the last column is orthogonal to the range of \mathbf{D} . The direction of the third column of \mathbf{U} is the direction in which no output torque is possible when $\text{rank}(\mathbf{D}) = 2$.

It is always the third singular value which goes to zero as a singular gimbal configuration is approached. Thus, preventing S_{33} from going to zero will ensure that the commanded gimbal rates are finite. Furthermore, we argue that it is not only unnecessary, but undesirable to change all of the gimbal rate commands when a singularity is approached, as is obviously accomplished through the singularity robust control law (see Equations (255) and (257)). The output torque requested by the Lyapunov control law, Equation (246), is not affected by the singularity of the gimbal cluster. It is the torque we would like to generate if possible. When we cannot because of a singular condition, there is no reason to alter all of the gimbal rates to avoid the singularity.

When \mathbf{D} is decomposed via SVD, Equation (243) becomes

$$\mathbf{l}_r = \mathbf{U}\mathbf{S}\mathbf{V}^T\dot{\boldsymbol{\delta}}_{\text{des}} \quad (260)$$

Some useful insight is provided when rewritten in the form

$$\mathbf{U}^T\mathbf{l}_r = \mathbf{S}\mathbf{V}^T\dot{\boldsymbol{\delta}}_{\text{des}} \quad (261)$$

When $S_{33} = 0$, the range of $\mathbf{S}\mathbf{V}^T$ is two-dimensional, and is the plane spanned by the first two columns of \mathbf{U} . The first two elements of the vector $\mathbf{U}^T\mathbf{l}_r$ remain the desired torque components in the range of $\mathbf{S}\mathbf{V}^T$. We argue that it is best not to alter S_{11} or S_{22} before inversion.

The question becomes one of determining what to do with the possible gimbal motions in the null space of \mathbf{D} . The singularity robust inverse technique would suggest letting

$$\left(\frac{1}{S_{33}}\right) \rightarrow \left(\frac{S_{33}}{S_{33}^2 + \alpha}\right)$$

Note that this function approximates $(1/S_{33})$ for large S_{33} , but goes back to zero at a singularity (for $\alpha \neq 0$).

It seems reasonable to expect maintaining the gimbal rates present prior to encountering the singularity would be preferable to attempting to stop the gimbal movement in the null direction as the singularity approaches. While this logic is sound in theory, since we are actually forced to deal with an acceleration steering law, the gimbal rates are never exactly what we desire and it is unlikely that the gimbal will transit the singularity in a direction exactly orthogonal to the singular direction. We therefore examine the rate steering equation of the form

$$\dot{\boldsymbol{\delta}}_{des} = \mathbf{V}_t \mathbf{S}_{SDA}^\dagger \mathbf{U}^T \mathbf{l}_r \quad (262)$$

where

$$\mathbf{S}_{SDA}^\dagger = \text{diag} \left(\frac{1}{S_{11}}, \frac{1}{S_{22}}, \frac{S_{33}}{S_{33}^2 + \alpha} \right) \quad (263)$$

We shall refer to the gimbal rates computed by Equation (262) as the *Singular Direction Avoidance* (SDA) steering law.

Of course, we should justify why choosing the gimbal rates in accordance with Equation (262) is an improvement over those computed by Equation (249), the SR steering law. Define as \mathbf{l}_p the torque produced by the gimbal rates of a cluster of CMGs. That is

$$\begin{aligned} \mathbf{l}_p &= \mathbf{D}\dot{\boldsymbol{\delta}} \\ &= \mathbf{U}\mathbf{S}\mathbf{V}^T\dot{\boldsymbol{\delta}} \\ &= \mathbf{U}\mathbf{S}_t\mathbf{V}_t^T\dot{\boldsymbol{\delta}} \end{aligned} \quad (264)$$

Choosing the gimbal rates in accordance with the SR steering law yields the gimbal rates given by Equation (255) so that

$$\mathbf{l}_{pSR} = \mathbf{U} \mathbf{S}_t \mathbf{S}_{SR}^\dagger \mathbf{U}^T \mathbf{l}_r \quad (265)$$

Near a singularity, this steering law does not produce the torque required. The error is

$$\mathbf{l}_r - \mathbf{l}_{pSR} = \mathbf{U} (\mathbf{1} - \mathbf{S}_t \mathbf{S}_{SR}^\dagger) \mathbf{U}^T \mathbf{l}_r \quad (266)$$

The norm of the error in the torque produced is therefore

$$\|\mathbf{l}_r - \mathbf{l}_{pSR}\| = \left\| \left(\begin{array}{ccc} \frac{\alpha}{S_{11}^2 + \alpha} & 0 & 0 \\ 0 & \frac{\alpha}{S_{22}^2 + \alpha} & 0 \\ 0 & 0 & \frac{\alpha}{S_{33}^2 + \alpha} \end{array} \right) \mathbf{U}^T \mathbf{l}_r \right\| \quad (267)$$

We use the same reduction to show that for the SDA approach

$$\|\mathbf{l}_r - \mathbf{l}_{pSDA}\| = \left\| \left(\begin{array}{ccc} 0 & 0 & 0 \\ 0 & 0 & 0 \\ 0 & 0 & \frac{\alpha}{S_{33}^2 + \alpha} \end{array} \right) \mathbf{U}^T \mathbf{l}_r \right\| \quad (268)$$

The error in the torque produced is therefore directly proportional to the magnitude of the torque required, but varies with direction. If \mathbf{l}_r is a unit vector, then the maximum error occurs in either case when \mathbf{l}_r lies solely in the direction of the smallest singular value (and is the same for either control law). The minimum error, however, occurs for the SR law when \mathbf{l}_r lies in the direction of the maximum singular value, but is always non-zero (assuming $\alpha \neq 0$). For the SDA law, the minimum error occurs (and is zero) if \mathbf{l}_r lies in the plane orthogonal to the direction of the minimum singular value (that is, in the range of the first two columns of \mathbf{U}).

We conclude that for the SR law

$$\frac{\alpha}{S_{11}^2 + \alpha} \leq \frac{\|\mathbf{l}_r - \mathbf{l}_{pSR}\|}{\|\mathbf{l}_r\|} \leq \frac{\alpha}{S_{33}^2 + \alpha} \quad (269)$$

whereas for the SDA law

$$0 \leq \frac{\|\mathbf{l}_r - \mathbf{l}_{p_{SDA}}\|}{\|\mathbf{l}_r\|} \leq \frac{\alpha}{S_{33}^2 + \alpha} \quad (270)$$

and that for any \mathbf{l}_r ,

$$\|\mathbf{l}_r - \mathbf{l}_{p_{SDA}}\| \leq \|\mathbf{l}_r - \mathbf{l}_{p_{SR}}\| \quad (271)$$

The error in the torque output resulting from the SDA control law is always less than or equal to that produced by the SR law. In some cases, the error might even be zero, whereas the SR law always produces some error.

5.3.4 The Singularity Avoidance Parameter. The choice of the singularity avoidance parameter, α , can of course have a major impact on a typical reorientation profile. Since the intent of the singularity avoidance is to effect a smooth reorientation and prevent large gimbal accelerations (and torque commands), a method of judging the smoothness of a maneuver is to observe gimbal angle histories, or possibly the output torque history. Numerous simulations using a singularity avoidance parameter based on Equation (250) indicated a tendency toward abrupt gimbal angle commands and angular velocity histories near singular configurations because the exponential term rises abruptly as the singularity is approached. Furthermore, the singularity parameter given by Equation (250) depends on the physical size of the system, since $\det(\mathbf{D}\mathbf{D}^T)$ has units of angular momentum squared. We therefore choose to non-dimensionalize the exponent.

For a typical CMG system, the contribution to \mathbf{D} from the first term of Equation (242) is much greater than the contribution from the second. For the physical model and reorientation profiles explored in this section, the difference is roughly seven orders of magnitude. Therefore

$$\mathbf{D} \approx -\mathbf{A}_t \text{diag}(\mathbf{h}_{swr}) \quad (272)$$

When \mathbf{D} is computed as in Equation (272), then

$$\mathbf{D}^T \mathbf{D} = \mathbf{V} \mathbf{S}^T \mathbf{S} \mathbf{V}^T \quad (273)$$

and since \mathbf{V} is an orthonormal matrix,

$$\text{trace}(\mathbf{D}^T \mathbf{D}) = \text{trace}(\mathbf{S}^T \mathbf{S}) \quad (274)$$

So, with

$$\mathbf{D}^T \mathbf{D} = \begin{bmatrix} \mathbf{a}_{t1}^T h_{swr1} \\ \mathbf{a}_{t2}^T h_{swr2} \\ \vdots \\ \mathbf{a}_{tN}^T h_{swrN} \end{bmatrix} \begin{bmatrix} \mathbf{a}_{t1} h_{swr1} & \mathbf{a}_{t2} h_{swr2} & \cdots & \mathbf{a}_{tN} h_{swrN} \end{bmatrix} \quad (275)$$

then

$$\text{trace}(\mathbf{D}^T \mathbf{D}) = h_{swr1}^2 + h_{swr2}^2 + \cdots + h_{swrN}^2 = \mathbf{h}_{swr}^T \mathbf{h}_{swr} = \text{constant} \quad (276)$$

which with Equation (273) implies

$$S_{11}^2 + S_{22}^2 + S_{33}^2 = \mathbf{h}_{swr}^T \mathbf{h}_{swr} = \text{constant} \quad (277)$$

When all N CMGs have identical spin momenta, h_{swr} , then

$$\sum_{i=1}^3 S_{ii}^2 = N h_{swr}^2 \quad (278)$$

This allows us to put a bound on the upper limit of the smallest singular value S_{33} , since when S_{33} is at its maximum, $S_{11} = S_{22} = S_{33}$. Therefore

$$S_{33} \leq \sqrt{\frac{N}{3}} h_{swr} \quad (279)$$

We define a non-dimensional variable

$$\sigma_{33} \equiv \sqrt{\frac{3}{N}} \left(\frac{S_{33}}{h_{swr}} \right) \quad (280)$$

so that

$$0 \leq \sigma_{33} \leq 1 \quad (281)$$

and choose as a singularity avoidance parameter

$$\alpha = \alpha_0 e^{-k_\sigma \sigma_{33}^2} \quad (282)$$

so that the response of the system is independent of system size. The constant k_σ may be selected as desired. Note also that the coefficient term, α_0 , also has units of angular momentum squared and should be adjusted to match the dimension of the system. In the following section, we compare the SR and SDA maneuvers, and we also compare maneuvers using the two singularity avoidance parameters.

5.4 Maneuver Examples

We now present some examples which are chosen to present the advantages of the proposed steering law. The physical model chosen is a rigid spacecraft with a cluster of 4 control moment gyros arranged in a pyramid configuration (see Oh and Vadali [42]). The parameters are taken directly from the example used by Oh and Vadali in order to compare selected results. The model data are listed in Table 1. Use of $\mathbf{I}_{sg} = \mathbf{I}_{gg} = \mathbf{0}$ does not affect the results.

5.4.1 Singular Direction Avoidance Example. We begin by examining the advantage of singular direction avoidance only. For this example, we choose an initial singular configuration of the CMGs which permits no torque output in the $[1, 1, 1]^T$ direction. Requesting a torque solely in this direction will result in no gimbal rate commands (and no motion). To show an advantage of the SDA law, we request the constant torque

Table 1 Spacecraft Physical Data for Singularity Avoidance Example

Item	Value	Units
\mathbf{h}_{swr}	$[1.8, 1.8, 1.8, 1.8]^T$	$kg\text{-}m^2/sec$
\mathbf{I}	$\text{diag}\{86.215, 85.070, 113.565\}$	$kg\text{-}m^2$
\mathbf{I}_{sw}	$\text{diag}\{0.05, 0.05, 0.05, 0.05\}$	$kg\text{-}m^2$
\mathbf{I}_{tw}	$\text{diag}\{0.03, 0.03, 0.03, 0.03\}$	$kg\text{-}m^2$
\mathbf{I}_{tg}	$\text{diag}\{0.01, 0.01, 0.01, 0.01\}$	$kg\text{-}m^2$
$\mathbf{I}_{sg}, \mathbf{I}_{gg}$	$\text{diag}\{0, 0, 0, 0\}$	$kg\text{-}m^2$
Pyramid Angle	54.74	deg

Table 2 SDA Example Simulation Data

Item	Value	Units
\mathbf{K}_δ	$\text{diag}\{100, 100, 100, 100\}$	sec^{-1}
α_0	0.5	$\text{kg}^2\text{-m}^4/\text{sec}^2$
δ_0	$[13.455, -13.455, -54.343, 54.343]^T$	degrees
$\dot{\delta}_0$	$[5.541, 9.204, 10.820, -1.983]^T$	degrees/sec
ω_0	$[0, 0, 0]^T$	degrees/sec
\mathbf{l}_r	$[0, -0.5, 0.5]^T$	$N\text{-m}$

$\mathbf{l}_r = [0, -0.5, 0.5]^T$, which is perpendicular to the singular direction. We also begin at a set of gimbal rates which are providing the desired torque at the beginning of the maneuver. Initial conditions and control law gain parameters are shown in Table 2.

Simulation results are shown in Figure 4. The top row of plots shows the desired (dashed line) and produced (solid line) torques in the body reference frame for the two control laws. The second row of plots shows the same torques presented in a reference frame using the columns of \mathbf{U} as basis vectors. Resolving components into this frame depicts how the control law affects the torque produced in the directions corresponding to the singular values. While the SR law produces torque deviations in all axes, the SDA law produces zero error in the plane orthogonal to the singular direction.

The deviation in the direction of the singularity deserves explanation. As the simulation progresses, the gimbals do not remain in a singular configuration. The direction of the smallest singular value changes, and it is the torque in the direction of the smallest singular value which is distorted due to the SDA control law. As the smallest singular value direction changes, \mathbf{l}_r is no longer exactly in the plane orthogonal to this most singular direction, whereupon the pseudoinverse calculated using the SDA law begins to produce a deviation.

Figure 4 also presents a comparison of the magnitude of the torque error for both laws. It is evident that the norm of the error is reduced for the SDA law (solid line) when compared with the SR law (dashed line). The residual error for both cases is caused by the actual gimbal rates lagging the desired rates. It can be reduced by increasing \mathbf{K}_δ in Equation (244). The singular value histories for both laws are also presented to illustrate

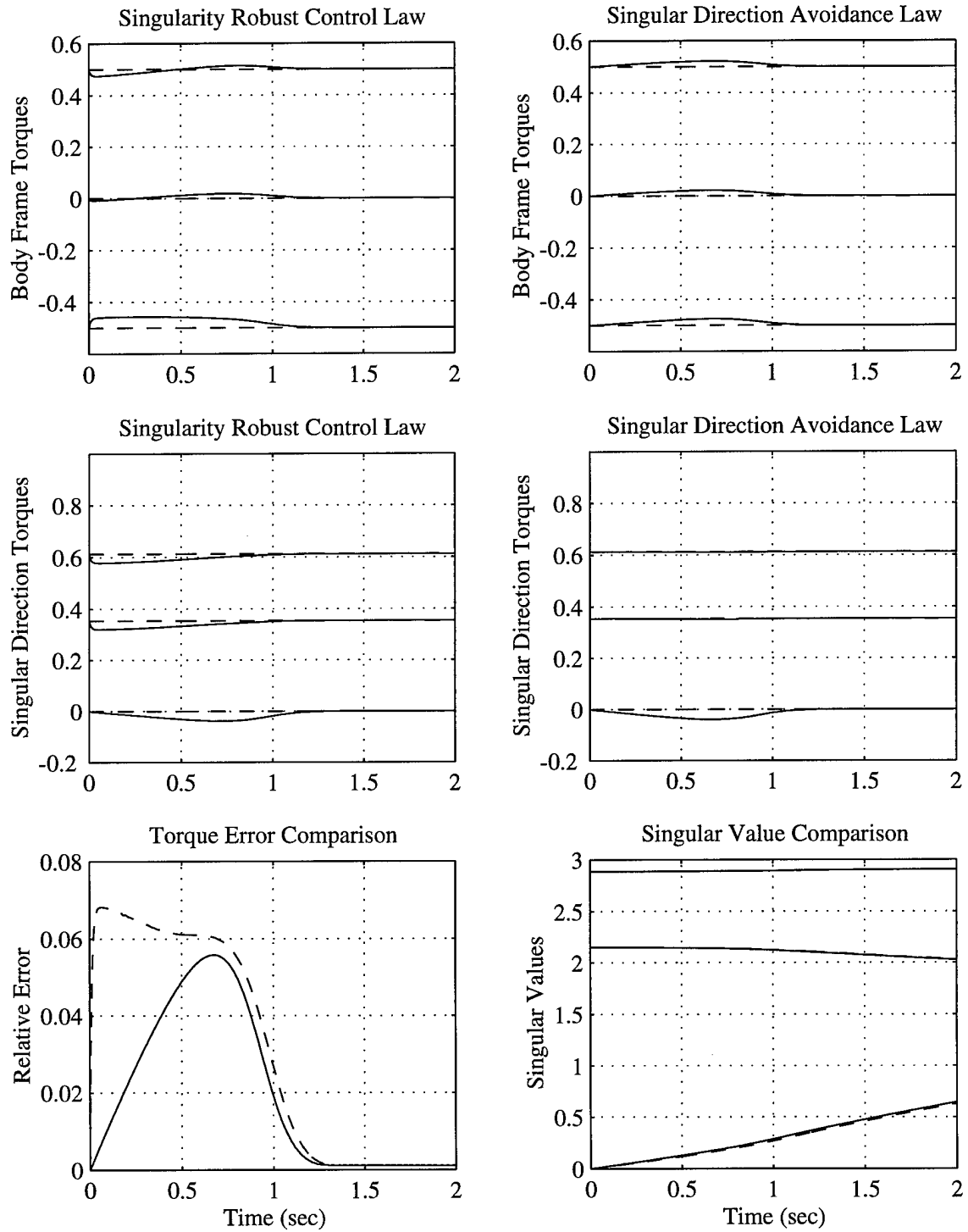


Figure 4 Torque Output Near a Singularity for the SDA and SR Steering Laws

the rate at which both control laws drive the gimbals away from the singularity. While this example is illustrative of the difference in the laws, it is somewhat artificial in that a singular condition is forced to exist at the start of the maneuver, a condition which is normally avoided during a reorientation.

5.4.2 Effect of the Singularity Avoidance Parameter. Figure 5 compares the resulting torque profiles for a reorientation maneuver started from a singular gimbal state. The plots show the torque produced (solid line) and the torque desired (dashed line). The simulation parameters are presented in Table 3. Case 1 uses the avoidance parameter based on Equation (250) and the SR law, whereas Case 2 uses Equation (282) with $k_\sigma = 10$ and the SDA law. Cases 1 and 2 use $\alpha_0 = 0.1$. Note the improvement in smoothness of the produced torque in Case 2. The third column of plots presents the same SDA law reorientation using Equation (282) and $\alpha_0 = 0.5$. The improvements evident in Cases 2 and 3 can be explained by the smoother and shallower rise of the singularity avoidance parameter function as the singularity approaches. Simply increasing α_0 for the singularity avoidance parameter given by Equation (250) does not improve the results. Using Equation (250) with $\alpha_0 = 0.5$ gives results which are similar to Case 1, except that the errors are larger.

Another measure of improvement in the steering law is the smoothness of the angular velocity history. The frequency content in the angular velocity components, for example, gives some insight into the tendency for a reorientation to excite vibrations in flexible appendages. An improvement here is evident from the angular velocity components pre-

Table 3 Singularity Avoidance Parameter Comparison Data

Item	Value	Units
k_0	1.0	$N\text{-}m$
\mathbf{K}_δ	$\text{diag}\{1, 1, 1, 1\}$	sec^{-1}
α_0 , Cases 1 & 2	0.1	$\text{kg}^2\text{-}m^4/\text{sec}^2$
α_0 , Case 3	0.5	$\text{kg}^2\text{-}m^4/\text{sec}^2$
δ_0	$[-90, 0, 90, 0]^T$	degrees
$\dot{\delta}_0$	$[0, 0, 0, 0]^T$	degrees/sec
ω_0, ω_f	$[0, 0, 0]^T$	degrees/sec
\mathbf{q}_0	$[0.5, 0.5, 0.5, 0.5]^T$	
\mathbf{q}_f	$[0, 0, 0, 1]^T$	

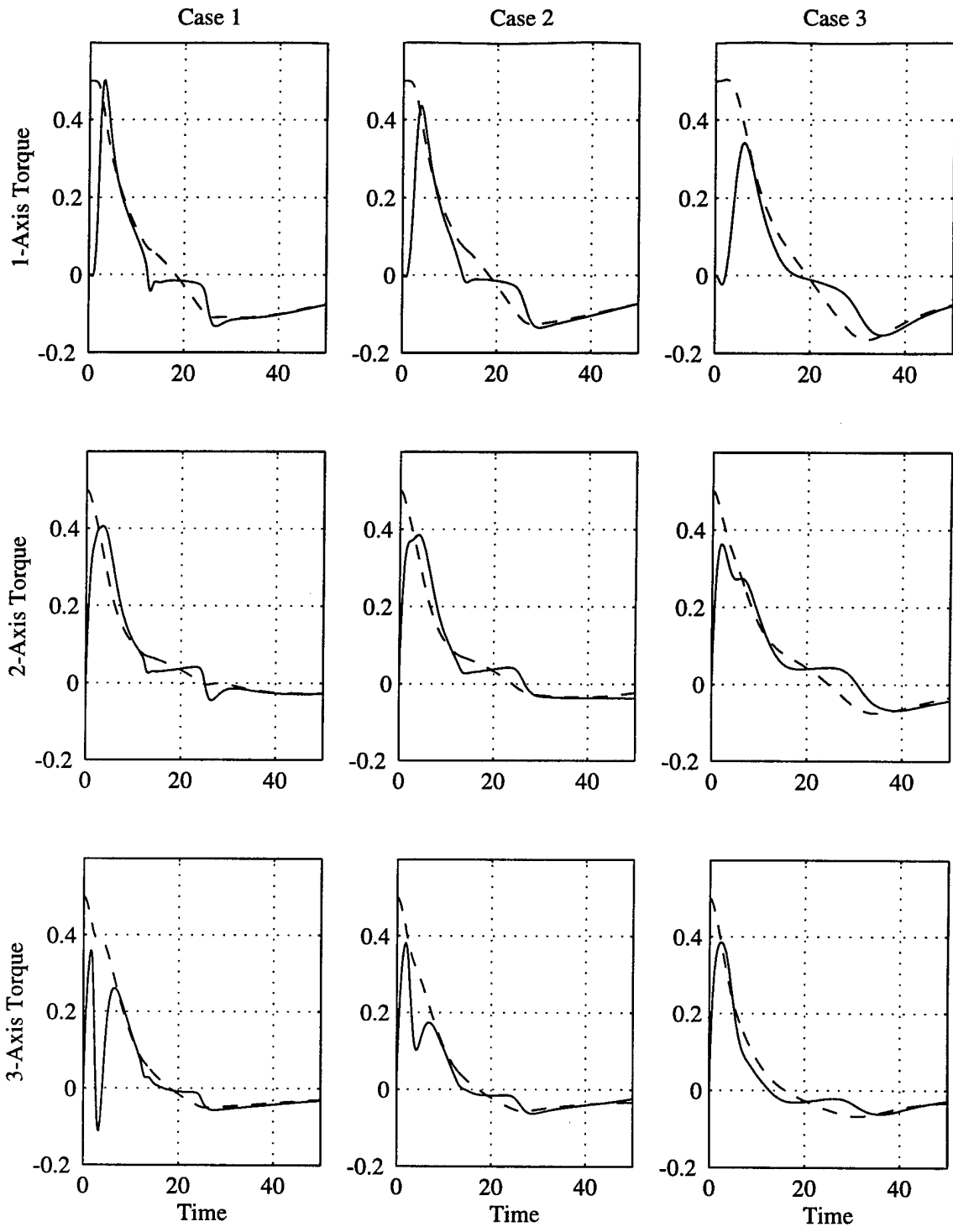


Figure 5 Torque Produced (—) and Torque Desired (---) for the Singularity Avoidance Parameter Example

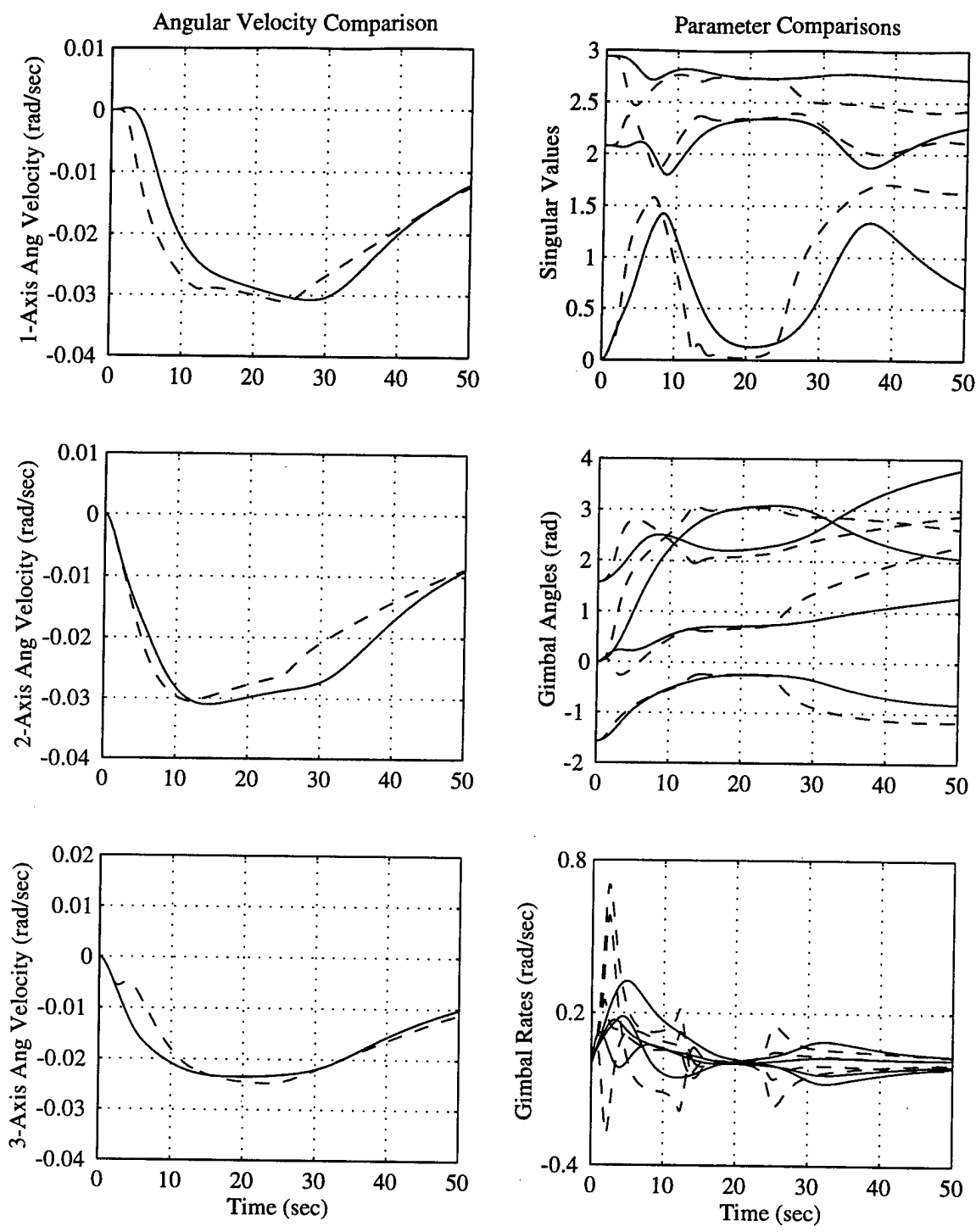


Figure 6 Reorientation Parameters for SDA (—) and SR (---) Control Laws

sented in Figure 6, which presents a direct comparison of Cases 1 and 3. Singular value and gimbal angle histories are also presented. The gimbal angle history is considerably smoother for the parameters of Case 3. Though the quaternion history is not presented, they are similar and are nearly identical at the 50 second point.

The gimbal angle rates shown in Figure 6 are very descriptive. Note the dramatic reduction in gimbal rates for the SDA law over the SR law. Rapid changes in gimbal rates are challenging for the CMG torque motors.

5.5 *The Stationary Platform Maneuver*

Stationary platform maneuvers (SPMs) are a class of gyrostat maneuvers investigated by Hall [21]. A spacecraft in which all of the angular momentum is contained in the momentum exchange devices will have zero angular velocity. A necessary (but not sufficient) condition for this state is that the momentum cluster have an angular momentum magnitude equal to the total system angular momentum magnitude. By controlling the rotors of a gyrostat in such a way that the maneuver remains near a branch of equilibrium motions for which the platform angular velocity is zero, then the angular velocity of the platform will remain small throughout the maneuver provided the rotor torques are small.

The low angular velocity resulting from execution of the SPM condition for a spacecraft with momentum wheels naturally leads to the question of its utility in the reorientation of flexible spacecraft. High angular velocities during a rest-to-rest maneuver imply high angular accelerations, which naturally tend to excite oscillations of any flexible appendages.

Existence of the SPM for a spacecraft with momentum wheels also raises the question of its existence for a spacecraft with control moment gyros. While following a stationary platform path with momentum wheels translates into following a hyper-ellipsoid in the space of wheel speeds, translation of the stationary platform condition into gimbal angle space for the CMG is considerably more complicated, as illustrated below.

5.5.1 Stationary Condition for the GMW. We start by investigating the case where all of the angular momentum is contained in the momentum storage devices. That

is, when $\boldsymbol{\omega} = \mathbf{0}$ in Equation (15). We also assume for this development that the linear momentum, \mathbf{p} , is constant, and without loss of generality equal to zero. This yields the stationary platform condition given by

$$\mathbf{h} = \mathbf{A}_s \mathbf{h}_{swa} + \mathbf{A}_g \mathbf{h}_{ga} \quad (283)$$

All combinations of \mathbf{h}_{swa} and \mathbf{h}_{ga} which maintain a constant \mathbf{h} will maintain a stationary platform. Note, however, that if $\mathbf{h}_{ga} \neq \mathbf{0}$, the gimbal rates are nonzero which implies \mathbf{A}_s is changing. This, in turn, requires varying spin axis torques to maintain a fixed \mathbf{h} . Explicitly, we must have

$$\dot{\mathbf{h}} = \mathbf{A}_s \dot{\mathbf{h}}_{swa} + \dot{\mathbf{A}}_s \mathbf{h}_{swa} + \mathbf{A}_g \dot{\mathbf{h}}_{ga} = \mathbf{0} \quad (284)$$

Since $\boldsymbol{\omega} = \mathbf{0}$, then Equation (284) becomes

$$\mathbf{A}_s \mathbf{g}_w - \mathbf{A}_t \text{diag} \delta \mathbf{h}_{swa} + \mathbf{A}_g \mathbf{g}_g = \mathbf{0} \quad (285)$$

which might be useful in the case where we desire to reorient the gimbals and wish to supply spin axis torques to maintain zero angular velocity.

We are most interested in the cases where \mathbf{h}_{ga} is zero (the gimbal rates are zero). In this case, we need only satisfy the condition

$$\mathbf{h} = \mathbf{A}_s \mathbf{h}_{swa} \quad (286)$$

Using the expression for \mathbf{A}_s in terms of the gimbal angles, then for a stationary platform with zero gimbal rates the total angular momentum must be

$$\mathbf{h} = [\mathbf{A}_{s0} \Delta^c - \mathbf{A}_{t0} \Delta^s] \mathbf{h}_{swa} \quad (287)$$

Equation (287) can be put in an alternate form by defining a new $N \times N$ matrix to be

$$\mathbf{H}_{swa} = \text{diag}(\mathbf{h}_{swa}) \quad (288)$$

so that we also have

$$\mathbf{h} = \mathbf{A}_{s0}\mathbf{H}_{swa} \cos \delta - \mathbf{A}_{t0}\mathbf{H}_{swa} \sin \delta \quad (289)$$

With multiple GMWs in the spacecraft, it might prove beneficial to exchange the momentum contributed by the individual GMWs with each other while maintaining the angular momentum of the system. We return to Equation (287) which gives \mathbf{h} as a function of the vector \mathbf{h}_{swa} and the gimbal angles δ . Taking the partial derivative of \mathbf{h} with respect to the vector of spin axis momenta, we have

$$\frac{\partial \mathbf{h}}{\partial \mathbf{h}_{swa}} = \mathbf{A}_{s0}\Delta^c - \mathbf{A}_{t0}\Delta^s \quad (290)$$

An expression for \mathbf{h} in alternate form is Equation (289). The partial derivative of \mathbf{h} with respect to the gimbal angles is therefore given by

$$\frac{\partial \mathbf{h}}{\partial \delta} = -\mathbf{A}_{s0}\mathbf{H}_{swa}\Delta^s - \mathbf{A}_{t0}\mathbf{H}_{swa}\Delta^c$$

which can also be written as

$$\frac{\partial \mathbf{h}}{\partial \delta} = -(\mathbf{A}_{s0}\Delta^s + \mathbf{A}_{t0}\Delta^c)\mathbf{H}_{swa} \quad (291)$$

A differential change in the body angular momentum vector then, can be expressed as

$$d\mathbf{h} = \frac{\partial \mathbf{h}}{\partial \mathbf{h}_{swa}}d\mathbf{h}_{swa} + \frac{\partial \mathbf{h}}{\partial \delta}d\delta \quad (292)$$

so that to maintain a constant angular momentum vector in body coordinates, any incremental change in δ should be accompanied by an appropriate change in \mathbf{h}_{swa} (or vice versa) to ensure $d\mathbf{h} = \mathbf{0}$. That is, we constrain the variation through the equation

$$(\mathbf{A}_{s0}\Delta^c - \mathbf{A}_{t0}\Delta^s)d\mathbf{h}_{swa} = (\mathbf{A}_{s0}\Delta^s + \mathbf{A}_{t0}\Delta^c)\mathbf{H}_{swa}d\delta \quad (293)$$

If the coefficient matrices are square (and nonsingular), then Equation (293) has a unique solution. If not, then either a least squares or minimum norm solution could be used. Note

also that the coefficient matrices $(\partial \mathbf{h} / \partial \mathbf{h}_{swa})$ and $(\partial \mathbf{h} / \partial \delta)$ are $3 \times N$, which means they have a nullspace of dimension at least $N - 3$. Variation of either \mathbf{h}_{swa} or δ in the direction of the nullspace of the corresponding coefficient matrix will also assure no variation in \mathbf{h} .

When Equation (287) is satisfied, the platform will be stationary. We are interested, however, in reorientation of the body. Note that the value of \mathbf{h} is free to vary as the body rotates, since \mathbf{h} is the angular momentum expressed in body coordinates. The magnitude of \mathbf{h} , however, is fixed if we assume no external torques are acting on the system. That is,

$$\mathbf{h}^T \mathbf{h} = h^2 = \text{constant} \quad (294)$$

when the external torque is zero. We define the *stationary platform condition* as the condition which exists when the magnitude of the cluster momentum equals the magnitude of the total momentum. That is

$$\mathbf{h}_c^T \mathbf{h}_c = h^2 = \text{constant} \quad (295)$$

Hall showed that, in the case of a gyrostat, maintaining the stationary platform condition during a slow maneuver results in a reorientation which keeps the angular velocity low.

5.5.2 Stationary Condition for the Momentum Wheel. In the case of a cluster of momentum wheels, we simply consider the restriction of GMWs to fixed gimbal axes. The condition of Equation (295) implies that

$$h^2 = \text{constant} = \mathbf{h}_{swa}^T \mathbf{A}_{s0}^T \mathbf{A}_{s0} \mathbf{h}_{swa} \quad (296)$$

For a spacecraft containing N momentum wheels, Equation (296) describes a hyper-ellipsoid of dimension N in the space spanned by $(h_{swa1}, 0, \dots, 0), (0, h_{swa2}, \dots, 0), \dots, (0, \dots, 0, h_{swaN})$, which we refer to as \mathbf{h}_{swa} -space. A requirement for a stationary platform is that the wheel momenta lie on the hyper-ellipsoid in \mathbf{h}_{swa} -space. We accomplish this by noting that the differentiation of Equation (296) results in the dynamical constraint

$$\mathbf{h}_{swa}^T \mathbf{A}_{s0}^T \mathbf{A}_{s0} \dot{\mathbf{h}}_{swa} = \mathbf{h}_{swa}^T \mathbf{A}_{s0}^T \mathbf{A}_{s0} \mathbf{g}_w = 0 \quad (297)$$

Of course, Equation (297) is satisfied when the wheel torques lie in the null space of \mathbf{A}_{s0} , but such “null motion” torques cause no motion. Thus, the applied torques must satisfy

$$(\mathbf{A}_{s0}\mathbf{g}_w)^T (\mathbf{A}_{s0}\mathbf{h}_{swa}) = 0 \quad (298)$$

5.5.3 Stationary Condition for the Control Moment Gyro. If we assume all of the GMWs have the same spin momentum, then

$$\mathbf{H}_{swa} = h_{swa}\mathbf{1} \quad (299)$$

where $\mathbf{1}$ is the $N \times N$ identity matrix. Also, with $\boldsymbol{\omega} = \mathbf{0}$, then the rotor relative angular momenta are identical to the absolute momenta. This means the stationary platform angular momentum vector must be

$$\mathbf{h} = h_{swr}(\mathbf{A}_{s0} \cos \delta - \mathbf{A}_{t0} \sin \delta) \quad (300)$$

To satisfy the stationary platform condition, we need

$$\cos \delta^T \mathbf{A}_{s0}^T \mathbf{A}_{s0} \cos \delta + \sin \delta^T \mathbf{A}_{t0}^T \mathbf{A}_{t0} \sin \delta - 2 \cos \delta^T \mathbf{A}_{s0}^T \mathbf{A}_{t0} \sin \delta = (h/h_{swr})^2 = \text{constant} \quad (301)$$

where we have used the fact that the transpose of a scalar is itself. We will refer to the satisfaction of Equation (301) as the *CMG stationary platform condition* and the set of all δ for which it is satisfied as the *stationary platform surface*, a surface which resides in δ -space and depends on the constant value of $(h/h_{swr})^2$.

We define the function F to be

$$F \equiv \frac{1}{2} \cos \delta^T \mathbf{A}_{s0}^T \mathbf{A}_{s0} \cos \delta + \frac{1}{2} \sin \delta^T \mathbf{A}_{t0}^T \mathbf{A}_{t0} \sin \delta - \cos \delta^T \mathbf{A}_{s0}^T \mathbf{A}_{t0} \sin \delta \quad (302)$$

A depiction of the three-dimensional surface described by Equation (302) when \mathbf{A}_{s0} is the 3×3 identity matrix ($F = 1/2$) is in Figure 7.

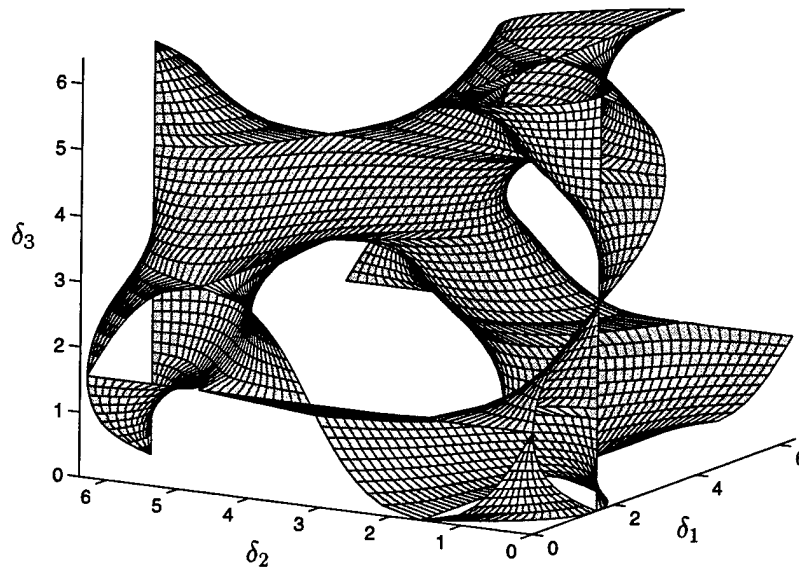


Figure 7 A CMG Stationary Platform Surface ($F = 1/2$)

Note that F is a function of only the gimbal angles. A differential change in F is strictly a result of a differential change in the gimbal angles. Thus

$$dF = \left(\frac{dF}{d\delta} \right) d\delta \quad (303)$$

Differential movement of the gimbals in the null space of $(dF/d\delta)$ will therefore maintain the stationary platform condition. Maintaining the gimbal velocity $\dot{\delta}$ in the null space of $(dF/d\delta)$ will accomplish the same. We also note that

$$\dot{F} = \left(\frac{dF}{d\delta} \right) \dot{\delta} \quad (304)$$

If we assume it is possible to control the gimbal angle rates directly, then the stationary platform condition is maintained by ensuring $\dot{F} = 0$.

Differentiation of the function F yields the matrix expression

$$\left(\frac{dF}{d\delta}\right) = -\cos(\delta^T)\mathbf{A}_{s0}^T\mathbf{A}_{s0}\Delta^s + \sin(\delta^T)\mathbf{A}_{t0}^T\mathbf{A}_{t0}\Delta^c - \cos(\delta^T)\mathbf{A}_{s0}^T\mathbf{A}_{t0}\Delta^c + \sin(\delta^T)\mathbf{A}_{t0}^T\mathbf{A}_{s0}\Delta^s \quad (305)$$

which is a $1 \times N$ matrix with a null space of dimension $N - 1$. For a cluster of 3 control moment gyros, for example, the stationary platform can be maintained by remaining on the two-dimensional stationary platform surface.

In reality, gimbals rates are integrals of gimbals accelerations and cannot be controlled directly. Assuming we have the capability to provide a desired torque to the gimbal axis, however, gimbals accelerations, $\ddot{\delta}$, can be controlled precisely. We ask then what the gimbals accelerations must be to maintain the SPC.

Differentiation of Equation (304) produces

$$\ddot{F} = \left(\frac{dF}{d\delta}\right)\dot{\delta} + \left(\frac{dF}{d\delta}\right)\ddot{\delta} \quad (306)$$

so that if we desire to hold $\ddot{F} = 0$, the gimbals accelerations may be computed by choosing gimbals accelerations such that

$$\left(\frac{dF}{d\delta}\right)\ddot{\delta} = -\left(\frac{dF}{d\delta}\right)\dot{\delta} \quad (307)$$

is satisfied. The coefficient of $\ddot{\delta}$ in Equation (307) can be computed as

$$\begin{aligned} \left(\frac{dF}{d\delta}\right) &= \dot{\delta}^T(\Delta^c\mathbf{A}_{t0} - \Delta^s\mathbf{A}_{s0})(\mathbf{A}_{s0}\Delta^s + \mathbf{A}_{t0}\Delta^c) \\ &\quad + (\cos\delta^T\mathbf{A}_{s0} + \sin\delta^T\mathbf{A}_{t0})(\mathbf{A}_{s0}\Delta^c - \mathbf{A}_{t0}\Delta^s)\text{diag}\dot{\delta} \end{aligned} \quad (308)$$

A minimum norm solution or other technique could be used to solve Equation (307), yielding gimbals accelerations which would maintain the stationary platform condition.

It is conceivable that in some instances we may be faced with a system state in which the stationary platform condition has been violated. That is

$$F \neq \frac{1}{2} \left(\frac{h}{h_{swr}}\right)^2$$

or else the rate of change of F as expressed by Equation (304) is not zero, implying that the trajectory departs the stationary platform surface. Consider a violation of the stationary platform condition where the deviation is given by

$$\Delta F = F - \frac{1}{2} \left(\frac{h}{h_{swr}} \right)^2 \quad (309)$$

To return to the stationary surface, we choose $\ddot{\delta}$ so that the second order equation

$$\ddot{F} + 2\zeta\omega_n\dot{F} + \omega_n^2\Delta F = 0 \quad (310)$$

has damped roots, thereby driving the stationary platform error exponentially back to zero. Choosing $\zeta = 1$, for example would provide critical damping, and the frequency ω_n should be selected so that a correction to the stationary platform condition occurs at a rate appropriate to the dynamical response of the spacecraft. Specifically, choosing a $\ddot{\delta}$ which satisfies

$$\left(\frac{\partial F}{\partial \delta} \right) \ddot{\delta} = - \left(\left(\frac{\partial \dot{F}}{\partial \delta} \right) + 2\zeta\omega_n \left(\frac{\partial F}{\partial \delta} \right) \right) \dot{\delta} - \omega_n^2 \left(F - \frac{1}{2} \left(\frac{h}{h_{swr}} \right)^2 \right) \quad (311)$$

will drive $\Delta F \rightarrow 0$, and return the cluster to the stationary platform condition should a deviation exist. The gimbals acceleration corrections given by Equation (311) are necessary because we do not have direct control of the gimbals rates.

5.6 Lyapunov Control with Stationary Platform Weighting

We now attempt to enforce the stationary platform condition while applying a Lyapunov control law. Since $\dot{\mathbf{h}}_c$ may contain components in the direction of \mathbf{h}_c , we seek to drive \mathbf{h}_c back to its original magnitude whenever a deviation is present. A candidate Lyapunov function based on the error in the magnitude of \mathbf{h}_c (deviation from the magnitude of \mathbf{h}) is

$$V_h = \frac{1}{4} (\mathbf{h}_c^T \mathbf{h}_c - \mathbf{h}^T \mathbf{h})^2 \quad (312)$$

Note $V_h = 0$ only when the magnitude of \mathbf{h}_c is equal to the magnitude of \mathbf{h} . The derivative of V_h is

$$\dot{V}_h = (\mathbf{h}_c^T \dot{\mathbf{h}}_c - \dot{\mathbf{h}}^T \mathbf{h}) \mathbf{h}_c^T \dot{\mathbf{h}}_c \quad (313)$$

so that we can ensure $\dot{V}_h \leq 0$ by choosing

$$\mathbf{h}_c^T \dot{\mathbf{h}}_c = k_2 (\mathbf{h}^T \mathbf{h} - \mathbf{h}_c^T \mathbf{h}_c), \quad k_2 \geq 0 \quad (314)$$

The minimum norm solution of Equation (314) is

$$\dot{\mathbf{h}}_c = k_2 (\mathbf{h}^T \mathbf{h} - \mathbf{h}_c^T \mathbf{h}_c) \frac{\mathbf{h}_c}{\mathbf{h}_c^T \mathbf{h}_c} \quad (315)$$

Now consider the ramifications of adding (315) to the control law of Equation (232) so that

$$\begin{aligned} \dot{\mathbf{h}}_c &= \mathbf{K}_1 (\boldsymbol{\omega} - \boldsymbol{\omega}_f) + k_0 \mathbf{G}^T (\mathbf{q}_f) \mathbf{q} - \mathbf{J} \dot{\boldsymbol{\omega}}_f - \boldsymbol{\omega}^\times (\mathbf{J} \boldsymbol{\omega} + \mathbf{h}_c) \\ &\quad - \frac{1}{2} \mathbf{J} (\boldsymbol{\omega} + \boldsymbol{\omega}_f) + k_2 (\mathbf{h}^T \mathbf{h} - \mathbf{h}_c^T \mathbf{h}_c) \frac{\mathbf{h}_c}{\mathbf{h}_c^T \mathbf{h}_c} \end{aligned} \quad (316)$$

which, recalling Equation (213), implies

$$\mathbf{J} \dot{\boldsymbol{\omega}} = -\mathbf{K}_1 (\boldsymbol{\omega} - \boldsymbol{\omega}_f) - k_0 \mathbf{G}^T (\mathbf{q}_f) \mathbf{q} + \mathbf{J} \dot{\boldsymbol{\omega}}_f + \frac{1}{2} \mathbf{J} (\boldsymbol{\omega}_f - \boldsymbol{\omega}) - k_2 (\mathbf{h}^T \mathbf{h} - \mathbf{h}_c^T \mathbf{h}_c) \frac{\mathbf{h}_c}{\mathbf{h}_c^T \mathbf{h}_c} \quad (317)$$

Equation (229) then becomes

$$\begin{aligned} \dot{V} &= -(\boldsymbol{\omega} - \boldsymbol{\omega}_f)^T \mathbf{K}_1 (\boldsymbol{\omega} - \boldsymbol{\omega}_f) - (\boldsymbol{\omega} - \boldsymbol{\omega}_f)^T \frac{k_2}{\mathbf{h}_c^T \mathbf{h}_c} (\mathbf{h}^T \mathbf{h} - \mathbf{h}_c^T \mathbf{h}_c) \mathbf{h}_c \\ &= -(\boldsymbol{\omega} - \boldsymbol{\omega}_f)^T \mathbf{K}_1 (\boldsymbol{\omega} - \boldsymbol{\omega}_f) - (\boldsymbol{\omega} - \boldsymbol{\omega}_f)^T \frac{k_2}{\mathbf{h}_c^T \mathbf{h}_c} ((\mathbf{J} \boldsymbol{\omega} + \mathbf{h}_c)^T (\mathbf{J} \boldsymbol{\omega} + \mathbf{h}_c) - \mathbf{h}_c^T \mathbf{h}_c) \mathbf{h}_c \\ &= -(\boldsymbol{\omega} - \boldsymbol{\omega}_f)^T \mathbf{K}_1 (\boldsymbol{\omega} - \boldsymbol{\omega}_f) - (\boldsymbol{\omega} - \boldsymbol{\omega}_f)^T \frac{k_2 \mathbf{h}_c}{\mathbf{h}_c^T \mathbf{h}_c} (\boldsymbol{\omega}^T \mathbf{J}^T \mathbf{J} \boldsymbol{\omega} + 2 \mathbf{h}_c^T \mathbf{J} \boldsymbol{\omega}) \end{aligned} \quad (318)$$

which when $\boldsymbol{\omega}_f = \mathbf{0}$, can be reduced to

$$\dot{V} = -\boldsymbol{\omega}^T \mathbf{K}_1 \boldsymbol{\omega} - \boldsymbol{\omega}^T k_2 (\mathbf{h}_c \boldsymbol{\omega}^T \mathbf{J}^T + 2 \mathbf{h}_c \mathbf{h}_c^T) \mathbf{J} \boldsymbol{\omega} \quad (319)$$

Since the first term of Equation (319) is already negative for all $\boldsymbol{\omega} \neq \mathbf{0}$, then the question of global stability with the modified control law reduces to the question of whether

$$(\mathbf{J}\boldsymbol{\omega})\mathbf{h}_c^T + 2\mathbf{h}_c\mathbf{h}_c^T = (\mathbf{J}\boldsymbol{\omega} + 2\mathbf{h}_c)\mathbf{h}_c^T \geq 0 \quad (\text{positive semidefinite}) \quad (320)$$

Since $\mathbf{J}\boldsymbol{\omega} + 2\mathbf{h}_c$ is an $N \times 1$ matrix and \mathbf{h}_c^T is $1 \times N$, then

$$\text{rank} \left((\mathbf{J}\boldsymbol{\omega} + 2\mathbf{h}_c)\mathbf{h}_c^T \right) = 1 \quad (321)$$

which implies that two of its eigenvalues are zero. Since the sum of the eigenvalues equals the trace, then the third eigenvalue must be the trace of $(\mathbf{J}\boldsymbol{\omega} + 2\mathbf{h}_c)\mathbf{h}_c^T$

$$\text{trace} \left((\mathbf{J}\boldsymbol{\omega} + 2\mathbf{h}_c)\mathbf{h}_c^T \right) = (\mathbf{J}\boldsymbol{\omega} + 2\mathbf{h}_c)^T \mathbf{h}_c \quad (322)$$

Therefore, Equation (320) is satisfied if and only if

$$(\mathbf{J}\boldsymbol{\omega} + 2\mathbf{h}_c)^T \mathbf{h}_c \geq 0 \quad (323)$$

The projection of $\mathbf{J}\boldsymbol{\omega} + 2\mathbf{h}_c$ onto \mathbf{h}_c could only be negative if $\|\mathbf{J}\boldsymbol{\omega}\| > \|2\mathbf{h}_c\|$. Therefore, a sufficient condition to satisfy Equation (323) is

$$\|\mathbf{J}\boldsymbol{\omega}\| \leq 2\|\mathbf{h}_c\| \quad (324)$$

For low angular velocities or large cluster momentum, Equation (324) will be satisfied guaranteeing the closed loop stability of the rigid body/GMW system when using the control law given by Equation (316).

The control law of Equation (316) does allow for deviation from the SPC to satisfy the kinematics, but also attempts to return the vector \mathbf{h}_c to the stationary platform value when a deviation does occur. The aggressiveness of the system in attempting to maintain the SPC is determined by k_2 . When $k_2 = 0$, the controller is guaranteed stable, but makes no attempt to maintain the SPC.

We make one additional observation. Since it is only required that $k_2 \geq 0$, it is permissible to allow it to vary. For example, using a variable k_2 such that

$$k_2 = \tilde{k}_2(1 - q_0), \quad \tilde{k}_2 > 0 \quad (325)$$

ensures that $k_2 \geq 0$ and relaxes the stationary platform constraint just as the body arrives at the destination quaternion (assuming $\mathbf{q}_f = [1 \ 0 \ 0 \ 0]^T$)².

5.7 Summary

In this chapter, we showed that control of a spacecraft using a momentum exchange device can be simplified by considering the rate of change of cluster momentum, $\dot{\mathbf{h}}_c$, as the control input. Once the necessary $\dot{\mathbf{h}}_c$ is determined, the input torques which produce the desired $\dot{\mathbf{h}}_c$ must be determined. A Lyapunov control law developed by Oh and Vadali which effects closed loop reorientations of a spacecraft is translated to the notation of this dissertation.

The problem of control moment gyro singularities is discussed, and the singular value decomposition is used to develop a singular direction avoidance law which decreases the torque error near a singularity. This new law, along with modification to the singularity avoidance parameter permits smoother reorientations near singular conditions. Some examples demonstrating these improvements are presented.

Finally, the stationary platform maneuver introduced by Hall for gyrostats is shown to have a parallel in the case of a spacecraft with a control moment gyro cluster. A method of reorienting a spacecraft while remaining arbitrarily close to the stationary platform surface is presented.

We now turn to numerical simulations which demonstrate the effectiveness of these control law improvements in the reorientations of spacecraft with flexible appendages.

²For any reorientation given by initial quaternions \mathbf{q}_0 and final quaternions \mathbf{q}_f , a transformation can be made such that $\mathbf{q}_f = [1 \ 0 \ 0 \ 0]^T$.

6. Simulation Results

In this section, the control laws previously developed are applied to two flexible spacecraft to examine their effectiveness. The maneuvers can be qualitatively compared by comparing the histories of the quaternions and angular velocities. They can also be quantitatively compared using cost functions which are dependent on such parameters as control inputs, total time for reorientation, and the deflections of the appendages.

We begin by examining a relatively small spacecraft with very light flexible appendages. The flexible appendages are chosen so that they have negligible impact on the dynamics of the reorientation. The effect of the reorientation profile on the flexible modes is investigated.

A mathematical model of the Hubble Space Telescope will also be developed. This development will demonstrate how the Euler-Bernoulli appendage model could be applied to a real spacecraft. The Hubble example also gives a feel for how the control laws apply to a spacecraft of a different scale than the first.

Before we take up the details of the flexible appendages, we should comment on the validity of the Lyapunov control law for the spacecraft/flexible appendage system. Derivation of the control law for the system began with Equation (210) and assumed perfect knowledge of $\dot{\omega}$ from Equation (213). This perfect knowledge of $\dot{\omega}$ is necessary to guarantee stability. If the appendages are small (or do not have a major effect on the system response), then Equation (213) is a good approximation. We should keep in mind, however, that stability is no longer guaranteed for the spacecraft with flexible appendages.

6.1 Reorientations of a Small Flexible Satellite

6.1.1 The Small Satellite Model. We again consider the small satellite model used for the examples of Chapter 5. Here, however, we reduce the number of wheels to only three, and orient them along the principal axes. The physical data for the model is given in Table 4. Three one meter long appendages are attached, each allowing flexure in a principal direction. The stiffness product, (EI) , is selected to provide a first mode

period of approximately 10 seconds. Note that the appendages are very light and do not significantly influence the dynamics of the satellite.

Table 4 Physical Data for the Small Flexible Satellite

Item	Value	Units
m	100	kg
\mathbf{I}	$\text{diag}\{86.215, 85.070, 113.565\}$	$kg\text{-}m^2$
\mathbf{I}_{sw}	$\text{diag}\{0.05, 0.05, 0.05\}$	$kg\text{-}m^2$
\mathbf{b}_1	$[1, 0, 0]^T$	m
\mathbf{b}_2	$[0, 1, 0]^T$	m
\mathbf{b}_3	$[0, 0, 1]^T$	m
\mathbf{r}_{01}	$[1, 0, 0]^T$	m
\mathbf{r}_{02}	$[0, 1, 0]^T$	m
\mathbf{r}_{03}	$[0, 0, 1]^T$	m
$\hat{\mathbf{n}}_1$	$[0, 0, 1]^T$	
$\hat{\mathbf{n}}_2$	$[1, 0, 0]^T$	
$\hat{\mathbf{n}}_3$	$[0, 1, 0]^T$	
ρ_1, ρ_2, ρ_3	0.1	kg/m
l_1, l_2, l_3	1.0	m
$(EI)_1, (EI)_2, (EI)_3$	0.0031935	$N\text{-}m^2$

6.1.2 Assumed Mode Shapes. The assumed modes method developed in Chapter 4 will be our tool for discretizing the flexible modes. For the assumed mode shapes, we choose comparison functions which are the actual solutions for an Euler-Bernoulli beam cantilevered in an inertially fixed object. Of course, the rigid spacecraft to which we attach the flexible appendages is not inertially fixed, and the functions described here are not the exact solutions. To represent the first mode of the appendage on a free floating body exactly would likely require an infinite number of assumed modes. These functions do represent the exact modal shapes as the mass of the spacecraft approaches infinity. We therefore expect that when the mass of the appendage is small with respect to the rigid hub, the mode shapes will converge rapidly (i.e. the first few mode shapes will closely represent the true solution).

The exact solution for the cantilevered beam is presented by several authors (see Craig [13] or Junkins and Kim [25]). The i -th mode shape, $\psi_i(x)$, for a beam of length l is

$$\psi_i(x) = \cosh(\lambda_i x) - \cos(\lambda_i x) - c_i(\sinh(\lambda_i x) - \sin(\lambda_i x)) \quad (326)$$

where

$$c_i = \frac{\cosh(\lambda_i l) + \cos(\lambda_i l)}{\sinh(\lambda_i l) + \sin(\lambda_i l)} \quad (327)$$

and the eigenvalues, λ_i , are solutions of the characteristic equation which results from imposing the boundary conditions given by Equation (165),

$$\cos \lambda l \cosh \lambda l + 1 = 0 \quad (328)$$

The first four solutions of Equation (328) are approximately

$$\begin{aligned} \lambda_1 l &= 1.8751 \\ \lambda_2 l &= 4.6941 \\ \lambda_3 l &= 7.8548 \\ \lambda_4 l &= 10.996 \end{aligned} \quad (329)$$

with corresponding modal frequencies

$$\omega_i = \frac{(\lambda_i l)^2}{l^2} \sqrt{\frac{EI}{\rho}} \quad (330)$$

It is worth noting that the second modal frequency is about six times the first modal frequency. The first four mode shapes are plotted in Figure 8.

6.1.3 Momentum Wheels. The cluster data for the small spacecraft with momentum wheels is in Table 5. The utility of the stationary platform maneuver is better demonstrated by setting the original spin momenta to higher values than in the example of Chapter 5.

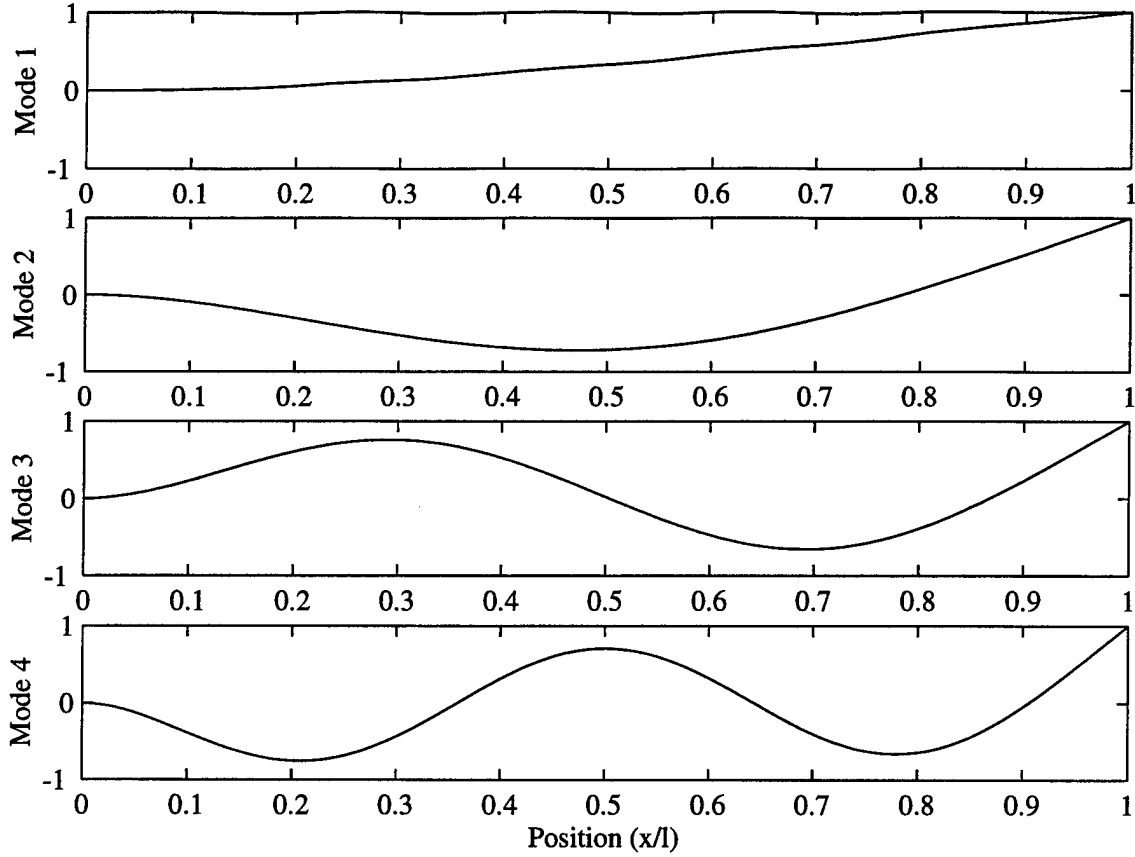


Figure 8 Cantilevered Beam Mode Shapes

To demonstrate the gyric effects of reorientations using a cluster of momentum wheels, we examine the effects of changing the spin momenta in a linear fashion between the initial values and the unique final values. Since the angular momentum in the inertial coordinate frame is constant, the final value of angular momentum in the body frame is

$$\mathbf{h}_{final} = \mathbf{C}_{final} \mathbf{C}_0^T \mathbf{h}_0 \quad (331)$$

so that we choose

$$\dot{\mathbf{h}}_c = \frac{\mathbf{h}_{final} - \mathbf{h}_0}{t_{man}} \quad (332)$$

where t_{man} is the desired maneuver time.

In the case of the stationary platform maneuver, we desire to maintain the magnitude of \mathbf{h}_c constant while changing its direction steadily to the final value \mathbf{h}_{final} . The angular

Table 5 Cluster Data for the Small Satellite with Momentum Wheels

Item	Value	Units
\mathbf{I}_{sw}	$\text{diag}\{0.05, 0.05, 0.05\}$	$kg\cdot m^2$
\mathbf{a}_{s1}	$[1, 0, 0]^T$	
\mathbf{a}_{s2}	$[0, 1, 0]^T$	
\mathbf{a}_{s3}	$[0, 0, 1]^T$	
\mathbf{h}_{swa0}	$[7.2, 7.2, 7.2]^T$	$kg\cdot m^2/sec$

change of the cluster angular momentum in the body frame is given by

$$\theta_{spm} = \arccos\left(\frac{\mathbf{h}_0^T \mathbf{h}_{final}}{\|\mathbf{h}_0\| \|\mathbf{h}_{final}\|}\right) \quad (333)$$

We define a plane in the body coordinate frame which contains \mathbf{h}_c and \mathbf{h}_{final} by a normal vector

$$\hat{\mathbf{e}}_{spm} = \frac{\mathbf{h}_c \times \mathbf{h}_{final}}{\|\mathbf{h}_c \times \mathbf{h}_{final}\|} \quad (334)$$

The cluster momentum \mathbf{h}_c will vary along a constant arc from \mathbf{h}_0 to \mathbf{h}_{final} if we maintain

$$\dot{\mathbf{h}}_c = \hat{\mathbf{e}}_{spm} \times \mathbf{h}_c \left(\frac{\theta_{spm}}{t_{man}}\right) \quad (335)$$

This cluster rate will maintain the stationary platform condition for any momentum exchange device.

Figures 9 through 11 show the results of the direct and stationary platform maneuvers for the small satellite when the cluster momentum is reoriented about the $(1, -2, 3)$ body axis through an angle of 2.856 radians. This corresponds to initial and final quaternions given by

$$\mathbf{q}_0 = \begin{bmatrix} 0.1423 \\ 0.2645 \\ -0.5291 \\ 0.7936 \end{bmatrix} \quad \mathbf{q}_f = \begin{bmatrix} 1 \\ 0 \\ 0 \\ 0 \end{bmatrix} \quad (336)$$

We set $t_{man} = 500$ seconds and show the dynamics for an extra 100 seconds after completion of the maneuver. Note in Figure 9 the drastic difference between the angular velocities (and consequently, the quaternion histories). While the rotor momenta follow only slightly

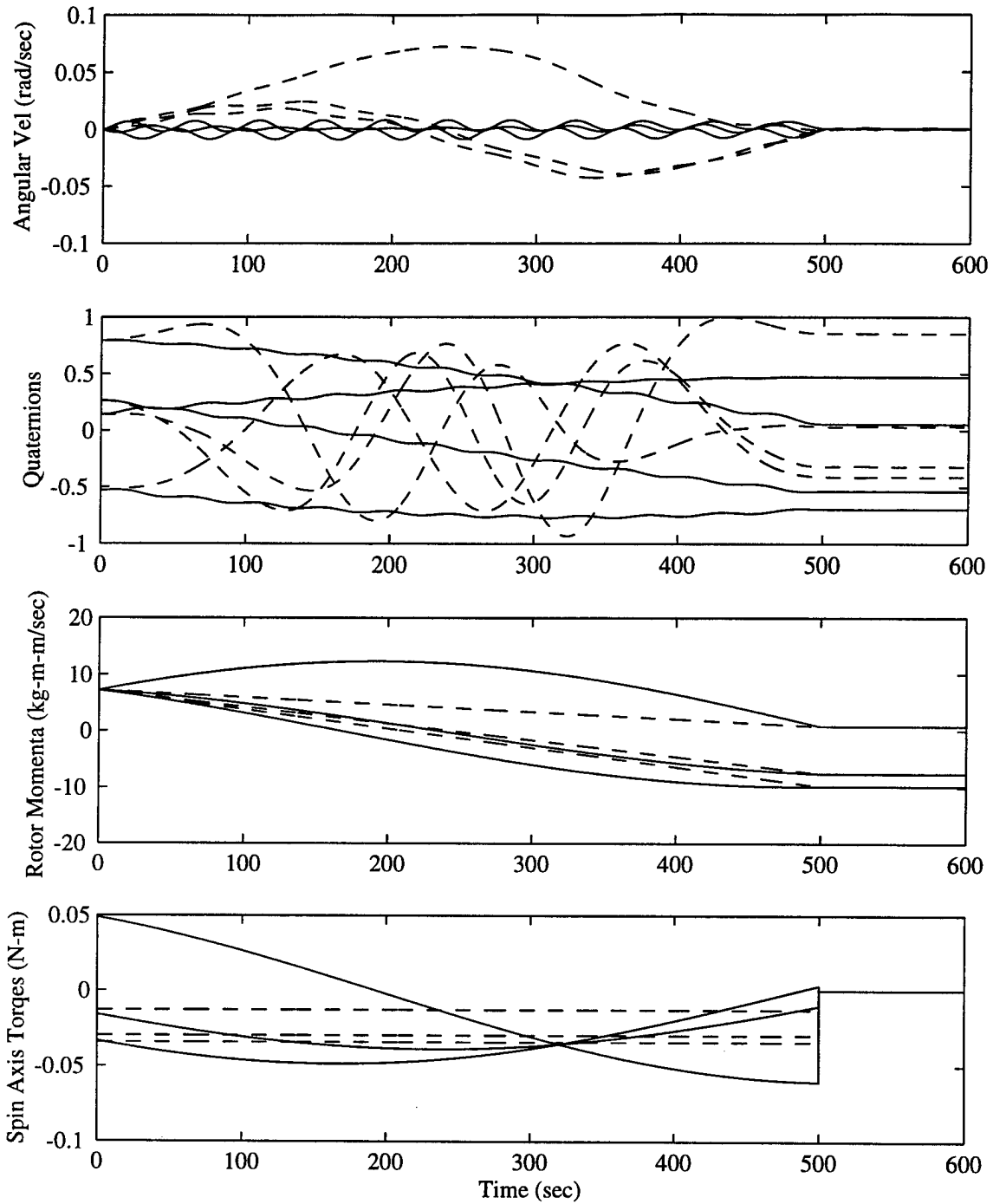


Figure 9 Reorientation Parameters for Stationary Platform (—) and Direct (---) Maneuvers Using Momentum Wheels

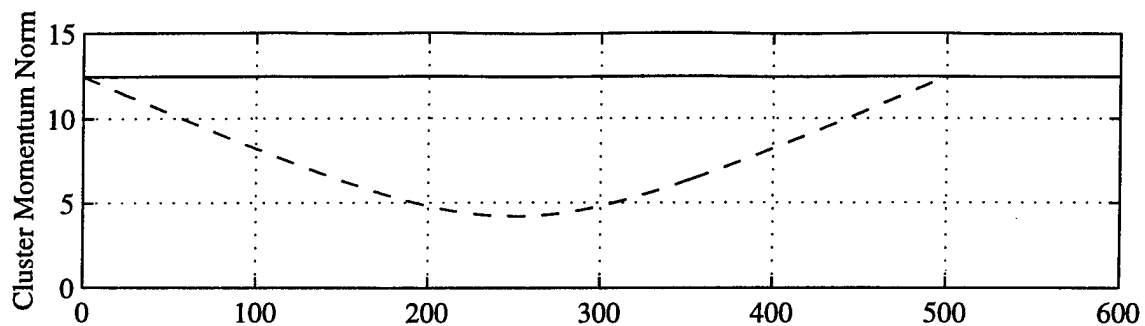


Figure 10 Cluster Norms for the Stationary Platform Maneuver (—) and Direct Maneuver (---) Using MWs

different profiles, the resultant reorientation is much better behaved for the stationary platform maneuver.

It is this behavior during the open-loop stationary platform maneuver which leads us to investigate its utility for reorientations of flexible structures. Neither the direct nor the stationary platform maneuver, however, accommodate kinematic considerations. Even should we be lucky enough to arrive at the final orientation with zero angular momentum in the body (and hence zero angular velocity), the kinematics are only satisfied to within a rotation about the angular momentum vector.

A comparison of the cluster norms is in Figure 10 for the direct and stationary platform maneuvers. The direct maneuver in particular demonstrates a large deviation from a constant norm. Since the magnitude of the total angular momentum of the system is constant (and equal to the initial cluster norm), a large deviation implies a large transfer of momentum to the body, which is evident in the quaternion history.

Because the excitations of the second assumed mode are generally several orders of magnitude smaller than those of the first mode, the appendage oscillations are very closely approximated by carrying only the first mode during the integration. As is evident from the appendage modal displacements shown in Figure 11, both maneuvers cause oscillations at the 0.1 Hz first modal frequency. The direct maneuver, however, produces higher deflections toward the middle of the maneuver profile. A plot of the total potential energy in the Euler-Bernoulli beams is the bottom plot of Figure 11. The total potential energy

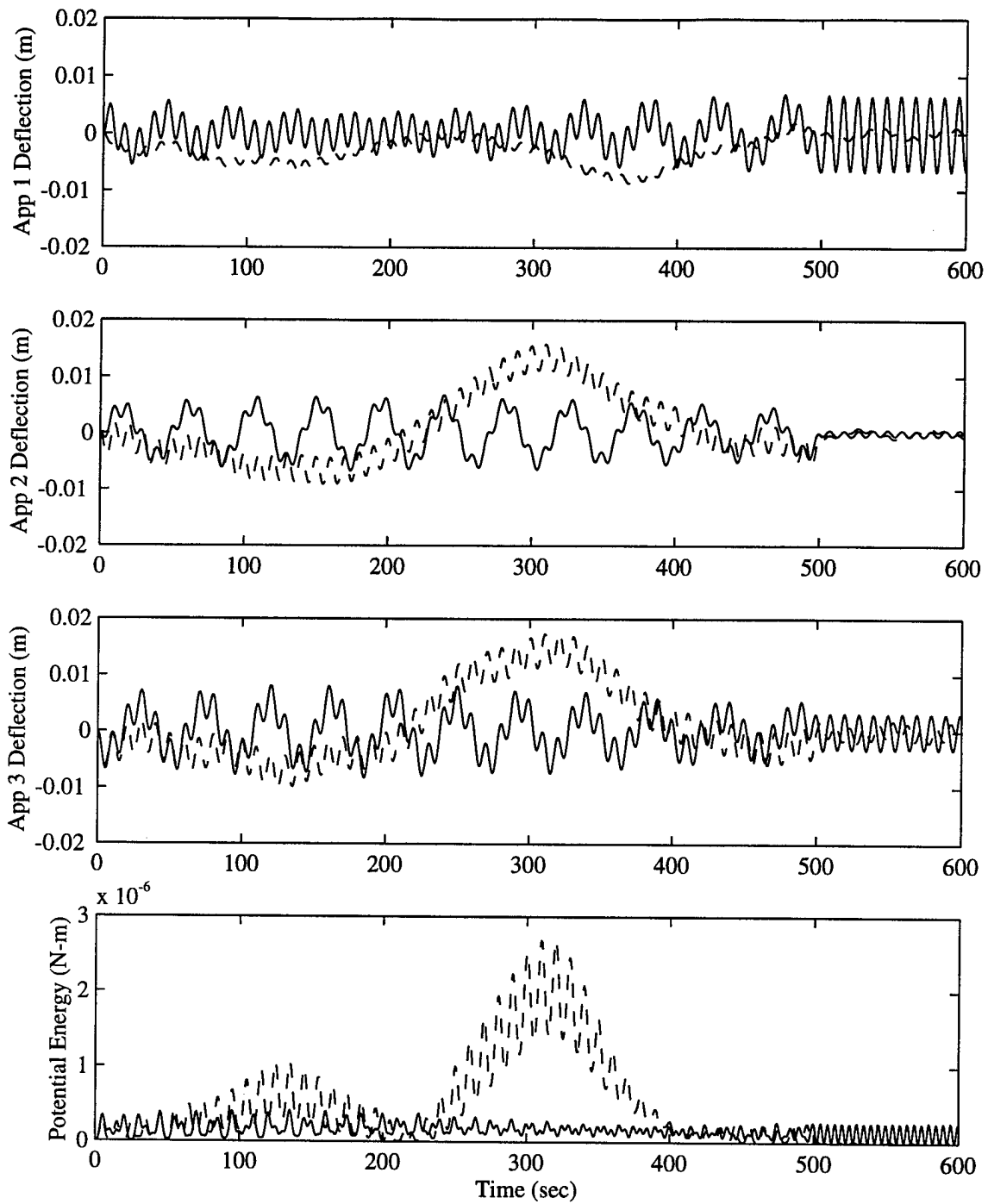


Figure 11 Appendage Excitations for Stationary Platform (—) and Direct (---) Maneuvers Using MWs

is useful as a scalar comparison of the appendage excitation for different maneuvers. Note that in this case, the total potential energy during the direct maneuver is generally higher than for the stationary platform maneuver.

Figures 12 and 13 show the results of a maneuver using the Lyapunov control law given by Equations (234) and (235), and the same law with the stationary platform weighting of Equation (315). The closed-loop law assumes knowledge of the inertia matrix. It also assumes perfect knowledge of $\dot{\omega}$, which can be computed for the rigid body, but not so simply for a flexible structure. It might be possible to measure it in the case of a flexible spacecraft. The gains for the Lyapunov maneuver were selected to accomplish the maneuver in roughly the same time as the direct and stationary platform maneuvers.

Because the Lyapunov maneuver begins the reorientation so abruptly (maximum torque is commanded at $t = 0$), most of the appendage oscillations are a result of the step torque command at initiation. These oscillations tend to obscure the benefits resulting from the new control laws. We therefore add a smoothing term to the torque commanded by the Lyapunov law. The cubic given by

$$\begin{aligned} k_{sm} &= 3 \left(\frac{t}{t_r} \right)^2 - 2 \left(\frac{t}{t_r} \right)^3, & 0 \leq t < t_r \\ k_{sm} &= 1, & t \geq t_r \end{aligned} \quad (337)$$

smoothly transitions from 0 to 1 over the period $0 \leq t \leq t_r$ with zero slope at $t = 0$ and $t = t_r$. We should point out that a variable coefficient multiplying the control law given by Equation (316) no longer guarantees that the Lyapunov function rate is negative semidefinite. When $t \geq t_r$, however, k_{sm} is again constant and the global asymptotic stability of the closed loop system (for the rigid body case) is once again guaranteed.

For these maneuvers, the angular velocity histories are really quite different, but it is difficult (based on ω) to choose the better maneuver. It is apparent from the quaternion history that the spacecraft takes a bit longer to achieve the desired final orientation when the stationary platform weighting is used. The plots of rotor momenta and spin axis torques show the slight differences in the control history.

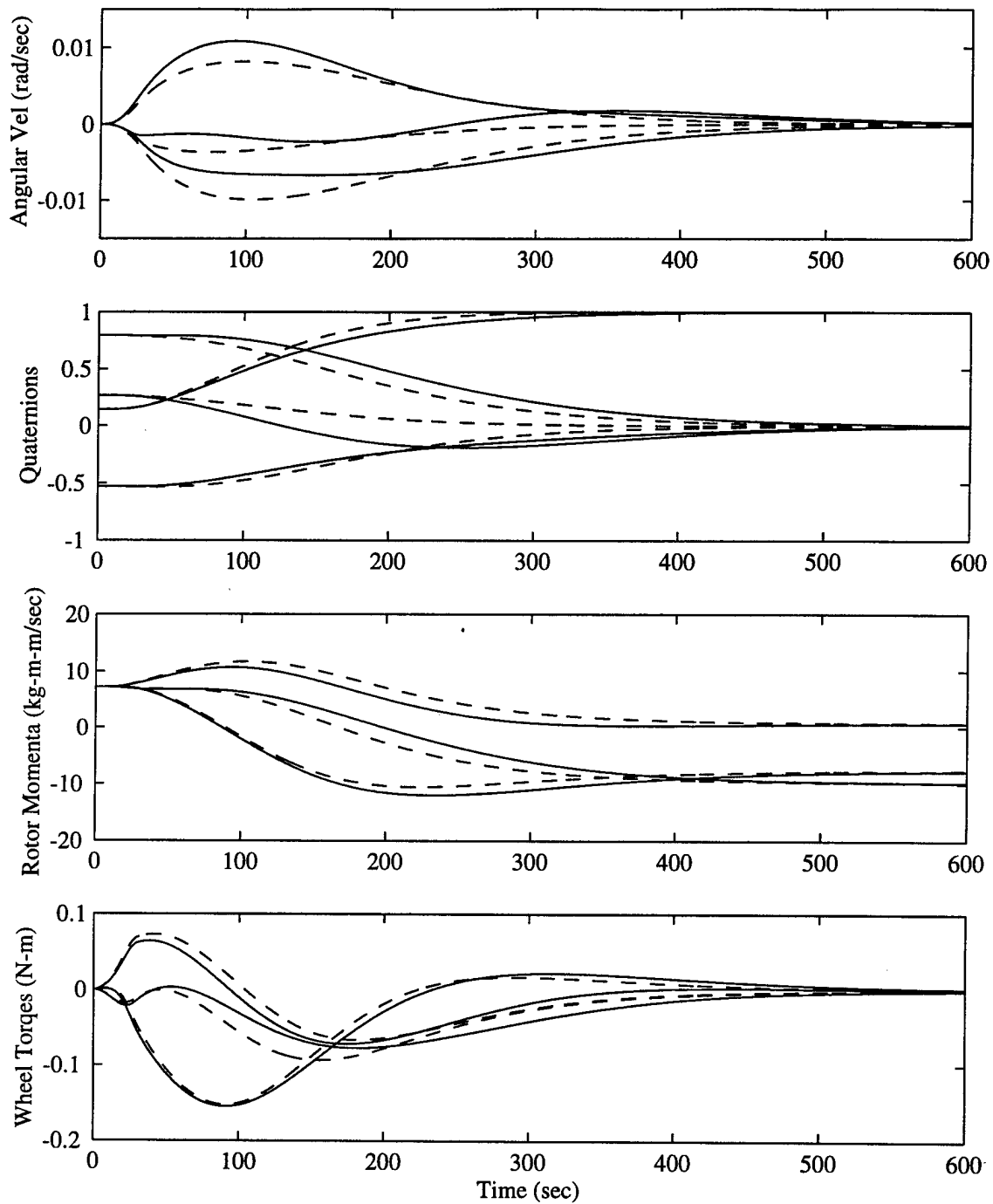


Figure 12 Reorientation Parameters for Lyapunov Maneuver With (—) and Without (---) Stationary Platform Weighting Using MWs

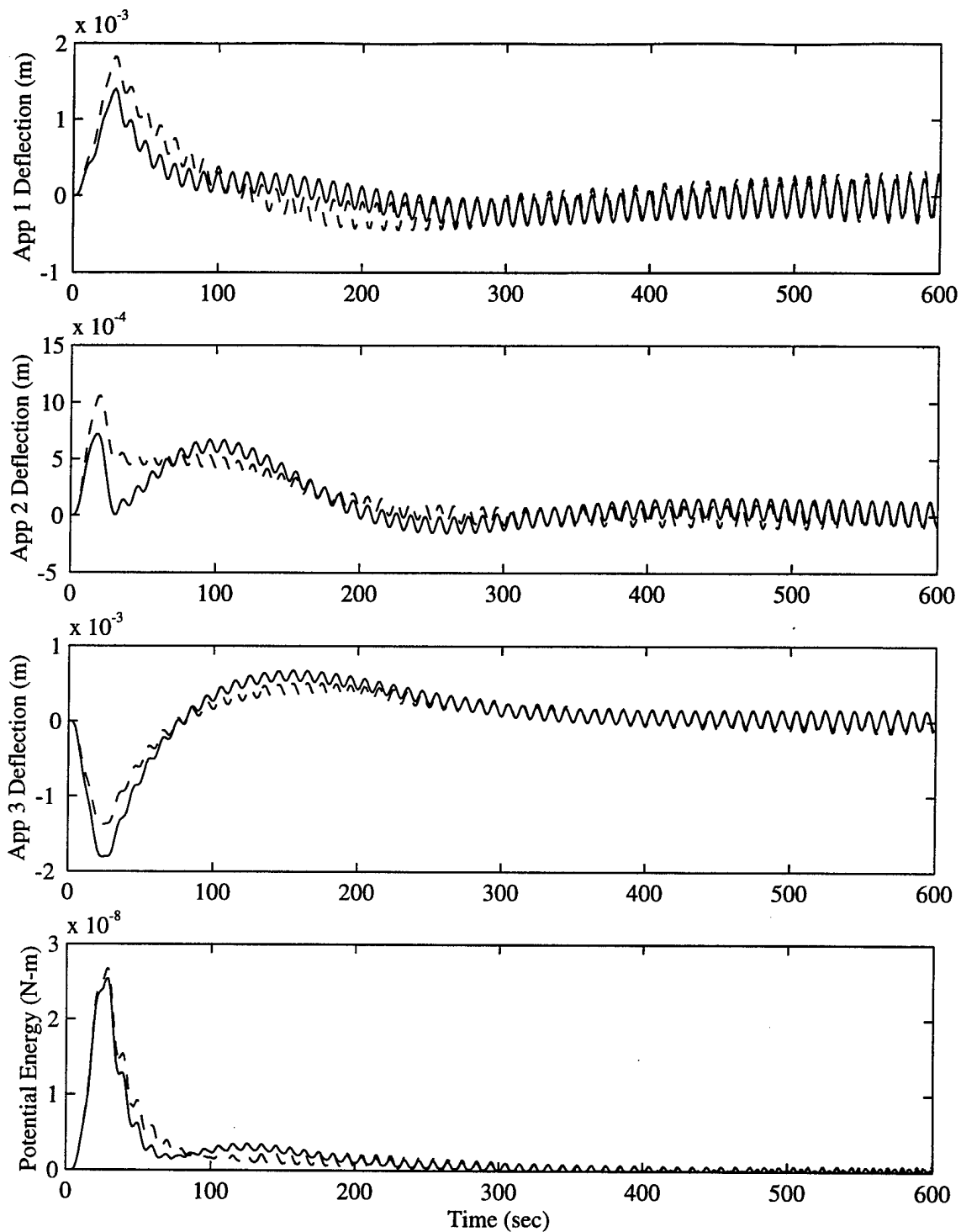


Figure 13 Appendage Excitations for Lyapunov Maneuver With (—) and Without (---) Stationary Platform Weighting Using MWs

Figure 13 presents the modal deflections of the appendages, along with a potential energy plot. Note that using the stationary platform weighting decreases the maximum deflection of the first two appendages, but increases the maximum deflection of the third appendage. The decrease in peak potential energy is only slight when the stationary platform weighting is used. It is not apparent that the stationary platform weighting provides a significant benefit for the spacecraft with momentum wheels.

6.1.4 Control Moment Gyros. A CMG cluster presents different challenges in the reorientation problem. We investigate the effects of applying the stationary platform condition for a CMG cluster to determine whether the behavior of a system with a CMG cluster is similar to that of a system with momentum wheels.

Changing the cluster momentum in the manner of Equation (332) may be impossible for a cluster of only three CMGs for reasons to be discussed subsequently. A direct maneuver more appropriate for the mechanization of control moment gyros is variation of the gimbal angles between initial and final values in a linear fashion. That is, given the final gimbal angles δ_{final} and the initial gimbal angles δ_0 , a direct maneuver for CMGs uses the law

$$\dot{\delta} = \frac{\delta_{final} - \delta_0}{t_{man}} \quad (338)$$

Execution of the stationary platform maneuver for the CMG cluster makes use of Equation (335) and an appropriate CMG control law (such as the SR or SDA law) to generate the desired $\dot{\mathbf{h}}_c$.

The stationary platform maneuver for the CMG cluster can be accomplished provided the initial cluster momentum lies inside the external momentum envelope for the cluster. For example, the cluster momentum envelope for a set of three orthogonal CMGs reaches a maximum of $\sqrt{6}h_{swr}$. (See Appendix D for a discussion of the momentum envelope of an orthogonal CMG cluster.) No component of the cluster momentum can be greater than $2h_{swr}$, since one of the three CMGs can only contribute in the plane orthogonal to that direction. In fact, the maximum *on* a principal axis is h_{swr} , since if the two non-orthogonal CMGs point along the axis, the orthogonal wheel always provides an off-axis component.

A stationary platform maneuver, therefore, using three orthogonal CMGs may not be possible when the cluster momentum is greater than h_{swr} .

Table 6 Cluster Data for Small Satellite with CMGs

Item	Value	Units
\mathbf{I}_{sw}	diag{0.05, 0.05, 0.05}	$kg\text{-}m^2$
\mathbf{I}_{tw}	diag{0.03, 0.03, 0.03}	$kg\text{-}m^2$
\mathbf{I}_{tg}	diag{0.01, 0.01, 0.01}	$kg\text{-}m^2$
$\mathbf{I}_{sg}, \mathbf{I}_{gg}$	diag{0, 0, 0}	$kg\text{-}m^2$
\mathbf{a}_{s10}	[1, 0, 0] ^T	
\mathbf{a}_{s20}	[0, 1, 0] ^T	
\mathbf{a}_{s30}	[0, 0, 1] ^T	
\mathbf{a}_{g1}	[0, 1, 0] ^T	
\mathbf{a}_{g2}	[0, 0, 1] ^T	
\mathbf{a}_{g3}	[1, 0, 0] ^T	
\mathbf{h}_{swr}	[7.2, 7.2, 7.2] ^T	$kg\text{-}m^2/sec$

The CMG cluster data for the small satellite is in Table 6. The results of direct and stationary platform maneuvers for the small satellite with CMGs are presented in Figure 14. We note from the angular velocity and quaternion history that, as for the momentum wheel case, the stationary platform maneuver for a cluster of CMGs is a considerable improvement over the direct maneuver. For this example, the gimbal rates were selected by using the actual inverse and permitting large gimbal rates to occur.

Whereas use of Equation (335) to maintain the stationary platform surface works perfectly in the case of momentum wheels, the second order effect of driving gimbal accelerations to achieve gimbal rates permits a deviation from the stationary platform surface in the CMG case, especially during periods of high gimbal rates commands. Just how closely the actual gimbal rates match the desired rates is determined by the gain \mathbf{K}_δ of Equation (244). Once the cluster momentum is in error, the control law of Equation (335) makes no attempt to correct \mathbf{h}_c to its original value. Addition of the gimbal acceleration corrections given by Equation (311) allows for a return to the desired cluster norm when a deviation does occur.

Figure 15 shows a comparison of the cluster norms and singular values for the direct and stationary platform maneuvers. It is evident that the cluster norm does remain

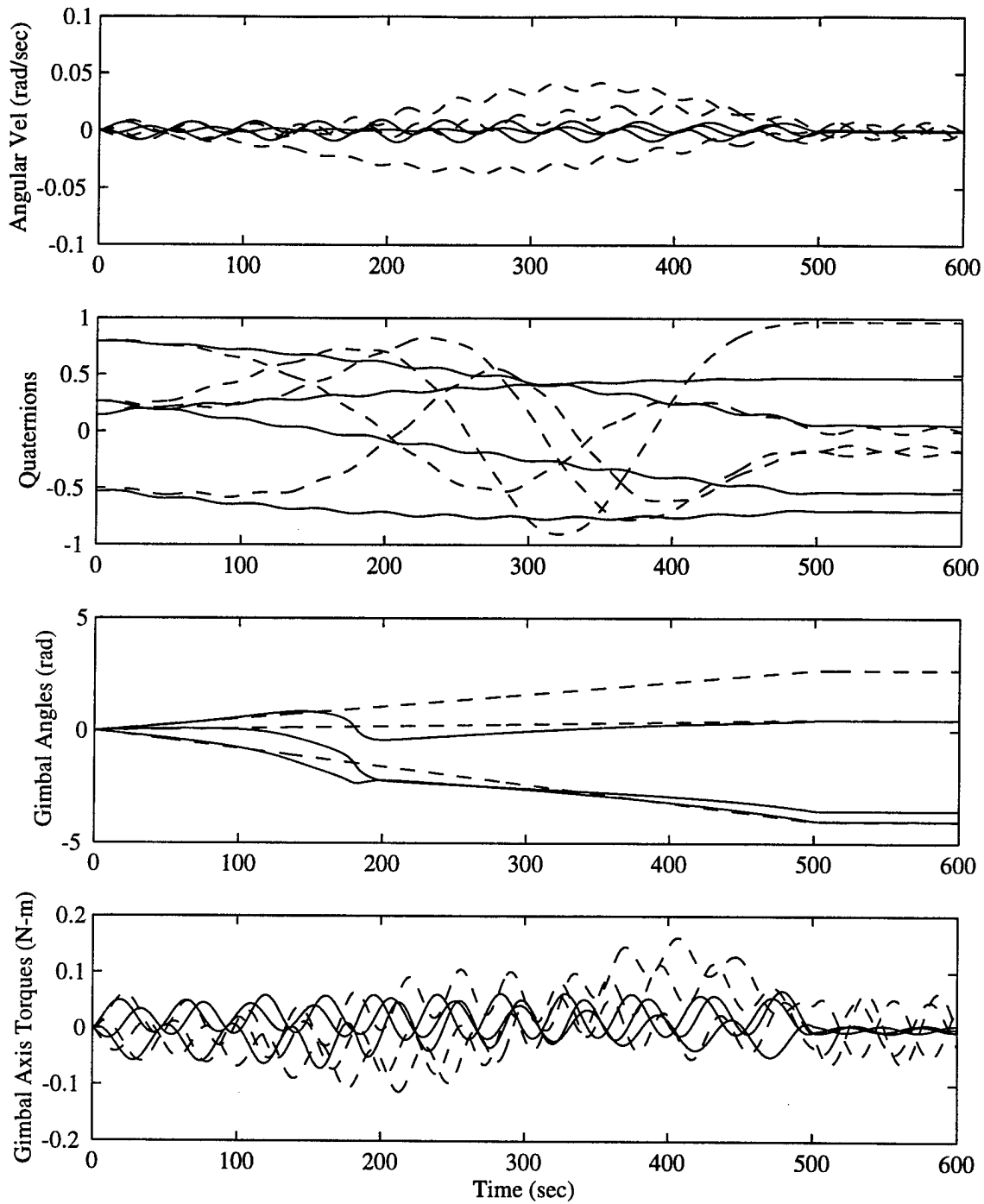


Figure 14 Reorientation Parameters for Stationary Platform (—) and Direct (---) Maneuvers Using CMGs

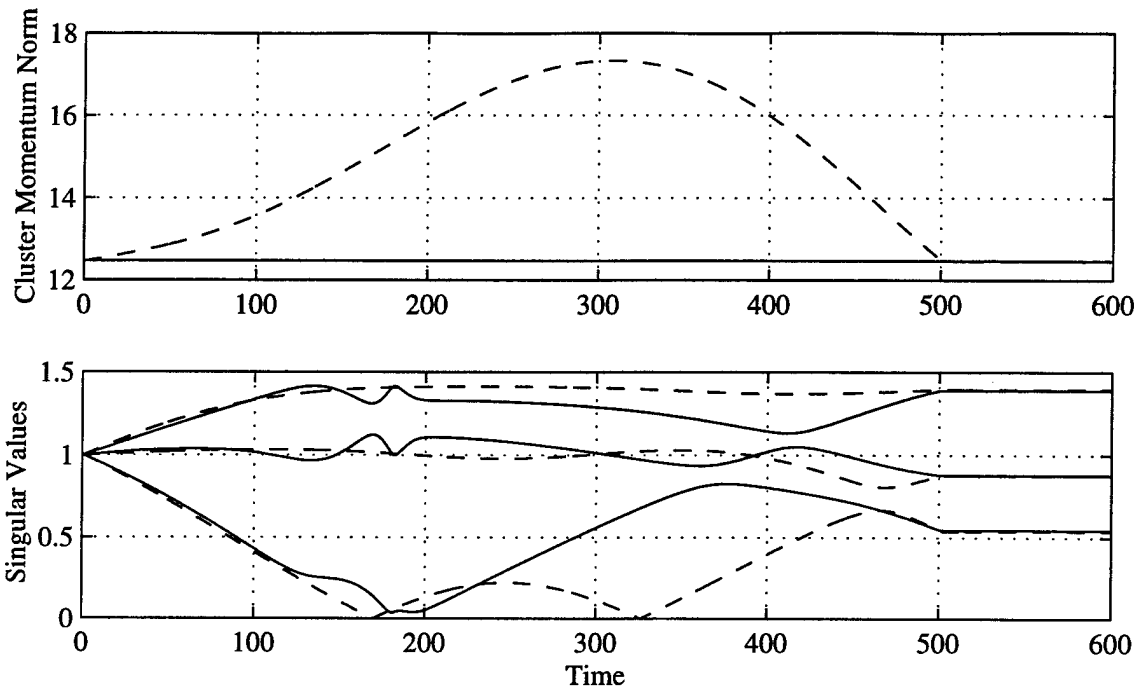


Figure 15 Cluster Norms and Singular Values for the Stationary Platform (—) and Direct Maneuvers (---) Using CMGs

constant during the stationary platform maneuver, whereas a large deviation from the stationary platform condition occurs during the direction maneuver. This large deviation implies that a significant amount of angular momentum has been transferred to the body of the spacecraft. Note also that the direct maneuver passes through two singularities (evident by a singular value going to zero), whereas the stationary platform maneuver approaches but does not actually reach a singularity. Appendage oscillations for the CMG stationary platform and direct maneuvers display the same characteristics as in the momentum wheel case.

We now present a comparison of four different control laws discussed in this dissertation for the small flexible satellite with the CMG cluster. Each maneuver is accomplished in approximately the same time. The four cases are:

1. Lyapunov control law only with gimbals rates computed by direct inversion of the \mathbf{D} matrix. Note that this will result in high gimbals rates near a singularity of the cluster ($k_0 = 0.35$).
2. Lyapunov law using the singularity-robust (SR) method for calculation of the gimbals rates. We use the law exactly as proposed by Oh and Vadali [42] ($k_0 = 0.35$, $\alpha_0 = 0.1$).
3. Lyapunov law using direct inversion for gimbals rates, but using stationary platform weighting ($k_0 = 0.35$, $\tilde{k}_2 = 0.1$, $\zeta = 1.0$, $\omega_n = 0.02\pi$).
4. Lyapunov law using the singular direction avoidance (SDA) method only ($k_0 = 0.35$, $\alpha_0 = 0.5$, $k_\sigma = 10$).

In all cases, the inputs were smoothed using the cubic smoothing function with $t_r = 20$ seconds.

The quaternion and gimbals angle histories for the four laws are presented in Figure 16. Note that all maneuvers are accomplished at approximately the same rate. The gimbals angle histories, however, are quite different during the maneuver. Note especially the rapid changes for Cases 1 and 2, whereas Cases 3 and 4 result in much smoother gimbals motion.

The modal deflections are presented in Figure 17, and it is evident that the different control laws produce significant differences in the magnitude of the oscillation. All of the control laws show a pronounced increase in vibration at approximately the 50 second point. This may be explained by noting the first plot of Figure 18, which shows the singular values of the CMG cluster during the reorientation. Note that Cases 1, 2, and 4 all become singular between 40 and 50 seconds. Case 3, the maneuver with stationary platform weighting, actually avoids the singularity. The singularity in this case is an external singularity, which is avoided by keeping the cluster momentum inside the external cluster envelope. It is interesting to note, however, that although Case 4 (the SDA law) does pass through a singularity, the gimbals rates remain very smooth.

The benefits of the proposed control laws are most vividly depicted in potential energy plot of Figure 18. Note especially the improvement resulting from the SDA law

(Case 4) over the SR law (Case 2), as well as the improvement stationary platform weighting (Case 3) provides to the basic Lyapunov control law (Case 1).

6.2 Reorientations of a Flexible Hubble Space Telescope

Of course, before actually flying the control laws proposed in this dissertation, simulation of their effects on the candidate spacecraft need to be numerically evaluated. In this section, we demonstrate the application of the mathematical models developed here to the Hubble Space Telescope with a control moment gyro cluster. We model the mass and inertia of the Hubble as closely as possible, and choose Euler-Bernoulli beams which represent the out-of-plane and in-plane bending of the two solar arrays. The in-plane bending stiffness is chosen to generate a first modal frequency of 0.4 Hz, and the out-of-plane stiffness to represent the lowest frequency mode at 0.1 Hz [40]. The physical data for the flexible model are presented in Table 7.

Because the reaction wheels on the Hubble are relatively small, we assign to them a larger momentum. Using the data for the actual wheels, the maneuvers are restricted to fairly slow rates. Slow maneuvers prove to be uninteresting from the viewpoint of structural excitations. The momenta and wheel sizes are set at 10 times the actual Hubble values. The zero gimbal angle spin axes are the actual reaction wheel spin axes of the Hubble. A gimbal axis is selected to represent a typical pyramid scheme. The cluster data are in Table 8.

The speed of the reorientations using CMGs is much faster than a typical Hubble reorientation. As is evident from the top plot of Figure 19, the spacecraft approaches the target quaternions in less than two minutes. The initial gimbal angles are selected so that the platform already possesses some angular momentum. The bottom plot shows the cluster norm histories. Whereas the cluster norm can be held as close to fixed as is desired by increasing the gain k_2 of Equation (315), the reorientation time increases with increasing gain.

Appendages 1 through 4 demonstrate almost identical oscillations, whereas appendages 5 and 6 are also similar. Modal deflections are shown in Figure 20. Keep in mind

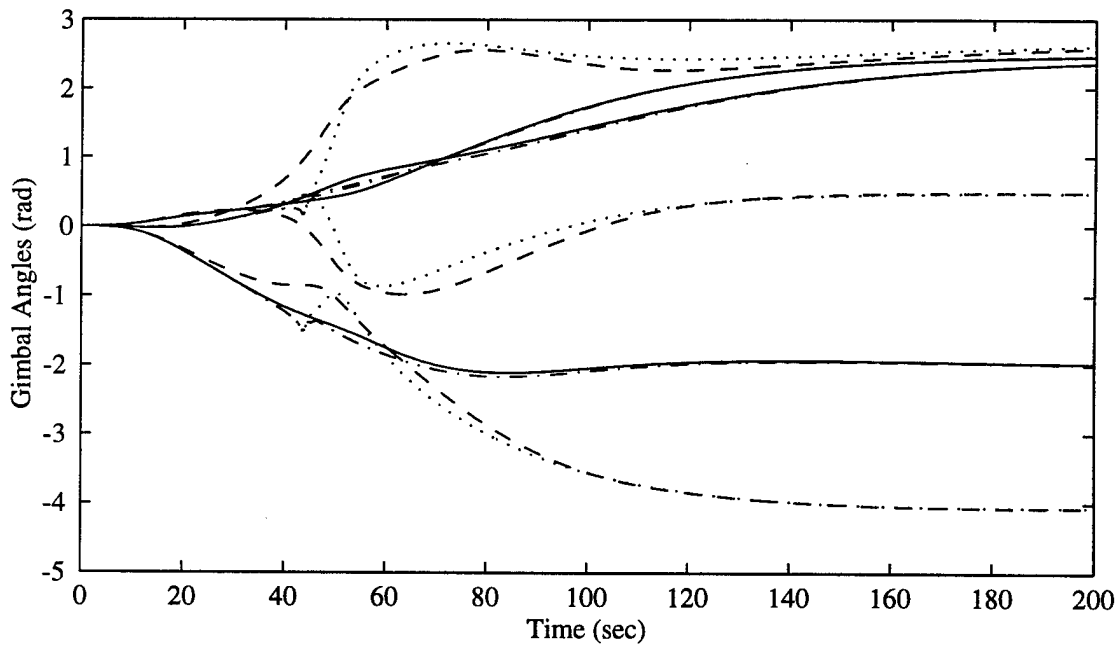
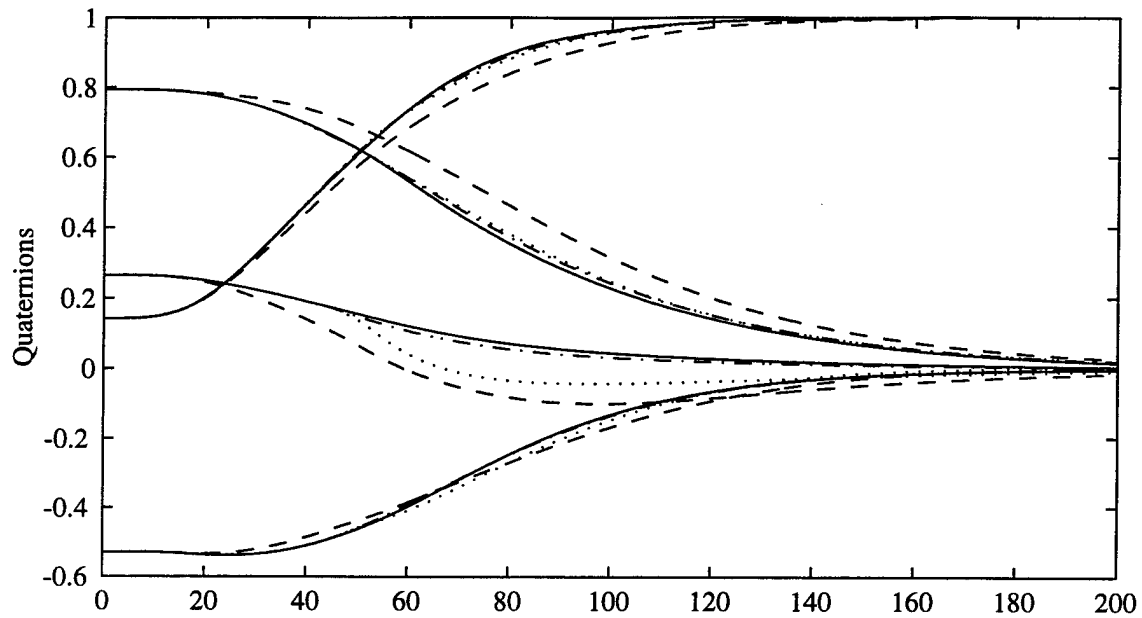


Figure 16 Reorientation Parameters for Four CMG Control Laws
 Case 1 (\cdots), Case 2 ($- \cdot -$), Case 3 ($---$), Case 4 ($—$)

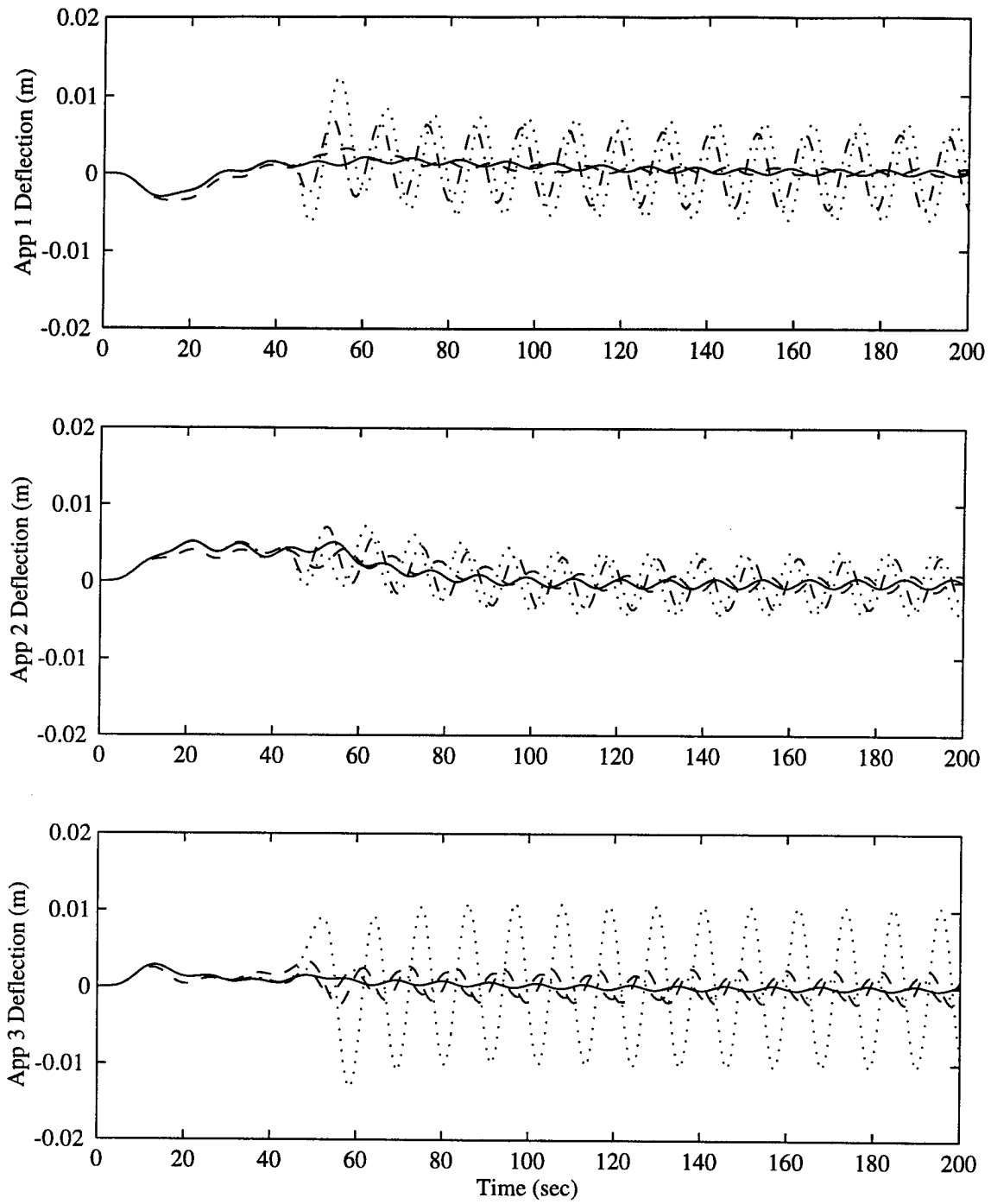


Figure 17 Modal Responses for Four CMG Control Laws
 Case 1 (···), Case 2 (- · -), Case 3 (---), Case 4 (—)

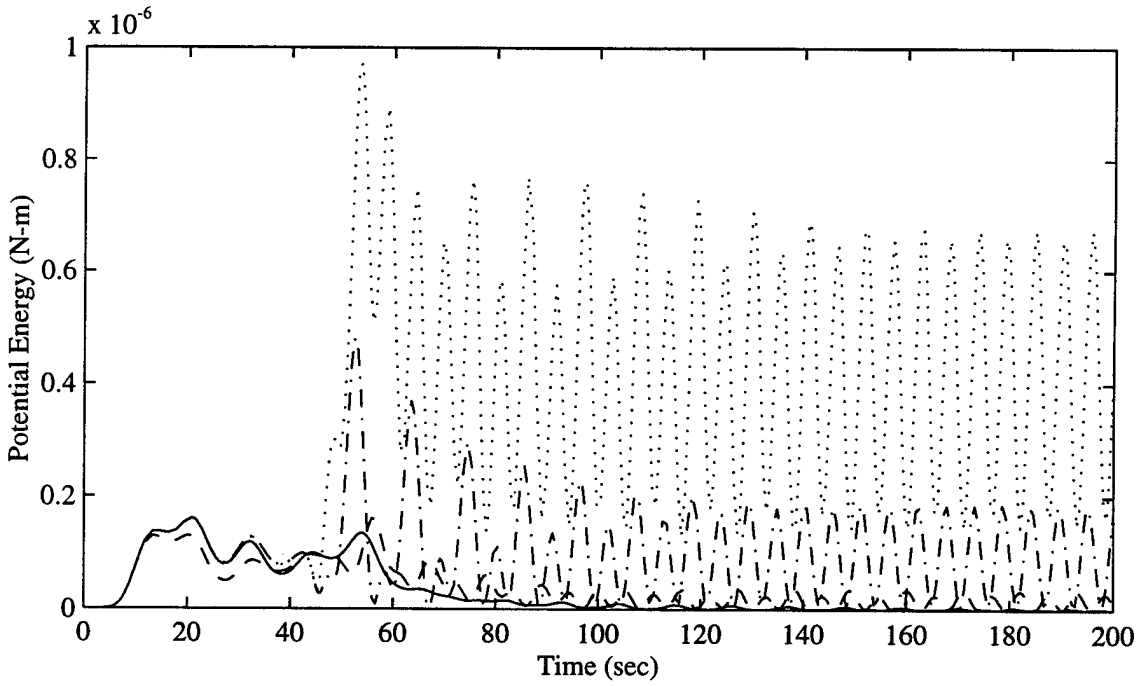
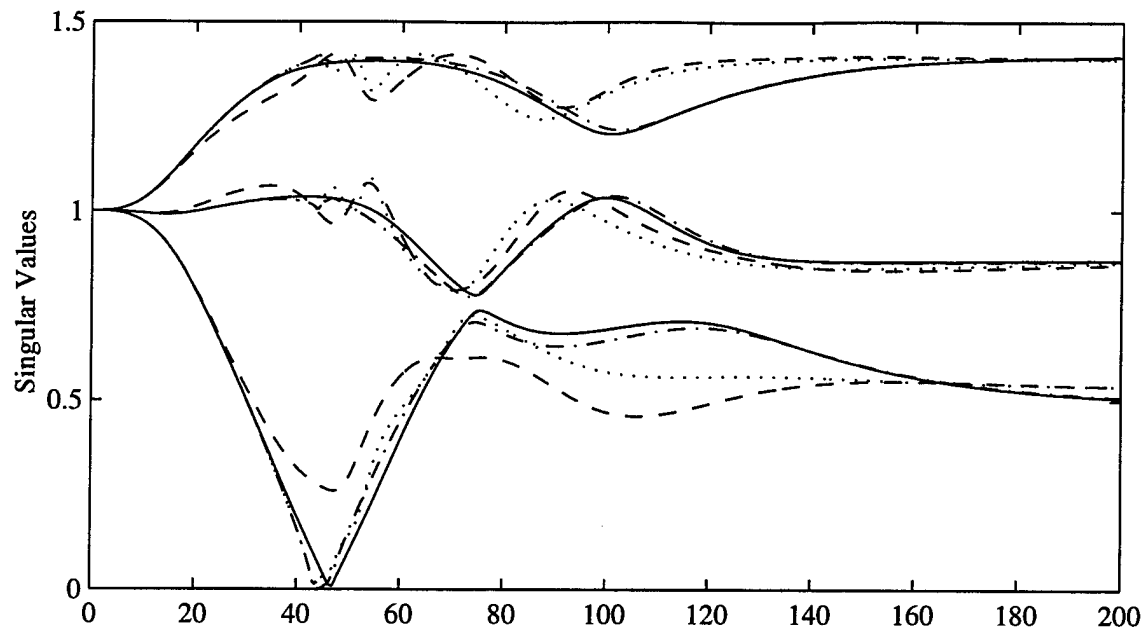


Figure 18 Singular Values and Potential Energy for Four CMG Control Laws
 Case 1 (\cdots), Case 2 ($- \cdot -$), Case 3 ($---$), Case 4 ($—$)

Table 7 Flexible Hubble Space Telescope Physical Data

Item	Value	Units
m	10788	kg
I	$\begin{bmatrix} 68322.26 & 37.15 & -1283.81 \\ 37.15 & 74130.14 & 53.96 \\ -1283.81 & 53.96 & 23504.51 \end{bmatrix}$	$kg\cdot m^2$
$\mathbf{b}_1, \mathbf{b}_2$	$[0, +4.0, +1.1]^T$	m
$\mathbf{b}_3, \mathbf{b}_4$	$[0, -4.0, +1.1]^T$	m
\mathbf{b}_5	$[0, +2.0, +1.1]^T$	m
\mathbf{b}_6	$[0, -2.0, +1.1]^T$	m
$\mathbf{r}_{01}, \mathbf{r}_{03}$	$[0, 0, +4.0]^T$	m
$\mathbf{r}_{02}, \mathbf{r}_{04}$	$[0, 0, -4.0]^T$	m
\mathbf{r}_{05}	$[0, +2.0, 0]^T$	m
\mathbf{r}_{06}	$[0, -2.0, 0]^T$	m
$\hat{\mathbf{n}}_1, \hat{\mathbf{n}}_3$	$[0, +1, 0]^T$	
$\hat{\mathbf{n}}_2, \hat{\mathbf{n}}_4$	$[0, -1, 0]^T$	
$\hat{\mathbf{n}}_5$	$[+1, 0, 0]^T$	
$\hat{\mathbf{n}}_6$	$[-1, 0, 0]^T$	
$\rho_1, \rho_2, \rho_3, \rho_4$	3.0625	kg/m
ρ_5, ρ_6	6.125	kg/m
l_1, l_2, l_3, l_4	4.0	m
l_5, l_6	2.0	m
$(EI)_1, (EI)_2, (EI)_3, (EI)_4$	25.037	$N\cdot m^2$
$(EI)_5, (EI)_6$	50.074	$N\cdot m^2$

that the modal parameters actually represent the tip deflection (in meters). The second mode of oscillation produces deflections roughly two orders of magnitude less than the first. Only the modal response of the first assumed mode is shown here. Perhaps the best scalar comparison of the two maneuvers is the potential energy in the appendages, shown as the last plot of Figure 20. Note that the stationary platform weighted maneuver produces smaller maximum appendage deflections.

6.3 Summary

In this chapter, the effectiveness of the control laws previously developed was evaluated using some candidate mathematical models of flexible satellites. The flexible appendages were modeled using assumed modes, which are the actual solutions for the Euler-Bernoulli beam cantilevered in an inertially fixed object. The various control laws were

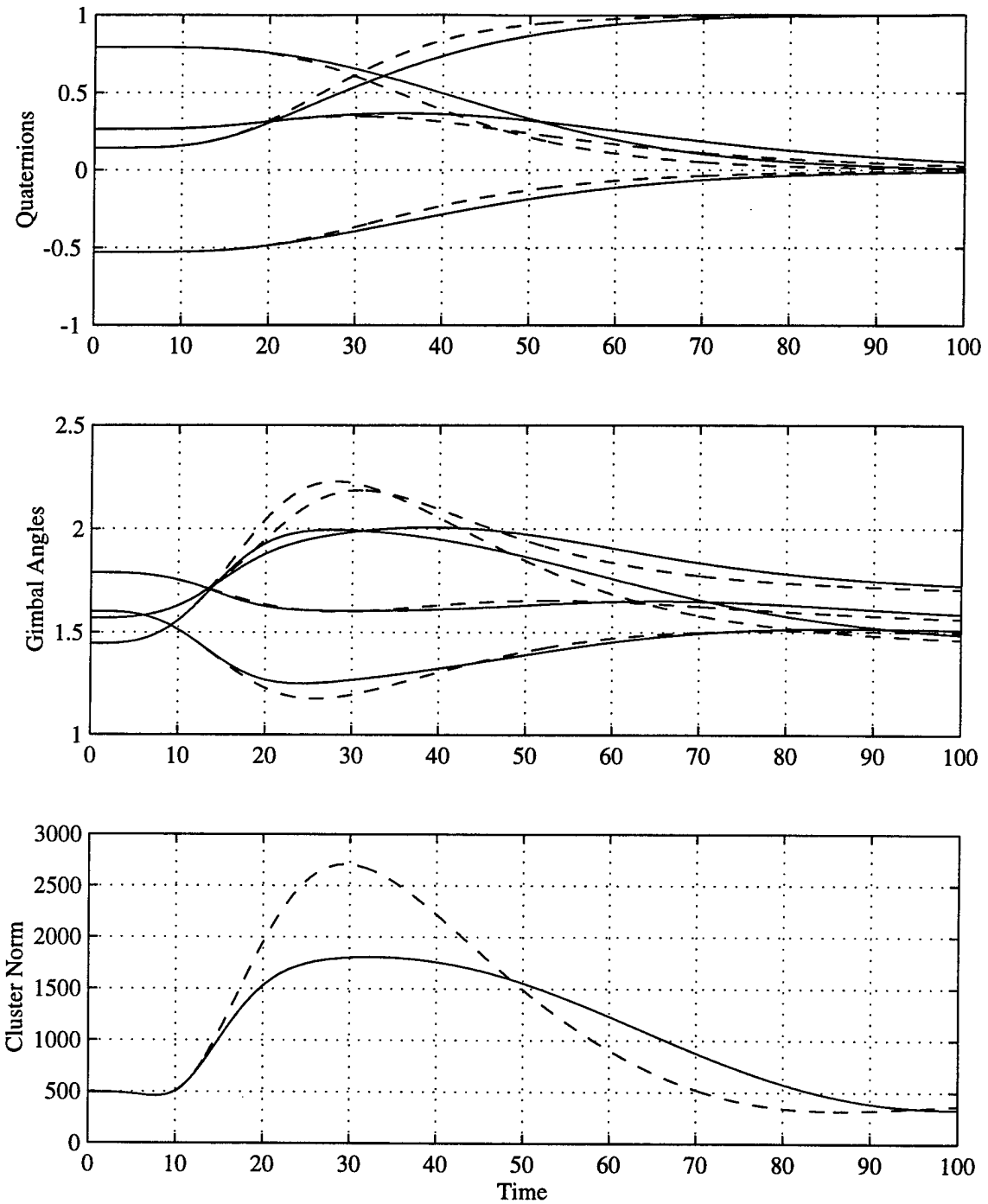


Figure 19 Hubble Reorientation Parameters for Lyapunov Maneuver With (—) and Without (---) Stationary Platform Weighting

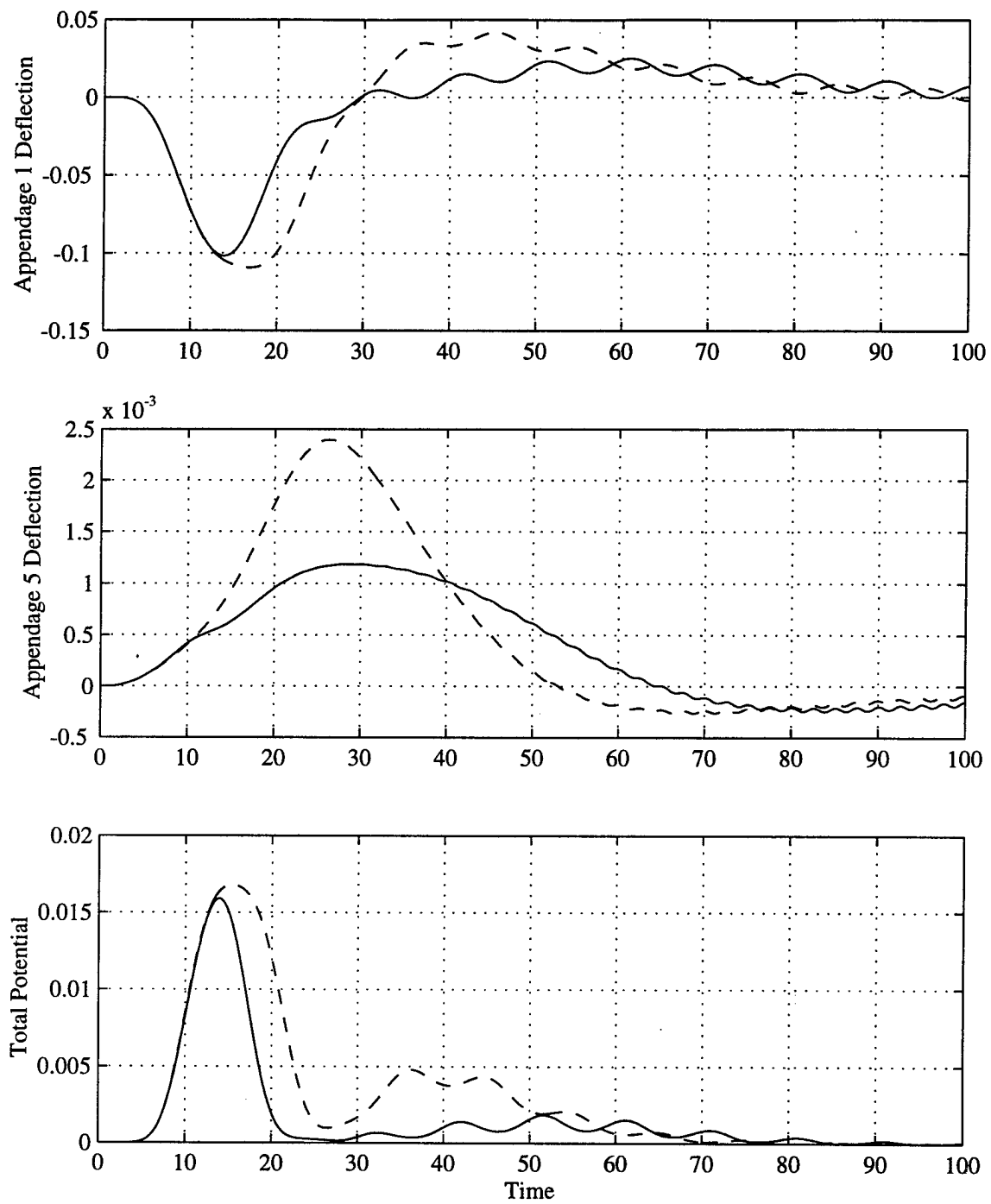


Figure 20 Hubble Appendage Excitations for Lyapunov Maneuver With (—) and Without (---) Stationary Platform Weighting

Table 8 Hubble Space Telescope CMG Cluster Data

Item	Value	Units
\mathbf{I}_{sw}	diag{8.62, 8.62, 8.62}	$kg\text{-}m^2$
\mathbf{I}_{tw}	diag{4.31, 4, 31, 4.31}	$kg\text{-}m^2$
$\mathbf{I}_{sg}, \mathbf{I}_{gg}, \mathbf{I}_{tg}$	diag{0, 0, 0, 0}	$kg\text{-}m^2$
\mathbf{a}_{s10}	$[-y/\sqrt{2}, -y/\sqrt{2}, +x]^T$	
\mathbf{a}_{s20}	$[-y/\sqrt{2}, -y/\sqrt{2}, -x]^T$	
\mathbf{a}_{s30}	$[-y/\sqrt{2}, +y/\sqrt{2}, +x]^T$	
\mathbf{a}_{s40}	$[-y/\sqrt{2}, +y/\sqrt{2}, -x]^T$	
\mathbf{a}_{g1}	$[+x/\sqrt{2}, +x/\sqrt{2}, +y]^T$	
\mathbf{a}_{g2}	$[+x/\sqrt{2}, +x/\sqrt{2}, -y]^T$	
\mathbf{a}_{g3}	$[+x/\sqrt{2}, -x/\sqrt{2}, +y]^T$	
\mathbf{a}_{g4}	$[+x/\sqrt{2}, -x/\sqrt{2}, -y]^T$	
	where $x = \cos(70^\circ), y = \sin(70^\circ)$	
\mathbf{h}_{swr}	$[3069, 3069, 3069]^T$	$kg\text{-}m^2/sec$

applied to compare oscillations of the appendages. In some examples, the torque commands were smoothed to prevent oscillations resulting from the startup torques from dominating the response. A reduction in oscillations of the appendages generally resulted when the singular direction avoidance law was used in lieu of the singularity-robust law. A profile which remains closer to the stationary platform surface was also shown to improve the smoothness of reorientation.

7. Summary and Conclusions

In this work, we develop the equations of motion for a rigid spacecraft with an imbedded cluster of gimballed momentum wheels. The Euler-Newton approach is used to find $6 + 3N$ differential equations (for an N GMW cluster) which describe the dynamics of the system. The control inputs are in the form of two $N \times 1$ torque matrices applied to the spin and gimballed axes. These equations of motion include the gimballed axis inertia effects often discarded in other developments. The approach taken is unique in that momenta components are grouped as three $N \times 1$ matrices, instead of the traditional $N \times 3$ vectors of individual torque components.

This approach permits much easier manipulation of the vector equations than does the summation notation used by Oh and Vadali [42]. Unique and simple equations of motion for spin and gimballed axis momenta are developed. The matrix formulation also yields simple matrix equations relating the system momenta and velocities, as well as system energy. Specialization of the gimballed momentum wheel equations to momentum wheel or single-gimballed control moment gyros is demonstrated.

Next, we formulate the equations of motion for a rigid body with an unlimited number of flexible appendages using the Lagrangian approach. The resultant set of hybrid equations could be solved numerically in a number of ways. We choose to apply the assumed modes method, yielding, for a body with p appendages for which we keep m modes each, a set of $6 + 2mp$ equations for the system dynamics.

Armed with these equations of motion, we seek control laws which smoothly reorient the flexible satellite. Though several reorientation schemes have been detailed in the literature, most laws showed oscillatory behavior when applied to a spacecraft possessing a significant amount of angular momentum, such as might be stored in an exchange cluster. We show that for spacecraft with any type of momentum cluster, the rate of change of cluster momentum can be viewed as the control input. This allows development of a control law in terms of the cluster momentum rate, which is then translated to spin axis torques for momentum wheels, or gimballed rates (and ultimately gimballed torques) for CMGs. A Lyapunov approach developed by Oh and Vadali is then used to find a globally asymp-

otic feedback law which drives the system to a desired target quaternion and zero angular velocity using the approach of this development.

The singularity problems of a control moment gyro cluster must be handled, and the new form of the equations of motion provides new insight into the nature of the problem. The Jacobian matrix which takes gimbal rates into output torques is closely related to a newly defined matrix of transverse unit vectors. It is shown that a typical technique of avoiding the singularity completely can be replaced with the alternative of avoiding only the singular direction. This singular direction avoidance technique also avoids the singularity, but always introduces less error into the output torque than does the commonly used singularity-robust law. Also, since the norm of the diagonal of the transformation matrix is nearly constant, the control law can be non-dimensionalized, allowing application independent of the spacecraft size. Some examples demonstrating these improvements are presented.

The promise demonstrated by the stationary platform maneuver motivates an investigation into its application to a control moment gyro cluster. For a cluster of momentum wheels, maintaining the stationary platform condition implies that we must remain on a hyper-ellipsoid in rotor momenta space. For the control moment gyro, however, the condition requires maintaining a surface in gimbal angle space which is considerably more complicated. The goal is to reorient the spacecraft while maintaining the stationary platform condition.

A modification to the Lyapunov control law is found which keeps the gimbal angles arbitrarily close to the stationary platform surface. We show that the addition of this law does not affect the guaranteed asymptotic stability of the original control law, so long as the body momentum is small relative to the cluster momentum.

Numerical simulations of the control laws are presented. The examples demonstrate that the singular direction avoidance law is generally an improvement over the singularity-robust law. Especially in the case of CMGs, a maneuver which remains closer to the stationary platform surface tends to keep the appendage oscillations smaller.

Further studies should investigate alternative methods of simultaneously satisfying the stationary platform and kinematical conditions. The feedback Lyapunov control law used throughout this work is certainly only one of many capable of effecting a reorientation maneuver. It seems likely that a reorientation could be achieved which would satisfy the kinematical constraints and maintain the stationary platform condition exactly.

Many of the control laws presented in this study can be altered by adjusting a gain which is a natural consequence of the control law development. One promising measure of the "cost" of a flexible spacecraft reorientation is the time integral of the potential energy in the flexible appendages. A study which compares the effects of this cost, along with others such as possibly control use or time, as a function of the control law gains might prove useful.

Actual implementation of the Lyapunov feedback control law depends on the ability to measure the quaternions and angular velocity. In addition, the noise in any measurement device used to provide these parameters to the control system could degrade the effectiveness of the control law and even the system closed loop stability. Some numerical simulations performed during this study indicate that the Lyapunov law is fairly robust in the presence of parameter variations, but the effects of random noise in the system were not evaluated. A careful study of the effects of noise should be conducted to determine the effectiveness of the proposed control laws for actual space hardware.

Finally, one interesting possibility not fully explored in this study is the use of a closed loop Lyapunov law as a dynamic tracker. That is, we could choose *a priori* the parameters \mathbf{q}_f and $\boldsymbol{\omega}_f$ as functions of time, and implement the Lyapunov law with these parameters as variables. Examples investigated during this study indicate that tracking is possible provided the required maneuver rates do not exceed a critical value.

Appendix A. Definitions, Kinematics, and Fundamentals

A.1 Notation

We begin this appendix with a review of the notation used in the dissertation. In general, vectors and dyadics which are independent of reference frame are denoted by a bold lower case and upper case respectively, and an arrow (e.g. $\vec{\mathbf{h}}$ and $\vec{\mathbf{I}}$). Matrices representing vectors and dyadics in a particular reference frame are denoted by the same bold character without the arrow. Unit vectors are denoted by bold characters with hats (e.g. $\hat{\mathbf{n}}$). The particular associated reference frame will be stated in the accompanying text or implied.

We indicate the transpose of a matrix with the superscript T, so $\mathbf{M}^T = \text{transpose}(\mathbf{M})$. A particularly useful notation allows us to express vector cross products in matrix multiplication form by defining the skew symmetric form of a vector. If

$$\mathbf{v} = \begin{bmatrix} v_1 \\ v_2 \\ v_3 \end{bmatrix} \quad (339)$$

then we define

$$\mathbf{v}^\times = \begin{bmatrix} 0 & -v_3 & v_2 \\ v_3 & 0 & -v_1 \\ -v_2 & v_1 & 0 \end{bmatrix} \quad (340)$$

so that in a particular coordinate system, for the case where $\vec{\mathbf{u}} \times \vec{\mathbf{v}} = \vec{\mathbf{w}}$, then

$$\mathbf{u}^\times \mathbf{v} = -\mathbf{v}^\times \mathbf{u} = \mathbf{w} \quad (341)$$

Note that the skew symmetric form of \mathbf{v}^\times makes it possible to make the occasionally convenient substitution

$$[\mathbf{v}^\times]^T = -\mathbf{v}^\times \quad (342)$$

The normal dot product of two vectors expressed in a particular coordinate frame, say for $\vec{\mathbf{u}} \cdot \vec{\mathbf{v}} = w$, is computed as

$$\mathbf{u}^T \mathbf{v} = \mathbf{v}^T \mathbf{u} = w \quad (343)$$

A.2 Transformation Matrices

We summarize relevant concepts regarding rotations of a rigid body in space. The orientation of a body-fixed reference frame relative to an inertial reference frame is most commonly described by a rotation matrix as follows. Suppose we are given a basis for the inertial reference frame and a basis for the body frame described by the sets of unit vectors

$$\mathcal{F}_i \equiv \begin{bmatrix} \hat{\mathbf{e}}_1 \\ \hat{\mathbf{e}}_2 \\ \hat{\mathbf{e}}_3 \end{bmatrix} \quad \text{and} \quad \mathcal{F}_b \equiv \begin{bmatrix} \hat{\mathbf{b}}_1 \\ \hat{\mathbf{b}}_2 \\ \hat{\mathbf{b}}_3 \end{bmatrix} \quad (344)$$

respectively. Hughes [23] refers to the objects \mathcal{F}_i and \mathcal{F}_b as *vectrices*. Note that the vectrix is a three-by-one matrix of vectors. A transformation between the frames can be written as

$$\begin{aligned} \hat{\mathbf{b}}_1 &= c_{11}\hat{\mathbf{e}}_1 + c_{12}\hat{\mathbf{e}}_2 + c_{13}\hat{\mathbf{e}}_3 \\ \hat{\mathbf{b}}_2 &= c_{21}\hat{\mathbf{e}}_1 + c_{22}\hat{\mathbf{e}}_2 + c_{23}\hat{\mathbf{e}}_3 \\ \hat{\mathbf{b}}_3 &= c_{31}\hat{\mathbf{e}}_1 + c_{32}\hat{\mathbf{e}}_2 + c_{33}\hat{\mathbf{e}}_3 \end{aligned} \quad (345)$$

or more compactly as

$$\begin{bmatrix} \hat{\mathbf{b}}_1 \\ \hat{\mathbf{b}}_2 \\ \hat{\mathbf{b}}_3 \end{bmatrix} = \begin{bmatrix} c_{11} & c_{12} & c_{13} \\ c_{21} & c_{22} & c_{23} \\ c_{31} & c_{32} & c_{33} \end{bmatrix} \begin{bmatrix} \hat{\mathbf{e}}_1 \\ \hat{\mathbf{e}}_2 \\ \hat{\mathbf{e}}_3 \end{bmatrix} = \mathbf{C}_{bi} \begin{bmatrix} \hat{\mathbf{e}}_1 \\ \hat{\mathbf{e}}_2 \\ \hat{\mathbf{e}}_3 \end{bmatrix} \quad (346)$$

The coefficients, c_{ij} , are called the *direction cosines* relating the bases, because

$$c_{ij} = \hat{\mathbf{e}}_i \cdot \hat{\mathbf{b}}_j = \cos \gamma_{ij} \quad i = 1, 2, 3 \quad j = 1, 2, 3 \quad (347)$$

where γ_{ij} is the angle between \hat{e}_i and \hat{b}_j .

Let a vector \vec{v} be expressed in both \mathcal{F}_b and \mathcal{F}_i :

$$\vec{v} = \beta_1 \hat{b}_1 + \beta_2 \hat{b}_2 + \beta_3 \hat{b}_3 = \alpha_1 \hat{e}_1 + \alpha_2 \hat{e}_2 + \alpha_3 \hat{e}_3 \quad (348)$$

The Greek coefficients are the *coordinates* of the vector \vec{v} in the respective reference frame.

Now

$$\begin{bmatrix} \beta_1 & \beta_2 & \beta_3 \end{bmatrix} \begin{bmatrix} \hat{b}_1 \\ \hat{b}_2 \\ \hat{b}_3 \end{bmatrix} = \begin{bmatrix} \alpha_1 & \alpha_2 & \alpha_3 \end{bmatrix} \begin{bmatrix} \hat{e}_1 \\ \hat{e}_2 \\ \hat{e}_3 \end{bmatrix} \quad (349)$$

so for a relationship between coordinates, we find

$$\begin{bmatrix} \beta_1 & \beta_2 & \beta_3 \end{bmatrix} \mathbf{C}_{bi} \begin{bmatrix} \hat{e}_1 \\ \hat{e}_2 \\ \hat{e}_3 \end{bmatrix} = \begin{bmatrix} \alpha_1 & \alpha_2 & \alpha_3 \end{bmatrix} \begin{bmatrix} \hat{e}_1 \\ \hat{e}_2 \\ \hat{e}_3 \end{bmatrix} \quad (350)$$

so that the transformation between coordinates in the body and inertial reference frames is

$$\mathbf{C}_{bi}^T \begin{bmatrix} \beta_1 \\ \beta_2 \\ \beta_3 \end{bmatrix} = \begin{bmatrix} \alpha_1 \\ \alpha_2 \\ \alpha_3 \end{bmatrix} \quad (351)$$

A transformation matrix between any pair of orthogonal, right-handed coordinate systems is orthonormal and obeys some useful relationships. Among them is the property

$$\mathbf{C}_{bi}^T = \mathbf{C}_{bi}^{-1} \quad (352)$$

which means that Equation (351) can also be written as

$$\begin{bmatrix} \beta_1 \\ \beta_2 \\ \beta_3 \end{bmatrix} = \mathbf{C}_{bi} \begin{bmatrix} \alpha_1 \\ \alpha_2 \\ \alpha_3 \end{bmatrix} \quad (353)$$

For a reference frame \mathcal{F}_b rotating relative to another reference frame, say \mathcal{F}_i , the relative rotational velocity can be expressed as a vector with three components. This vector is called the *angular velocity* and we denote it ω_{bi} which is read as “the angular velocity of \mathcal{F}_b relative to \mathcal{F}_i .” Since we will make constant use of the angular velocity of a body with respect to the inertial frame, we will use the symbol ω for the more explicit ω_{bi} . Any other angular velocities will be specifically subscripted. If the angular velocity is expressed in body components, then the transformation matrix satisfies

$$\dot{C}_{bi} = -\omega^\times C_{bi} \quad (354)$$

where we emphasize that the components are expressed in \mathcal{F}_b . An excellent development of transformation matrices and their unique properties is given by Hughes [23].

A.3 Eigenaxis Rotations

The rotation of any body with one point fixed (for example, the center of mass) can be reduced to a rotation about a fixed axis through the point. This observation was made by Euler and is known as *Euler's Theorem*. Hughes [23] derives the equations which relate the eigenaxis (the set of points which remains fixed in space) and angle of rotation about it (the eigenangle) in terms of the general rotation matrix.

We denote the axis of rotation by the unit vector \hat{a} . The direction of \hat{a} is of course parallel to the axis of rotation, but may be arbitrarily selected to be a vector in either of two directions. The axis of rotation is the same before and after the rotation (by definition), so we must have

$$C\hat{a} = \hat{a} \quad (355)$$

which is recognized as an eigenvalue problem (with a unitary eigenvalue). Through some geometrical considerations, it can be demonstrated that in terms of the axis of rotation and the rotation angle ϕ , the rotation matrix is given by

$$C = \cos \phi \mathbf{1} + (1 - \cos \phi) \hat{a} \hat{a}^T - \sin \phi \hat{a}^\times \quad (356)$$

Of course, we might be just as interested in computing the axis of rotation and total rotation angle about it in terms of the rotation matrix. They can be calculated as

$$\phi = \arccos\left(\frac{\text{trace}(\mathbf{C}) - 1}{2}\right) \quad (357)$$

and

$$\hat{\mathbf{a}}^\times = \frac{1}{2 \sin \phi} (\mathbf{C}^T - \mathbf{C}) \quad (358)$$

allowing the components of $\hat{\mathbf{a}}$ to be extracted from $\hat{\mathbf{a}}^\times$. The solution for the eigenangle is not unique, but picking the eigenangle produces a unique eigenaxis. A rotation corresponding to an eigenaxis/eigenangle pair is exactly the same as an equal but opposite rotation about the negative of the eigenaxis.

Relationships between angular velocity and the eigenaxis/eigenangle parameters are useful when we wish to prescribe maneuvers referred to the eigenaxis, for instance during a pure eigenaxis rotation. Hughes shows that the angular velocity can be expressed in terms of the eigenaxis parameters as

$$\boldsymbol{\omega} = \dot{\phi} \hat{\mathbf{a}} - (1 - \cos \phi) \hat{\mathbf{a}}^\times \dot{\hat{\mathbf{a}}} + \sin \phi \dot{\hat{\mathbf{a}}}^\times \quad (359)$$

so that for a rotation about a fixed axis

$$\boldsymbol{\omega} = \dot{\phi} \hat{\mathbf{a}} \quad (360)$$

The inverse of Equation (359) is given by the two equations

$$\dot{\phi} = \hat{\mathbf{a}}^T \boldsymbol{\omega} \quad (361)$$

$$\dot{\hat{\mathbf{a}}} = \frac{1}{2} \left(\hat{\mathbf{a}}^\times - \cot \frac{\phi}{2} \hat{\mathbf{a}}^\times \hat{\mathbf{a}}^\times \right) \boldsymbol{\omega} \quad (362)$$

Note the presence of the trigonometric term in Equation (362). This can be costly during numerical integration for the kinematics. While the eigenaxis and eigenangle are relatively intuitive parameters for expressing attitude, we next turn to an alternative set

which is similarly intuitive, but also provides the benefit of avoiding trigonometric relations in the kinematical equations.

A.4 Quaternions

A four-parameter set suitable for kinematic computations has emerged as perhaps the most popular choice for describing the orientations of a rigid body in space. This set of parameters, often called *Euler parameters*, shall be referred to here as *quaternions*. These parameters have the important advantage of avoiding singularities everywhere, and also of avoiding trigonometric relationships in the kinematical equations of motion.

We define the quaternions as

$$\mathbf{q} = \begin{bmatrix} q_0 \\ q_1 \\ q_2 \\ q_3 \end{bmatrix} = \begin{bmatrix} q_0 \\ \tilde{\mathbf{q}} \end{bmatrix} \in \mathfrak{R}^4 \quad (363)$$

where

$$q_0 = \cos\left(\frac{\phi}{2}\right) \quad \text{and} \quad \tilde{\mathbf{q}} = \hat{\mathbf{a}} \sin\left(\frac{\phi}{2}\right) \quad (364)$$

Of course, using four parameters to describe three degrees of freedom implies redundancy. This is evident in that

$$q_0^2 + \tilde{\mathbf{q}}^T \tilde{\mathbf{q}} = 1 \quad (365)$$

Conversion between the rotation matrix and quaternions is easily accomplished using the relationships

$$\mathbf{C} = (q_0^2 - \tilde{\mathbf{q}}^T \tilde{\mathbf{q}})\mathbf{1} + 2\tilde{\mathbf{q}}\tilde{\mathbf{q}}^T - 2q_0\tilde{\mathbf{q}}^\times \quad (366)$$

and

$$q_0 = \pm \frac{1}{2} \sqrt{(1 + \text{trace}(\mathbf{C}))} \quad (367)$$

$$\tilde{\mathbf{q}} = \frac{1}{4q_0} \begin{bmatrix} c_{23} - c_{32} \\ c_{31} - c_{13} \\ c_{12} - c_{21} \end{bmatrix} \quad (368)$$

where the c_{ij} are the direction cosines of the transformation matrix.

The usefulness of quaternions becomes most evident in the following kinematic relationship for quaternion rates in terms of the body angular velocity

$$\dot{q}_0 = -\frac{1}{2}\tilde{\mathbf{q}}^T\boldsymbol{\omega} \quad (369)$$

$$\dot{\tilde{\mathbf{q}}} = \frac{1}{2}(\tilde{\mathbf{q}}^\times + q_0\mathbf{1})\boldsymbol{\omega} \quad (370)$$

and conversely, the angular velocities in terms of quaternions and rates are

$$\boldsymbol{\omega} = \frac{2}{q_0} (q_0^2\mathbf{1} - q_0\tilde{\mathbf{q}}^\times + \tilde{\mathbf{q}}\tilde{\mathbf{q}}^T)\dot{\tilde{\mathbf{q}}} \quad (371)$$

These equations allow us to integrate for the quaternions given a history for the angular velocities. Note the absence of trigonometric terms in Equations (369) and (370). The simple matrix forms of these equations make them very suitable for numerical implementation. It is the dynamical equations of the rigid body which must be solved for angular velocities. We now present a brief review of the rigid body equations of motion.

A.5 Rigid Body Equations of Motion

Here we summarize the equations of motion for a general rigid body. Hughes [23] provides the notation for this work, and is an excellent source for further explanation of the concepts summarized in this section. The developments for the rigid body will serve as a useful starting point for the development of the flexible structure and will also be necessary to develop the equations of motion for the body with imbedded momentum storage devices. The equations which describe the dynamics of momentum wheels and control moment gyroscopes are special cases of the equations summarized in this section.

We consider the rigid body B as a continuum of mass and define the first and second moments of inertia of the rigid body as

$$\vec{c} \equiv \int_B \vec{r} \sigma(\vec{r}) dV \quad (372)$$

and

$$\vec{J} \equiv \int_B (r^2 \vec{1} - \vec{r} \vec{r}^T) \sigma(\vec{r}) dV \quad (373)$$

respectively, where $\sigma(\vec{r})$ is the mass density at \vec{r} . Then the linear momentum \vec{p} and angular momentum of the body \vec{h}_0 about an origin, 0 , can be expressed as

$$\vec{p} = m \vec{v}_0 + \vec{\omega} \times \vec{c} \quad (374)$$

$$\vec{h}_0 = \vec{c} \times \vec{v}_0 + \vec{J} \cdot \vec{\omega} \quad (375)$$

where \vec{v}_0 is the velocity of the origin, $\vec{\omega}$ the angular velocity of the body, and m is the body mass. Note we have generalized the above quantities to any point, 0 , in the body.

The equations of motion, then, come from the application of Newton/Euler principles to the quantities described by Equations (374) and (375). That is,

$$\dot{\vec{p}} = \vec{f} \quad (376)$$

$$\dot{\vec{h}}_0 = -\vec{v}_0 \times \vec{p} + \vec{g}_0 \quad (377)$$

where \vec{f} is the total external force vector and \vec{g}_0 is the external moment vector about 0 .

These equations simplify somewhat in the case of a rigid body if we choose the origin to be the mass center so that Equations (374) and (375) reduce to (with $\vec{c} = \vec{0}$)

$$\vec{p} = m \vec{v}_c \quad (378)$$

$$\vec{h}_c = \vec{J}_c \cdot \vec{\omega} \quad (379)$$

and the dynamical Equation (377) is reduced to

$$\dot{\vec{p}} = \vec{g}_c \quad (380)$$

since \vec{v}_c is parallel to \vec{p} . The new subscript c denotes properties at or about the mass center.

When we must finally resort to replacing the vectors with numbers representing coordinates in a reference frame, then we must keep in mind that the dynamical Equations (376) and (377) only apply in the inertial reference frame. In a frame rotating with respect to the inertial at angular velocity ω , then the component rates must be computed as

$$\dot{\mathbf{p}} + \omega^\times \mathbf{p} = \mathbf{f} \quad (381)$$

$$\dot{\mathbf{h}}_0 + \omega^\times \mathbf{h}_0 = -\mathbf{v}_0 \times \mathbf{p} + \mathbf{g}_0 \quad (382)$$

Note the absence of arrows above the variables, indicating we have written the equations as components in a specific reference frame. We typically focus on a zero external force scenario. We are also free to choose the initial linear momentum as zero ($\vec{p} = \vec{0}$) giving also $\dot{\vec{p}} = \vec{0}$, which implies $\vec{p} = \vec{0}$ for all time. Therefore may sometimes discard the dynamical Equation (376).

Finally, an expression for the total kinetic energy of the rigid body is

$$T = \frac{1}{2} \omega^T \mathbf{I} \omega + \frac{1}{2} m \mathbf{v}^T \mathbf{v} + \omega^T \mathbf{c}^\times \mathbf{v} \quad (383)$$

which is important, not only for its usefulness in Lagrangian formulation of the dynamical equations, but provides a first integral of the system when all of the forces are conservative.

Appendix B. Simultaneous Eigenaxis and Stationary Platform Rotations

Consider the question of whether it is possible to do an eigenaxis rotation and simultaneously maintain the stationary platform condition. For an eigenaxis rotation of a body about a fixed axis $\hat{\mathbf{a}}$ at an angular rate $\dot{\phi}$, we have

$$\boldsymbol{\omega} = \dot{\phi}\hat{\mathbf{a}} \quad (384)$$

and

$$\dot{\boldsymbol{\omega}} = \ddot{\phi}\hat{\mathbf{a}} \quad (385)$$

The total angular momentum of the body plus cluster is

$$\mathbf{h} = \mathbf{J}\boldsymbol{\omega} + \mathbf{h}_c \quad (386)$$

With no external torque and constant \mathbf{J}

$$\mathbf{J}\dot{\boldsymbol{\omega}} + \dot{\mathbf{h}}_c + \boldsymbol{\omega} \times \mathbf{J}\boldsymbol{\omega} + \boldsymbol{\omega} \times \mathbf{h}_c = \mathbf{0} \quad (387)$$

and inserting (384) and (385), then the cluster's momentum must change as

$$\dot{\mathbf{h}}_c = -\dot{\phi}^2 \hat{\mathbf{a}} \times \mathbf{J}\hat{\mathbf{a}} - \dot{\phi} \hat{\mathbf{a}} \times \mathbf{h}_c - \ddot{\phi} \mathbf{J}\hat{\mathbf{a}} \quad (388)$$

We now attempt to enforce the stationary platform condition, which implies that the magnitude of \mathbf{h}_c is constant. Therefore, we seek a vector \mathbf{v} such that

$$\dot{\mathbf{h}}_c = -\mathbf{v} \times \mathbf{h}_c = \mathbf{h}_c \times \mathbf{v} \quad (389)$$

which must satisfy

$$\mathbf{h}_c \times \mathbf{v} = -(\dot{\phi}\hat{\mathbf{a}}) \times (\dot{\phi}\mathbf{J}\hat{\mathbf{a}} + \mathbf{h}_c) - \ddot{\phi}\mathbf{J}\hat{\mathbf{a}} \quad (390)$$

The matrix, $\mathbf{h}_c \times$, is a rank 2 matrix. This implies that, in general, Equation (390) is overdetermined and does not have a solution, \mathbf{v} . Therefore, it is generally impossible to

accomplish a rest-to-rest eigenaxis rotation and simultaneously maintain the stationary platform condition.

Appendix C. Singularity Attraction Using Pseudoinverse Steering

Equation (248) of Chapter 5 gives the minimum 2-norm solution for the gimbal rates when we desire to generate the torque \mathbf{l}_r . It is often claimed in the literature that choosing the gimbal rates using this relationship actually encourages singularities in a CMG cluster (see, for example [4, 43]). The argument is that the minimum norm solution tends to avoid movement of gimbals which are contributing to the singularity. This phenomenon was not observed during this dissertation research.

Consider the gimbal rate to torque relation given by

$$\mathbf{D}\dot{\boldsymbol{\delta}} = \mathbf{l}_r \quad (391)$$

where \mathbf{D} is the Jacobian matrix given by

$$\mathbf{D} = -\mathbf{A}_t = -\mathbf{A}_{t0}\Delta^c - \mathbf{A}_{s0}\Delta^s \quad (392)$$

Equation (392) results when we assume that each CMG has unit magnitude spin momentum.

It is possible to choose the geometry of a three CMG cluster such that

$$\mathbf{D} = \begin{bmatrix} \sin \delta_1 & \cos \delta_2 & 0 \\ \cos \delta_1 & 0 & \sin \delta_3 \\ 0 & \sin \delta_2 & \cos \delta_3 \end{bmatrix} \quad (393)$$

In general, either of two CMGs may be used to provide torque in a specific direction. Suppose we are interested in exactly achieving the desired torque in a 1-axis direction of magnitude l_{r1} while the other components are free. Then we need only enforce the relation

$$\begin{bmatrix} \sin \delta_1 & \cos \delta_2 \end{bmatrix} \begin{bmatrix} \dot{\delta}_1 \\ \dot{\delta}_2 \end{bmatrix} = \mathbf{d} \begin{bmatrix} \dot{\delta}_1 \\ \dot{\delta}_2 \end{bmatrix} = l_{r1} \quad (394)$$

which is an underdetermined problem. Employing the pseudoinverse which gives the minimum norm solution (i.e., $\mathbf{d}^\dagger = \mathbf{d}^T(\mathbf{d}\mathbf{d}^T)^{-1}$) yields the gimbal rate steering law

$$\begin{bmatrix} \dot{\delta}_1 \\ \dot{\delta}_2 \end{bmatrix} = \frac{1}{\sin^2 \delta_1 + \cos^2 \delta_2} \begin{bmatrix} \sin \delta_1 \\ \cos \delta_2 \end{bmatrix} l_{r1} \quad (395)$$

Equation (395) does not have a solution when

$$m \equiv \sin^2 \delta_1 + \cos^2 \delta_2 = 0 \quad (396)$$

given by the set

$$\begin{bmatrix} \delta_1 \\ \delta_2 \end{bmatrix} = \left\{ \begin{bmatrix} 0 \\ \pi/2 \end{bmatrix}, \begin{bmatrix} 0 \\ 3\pi/2 \end{bmatrix}, \begin{bmatrix} \pi \\ \pi/2 \end{bmatrix}, \begin{bmatrix} \pi \\ 3\pi/2 \end{bmatrix} \right\} \quad (397)$$

We refer to m as the singularity measure. We wish to avoid the condition $m = 0$. Observe that

$$\dot{m} = \frac{dm}{d\delta} \dot{\delta} \quad (398)$$

and since $m \geq 0$, then a condition in which $\dot{m} < 0$ drives the system toward a singularity.

In this case

$$\dot{m} = 2 \begin{bmatrix} \sin \delta_1 \cos \delta_1 & -\sin \delta_2 \cos \delta_2 \end{bmatrix} \begin{bmatrix} \sin \delta_1 \\ \cos \delta_2 \end{bmatrix} \frac{l_{r1}}{\sin^2 \delta_1 + \cos^2 \delta_2} \quad (399)$$

$$= \frac{2(\sin^2 \delta_1 \cos \delta_1 - \cos^2 \delta_2 \sin \delta_2)}{\sin^2 \delta_1 + \cos^2 \delta_2} l_{r1} \quad (400)$$

The regions where \dot{m} are positive and negative are labeled in Figure 21. The quiver arrows depict the direction of flow based on the gimbal rates of Equation (395). Each of the singular points are characterized by a specific type of flow. The gimbal motion near the singularity at $(0, 3\pi/2)$ is actually away from the singular state (for $l_{r1} > 0$), while motion near the singularity at $(\pi, \pi/2)$ is toward the singularity. The singularities at $(0, \pi/2)$ and $(\pi, 3\pi/2)$ are saddle points. The gimbal angles cannot (in general) drive to either of these

points. We see, therefore, that of the four singular gimbal configurations, only one of them tends to attract the gimbal angles. Note that if we choose $l_{r1} < 0$, then the regions of positive and negative \dot{m} will switch, but so will the direction of flow.

It is not surprising that the flow is everywhere toward the singularity at $(\pi, \pi/2)$, since we are in effect requesting a continuous torque output from the cluster, and it only has a finite amount of momentum to give in the 1-axis direction. If we only request torque for a finite length of time, then the flow will continue toward the external singularity until $l_{r1} = 0$, at which time the gimbal rates also become zero.

At $(\pi, \pi/2)$, the spin axes of both gimbals lie in the 1-axis direction. At this point, the CMGs can provide no more momentum exchange in that direction, and are therefore at an *external* singularity. Furthermore, no null motion exists which will allow movement away from the singularity. In a similar way, the point $(0, 3\pi/2)$ is where the spin axes of both CMGs point in the negative 1-axis direction. Here we have plenty of momentum available to reorient in the positive 1-axis direction. The other two singular points, however, correspond to the physical situation where the spin axes point opposite each other. These are *internal* singularities.

Consider now the possibility of null motion for the 2 CMGs. That is, motion for which the torque output in the 1-axis direction is zero. The torque output is zero only when the gimbal rates lie in the null space of \mathbf{d} . This motion is perpendicular to the quiver arrows in Figure 21. Departing the singularities at $(0, 3\pi/2)$ and $(\pi, \pi/2)$ in a direction perpendicular to \mathbf{d} is not possible. It is not possible, therefore, to depart these singularities using null motion. Singularities which may not be departed using null motion are often called *elliptic* singularities.

On the other hand the singularities at $(0, \pi/2)$ and $(\pi, 3\pi/2)$ do allow for escape using null motion. Adding a component to $\dot{\delta}$ along the $\pm 45^\circ$ direction will not affect the torque output. These singularities are often called *hyperbolic* singularities. See Margulies and Aubrun [32] for further discussion.

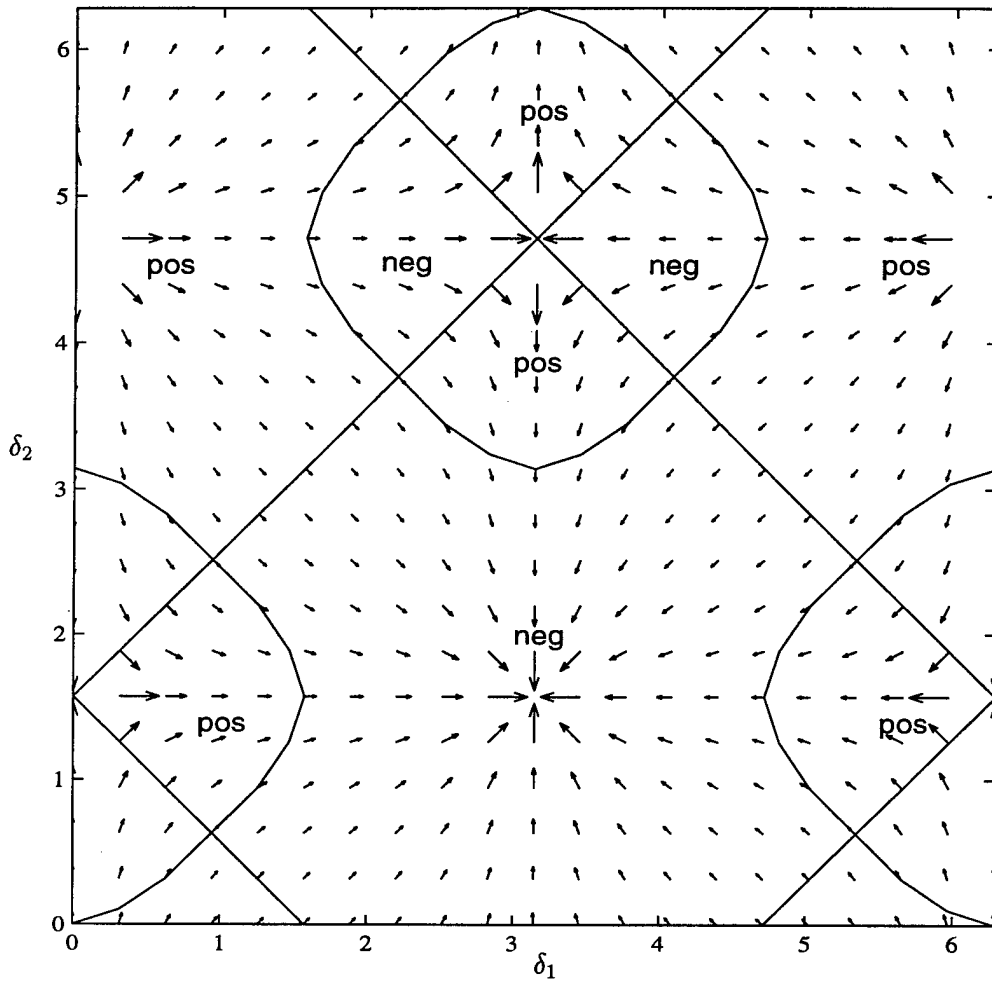


Figure 21 Gimbal Angle Flow for Pseudoinverse Steering Law

Appendix D. Orthogonal CMG Cluster Envelope

A cluster of three or more non-coplanar momentum wheels are capable of attaining any desired cluster momentum. The same is not true for a cluster of control moment gyros. Since the wheel speeds are fixed, a CMG cluster can produce only a finite momentum in a specified direction. The momentum limit in that direction is determined by the arrangement and number of CMGs, and the spin momenta of the CMGs. In general, computation of the momentum limit in any specific direction is quite complicated. An excellent geometric treatment of single gimbal control moment gyro clusters is in Margulies and Aubrun [32].

In Chapter 5, we make some claims regarding limitations on the cluster momentum in certain directions. Here we attempt to provide some insight into the nature of an orthogonal cluster momentum envelope.

Suppose we have a cluster of 3 control moment gyros in an orthogonal arrangement such that

$$\mathbf{A}_{s0} = \begin{bmatrix} 1 & 0 & 0 \\ 0 & 1 & 0 \\ 0 & 0 & 1 \end{bmatrix} \quad (401)$$

$$\mathbf{A}_g = \begin{bmatrix} 0 & 0 & 1 \\ 1 & 0 & 0 \\ 0 & 1 & 0 \end{bmatrix} \quad (402)$$

$$\mathbf{A}_{t0} = \begin{bmatrix} 0 & 1 & 0 \\ 0 & 0 & 1 \\ 1 & 0 & 0 \end{bmatrix} \quad (403)$$

When the gimbal rates are zero, the cluster momentum relative to the body is simply

$$\mathbf{h}_c = \mathbf{A}_s \mathbf{h}_{swr} \quad (404)$$

and for uniform CMG spin momenta of h_{swr} , the 3 scalar equations for the momentum of the cluster (from Equation (29)) are

$$\begin{aligned} h_{swr}(\cos \delta_1 - \sin \delta_2) &= h_1 \\ h_{swr}(\cos \delta_2 - \sin \delta_3) &= h_2 \\ h_{swr}(\cos \delta_3 - \sin \delta_1) &= h_3 \end{aligned} \quad (405)$$

where $\mathbf{h} = [h_1 \ h_2 \ h_3]^T$. It is evident from Equations (405) that no principal component of the cluster momentum can be greater than $2h_{swr}$.

Of interest are the angles for which the cluster has maximum and minimum momentum magnitude. It is easy to confirm that the square of the magnitude of \mathbf{h} is

$$h^2 = h_{swr}^2 (3 - 2(\cos \delta_1 \sin \delta_2 + \cos \delta_2 \sin \delta_3 + \cos \delta_3 \sin \delta_1)) \quad (406)$$

The extrema of Equation (406) occur when

$$\frac{\partial h^2}{\partial \delta_1} = \frac{\partial h^2}{\partial \delta_2} = \frac{\partial h^2}{\partial \delta_3} = 0 \quad (407)$$

yielding the 3 equations

$$\begin{aligned} \sin \delta_1 \sin \delta_2 &= \cos \delta_3 \cos \delta_1 \\ \sin \delta_2 \sin \delta_3 &= \cos \delta_1 \cos \delta_2 \\ \sin \delta_3 \sin \delta_1 &= \cos \delta_2 \cos \delta_3 \end{aligned} \quad (408)$$

which can ultimately be manipulated to reach the requirements that

$$\cos^2 \delta_1 = \cos^2 \delta_2 = \cos^2 \delta_3 = \frac{1}{2} \quad (409)$$

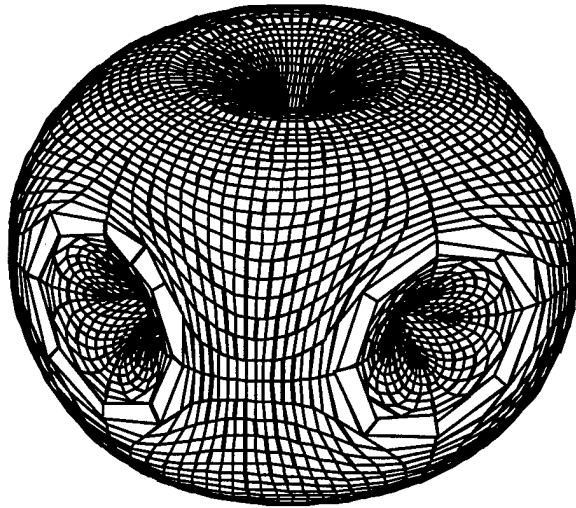


Figure 22 External Momentum Envelope for a Three CMG Orthogonal Cluster

So each gimbal angle must be $\frac{\pi}{4}$ plus integer multiples of $\frac{\pi}{2}$. It should not be too difficult to convince the reader that since

$$\cos \delta_i = \pm \frac{1}{\sqrt{2}} \quad i = 1, 2, 3 \quad (410)$$

then

$$\sin \delta_i = \pm \frac{1}{\sqrt{2}} \quad i = 1, 2, 3 \quad (411)$$

also. The maximum possible value of h^2 is therefore

$$\begin{aligned} h^2 &= h_{swr}^2 \left(3 - 2 \left(-\frac{1}{2} - \frac{1}{2} - \frac{1}{2} \right) \right) \\ &= 6h_{swr}^2 \end{aligned} \quad (412)$$

and occurs, for example, at $(\delta_1, \delta_2, \delta_3) = (\frac{3\pi}{4}, \frac{3\pi}{4}, \frac{3\pi}{4})$. Since $h^2 \geq 0$, we note that the the minimum is indeed zero and occurs, for example, when $(\delta_1, \delta_2, \delta_3) = (\frac{\pi}{4}, \frac{\pi}{4}, \frac{\pi}{4})$. The momentum envelope is depicted in Figure 22.

Bibliography

1. Barbera, F. J. and P. W. Likins. "Liapunov Stability Analysis of Spinning Flexible Spacecraft," *AIAA Journal*, 11(4):457-466 (1973).
2. Barbieri, E. and U. Ozguner. "A New Minimum-Time Control Law for a One-Mode Model of a Flexible Slewing Structure," *IEEE Transactions of Automatic Control*, 38(1):142-146 (1993).
3. Bedrossian, N. S., J. Paradiso, E. V. Bergmann and D. Rowell. "Redundant Single Gimbal Control Moment Gyroscope Singularity Analysis," *Journal of Guidance, Control, and Dynamics*, 13(6):1096-1101 (1990).
4. Bedrossian, N. S., J. Paradiso, E. V. Bergmann and D. Rowell. "Steering Law Design for Redundant Single-Gimbal Control Moment Gyroscopes," *Journal of Guidance, Control, and Dynamics*, 13(6):1083-1089 (1990).
5. Bell, M. J. and J. L. Junkins. "Near Minimum-Time Three Dimensional Maneuvers of Rigid and Flexible Spacecraft," *The Journal of the Astronautical Sciences*, 42(4):421-438 (1994).
6. Bilimoria, K. D. and B. Wie. "Time-Optimal Three-Axis Reorientation of a Rigid Spacecraft," *Journal of Guidance, Control, and Dynamics*, 16(3):446-452 (1993).
7. Bishop, R. H., S. J. Paynter and J. W. Sunkel. "Adaptive Control of Space Station with Control Moment Gyros," *IEEE Control Systems Magazine*, 12(5):23-27 (1992).
8. Byers, R. M. and S. R. Vadali. "Quasi-Closed-Form Solution to the Time-Optimal Rigid Spacecraft Reorientation Problem," *Journal of Guidance, Control, and Dynamics*, 16(3):453-461 (1993).
9. Byers, R. M., S. R. Vadali and J. L. Junkins. "Near-Minimum Time, Closed-Loop Slewing of Flexible Spacecraft," *Journal of Guidance, Control, and Dynamics*, 13(1):57-65 (1990).
10. Carrington, C. K. and J. L. Junkins. "Nonlinear Feedback Control of Spacecraft Slew Maneuvers," *The Journal of the Astronautical Sciences*, 32(1):29-45 (1984).
11. Cherchas, D. B. and P. C. Hughes. "Attitude Stability of a Dual-Spin Satellite with a Large Flexible Solar Array," *Journal of Spacecraft and Rockets*, 10(2):126-132 (1973).
12. Cochran, John E., Ping-Huei Shu and Stephen D. Rew. "Attitude Motion of Asymmetric Dual-Spin Spacecraft," *Journal of Guidance, Control, and Dynamics*, 5(1):37-42 (1982).
13. Craig, Jr., R. R. *Structural Dynamics: An Introduction to Computer Methods*. New York: Wiley & Sons, 1981.
14. Creamer, G., P. DeLaHunt, S. Gates and M. Levenson. "Attitude Determination and Control of Clementine During Lunar Mapping," *Journal of Guidance, Control, and Dynamics*, 19(3):505-511 (1996).

15. Cristi, R., J. Burl and N. Russo. "Adaptive Quaternion Feedback Regulation for Eigenaxis Rotations," *Journal of Guidance, Control, and Dynamics*, 17(6):1287–1291 (1994).
16. Gale, A. H. and P. W. Likins. "Influence of Flexible Appendages on Dual-Spin Spacecraft Dynamics and Control," *Journal of Spacecraft and Rockets*, 7(9):1049–1056 (1970).
17. Grote, P. B., J. C. McMunn and R. Gluck. "Equations of Motion of Flexible Spacecraft," *Journal of Spacecraft and Rockets*, 8(6):561–567 (1971).
18. Hall, C. D. "Spinup Dynamics of Gyrostats," *Journal of Guidance, Control, and Dynamics*, 18(5):1177–1183 (1995).
19. Hall, C. D. and R. H Rand. "Spinup Dynamics of Axial Dual-Spin Spacecraft," *Journal of Guidance, Control, and Dynamics*, 17(1):30–37 (1994).
20. Hall, Christopher D. "Momentum Transfer in Two-Rotor Gyrostats," *Journal of Guidance, Control, and Dynamics*, 19(5):1157–1161 (1996).
21. Hall, Christopher D. "Stationary-Platform Maneuvers of Gyrostat Satellites." In Kirk, C. and D. Inman, editors, *Dynamics and Control of Structures in Space III*, pages 337–348, Southampton: Computational Mechanics Publications, 1996.
22. Hoelscher, B. R. and S. R. Vadali. "Optimal Open-Loop and Feedback Control Using Single Gimbal Control Moment Gyroscopes," *The Journal of the Astronautical Sciences*, 42(2):189–206 (1994).
23. Hughes, Peter C. *Spacecraft Attitude Dynamics*. New York: Wiley & Sons, 1986.
24. Jacot, A. D. and D. J. Liska. "Control Moment Gyros in Attitude Control," *Journal of Spacecraft and Rockets*, 3(9):1313–1320 (1966).
25. Junkins, J. L. and Y. Kim. *Introduction to Dynamics and Control of Flexible Structures*. Washington, D.C.: AIAA, 1993.
26. Junkins, J. L. and J. D. Turner. *Optimal Spacecraft Rotational Maneuvers*. Amsterdam: Elsevier, 1986.
27. Keat, J. E. "Dynamical Equations of Nonrigid Satellites," *AIAA Journal*, 8(7):1344–1345 (1970).
28. Li, Z. and P. M. Bainum. "3-D Maneuver and Vibration Control of Flexible Spacecraft Using the Momentum Exchange Feedback Control Concept," *The Journal of the Astronautical Sciences*, 42(2):175–188 (1994).
29. Likins, P. W. and G. E. Fleischer. "Results of Flexible Spacecraft Attitude Control Studies Utilizing Hybrid Coordinates," *Journal of Guidance, Control, and Dynamics*, 8(3):264–273 (1971).
30. Likins, P. W., G. T. Tseng and D. L. Mingori. "Stable Limit Cycles due to Nonlinear Damping in Dual-Spin Spacecraft," *Journal of Spacecraft and Rockets*, 8(6):568–574 (1971).

31. Long, T. "Satellite Attitude Control in the Equivalent Axis Frame," *Acta Astronautica*, 26(5):299-305 (1992).
32. Margulies, G. and J. N. Aubrun. "Geometric Theory of Single-Gimbal Control Moment Gyro Systems," *The Journal of the Astronautical Sciences*, 26(2):159-191 (1978).
33. Mazzoleni, A. P., C. D. Hall and M. C. Stabb. "Double Averaging Approach to the Study of Spinup Dynamics of Flexible Satellites," *Journal of Guidance, Control, and Dynamics*, 19(1):54-59 (1996).
34. Meirovitch, L. and R. A. Calico. "A Comparative Study of Stability Methods for Flexible Satellites," *AIAA Journal*, 11(1):91-98 (1973).
35. Meirovitch, L. and Stemple T. "Hybrid Equations of Motion for Flexible Multi-body Systems Using Quasicoordinates," *Journal of Guidance, Control, and Dynamics*, 18(4):678-688 (1995).
36. Meirovitch, Leonard. *Methods of Analytical Dynamics*. New York: McGraw-Hill Publishing Company, 1970.
37. Mingori, D. L., G. T. Tseng and P. W. Likins. "Constant and Variable Amplitude Limit Cycles in Dual-Spin Spacecraft," *Journal of Spacecraft and Rockets*, 9(11):825-830 (1972).
38. Modi, V. J. "Attitude Dynamics of Satellites with Flexible Appendages - A Brief Review," *Journal of Spacecraft and Rockets*, 11(11):743-751 (1974).
39. Nakamura, Yoshihiko. *Advanced Robotics Redundancy and Optimization*. Reading, Massachusetts: Addison-Wesley Publishing Company, 1991.
40. Nurre, G. S. and J. D. Sharkey. "Preservicing Mission, On-Orbit Modifications to Hubble Space Telescope Pointing Control System," *Journal of Guidance, Control, and Dynamics*, 18(2):222-229 (1995).
41. O'Connor, B. J. and L. A. Morine. "A Description of the CMG and Its Application to Space Vehicle Control," *Journal of Spacecraft and Rockets*, 6(3):225-231 (1969).
42. Oh, H. S. and S. R. Vadali. "Feedback Control and Steering Laws for Spacecraft Using Single Gimbal Control Moment Gyros," *The Journal of the Astronautical Sciences*, 39(2):183-203 (1994).
43. Paradiso, Joseph A. "Global Steering of Single Gimballed Control Moment Gyroscopes Using a Directed Search," *Journal of Guidance, Control, and Dynamics*, 15(5):1236-1244 (1992).
44. Quinn, Roger D. "Equations of Motion for Structures in Terms of Quasi-Coordinates," *Journal of Applied Mechanics*, 57:745-749 (1990).
45. Reyhanoglu, M. and N. H. McClamroch. "Planar Reorientation Maneuvers of Space Multibody Systems Using Internal Controls," *Journal of Guidance, Control, and Dynamics*, 15(6):1475-1480 (1992).

46. Schultz, G. W. *Sub-Optimal Control of Rigid Spacecraft Reorientation Using Three Momentum Wheels*. MS thesis, Air Force Institute of Technology, Wright-Patterson AFB, Ohio, December 1995.
47. Scrivener, S. L. and R. C. Thompson. "Survey of Time-Optimal Attitude Maneuvers," *Journal of Guidance, Control, and Dynamics*, 17(2):225-233 (1994).
48. Singh, S. N. and T. C. Bossart. "Exact Feedback Linearization and Control of Space Station Using CMG," *IEEE Transactions on Automatic Control*, 38(1):184-187 (1993).
49. Sparks, D. W. and J. N. Juang. "Survey of Experiments and Experimental Facilities for Control of Flexible Structures," *Journal of Guidance, Control, and Dynamics*, 15(4):801-816 (1992).
50. Stabb, M. C. and A. L. Schlack. "Pointing Accuracy of a Dual-Spin Satellite due to Torsional Appendage Vibrations," *Journal of Guidance, Control, and Dynamics*, 16(4):630-635 (1993).
51. Vadali, S. R., M. T. Carter, T. Singh and N. S. Abhyankar. "Near-Minimum-Time Maneuvers of Large Structures: Theory and Experiments," *Journal of Guidance, Control, and Dynamics*, 18(6):1380-1385 (1995).
52. Vadali, S. R. and S. Krishnan. "Suboptimal Command Generation for Control Moment Gyroscopes and Feedback Control of Spacecraft," *Journal of Guidance, Control, and Dynamics*, 18(6):1350-1354 (1995).
53. Vadali, S. R., H. S. Oh and S. R. Walker. "Preferred Gimbal Angles for Single Gimbal Control Moment Gyros," *Journal of Guidance, Control, and Dynamics*, 13(6):1090-1095 (1990).
54. Vadali, S. R., T. Singh and M. T. Carter. "Computation of Near-Minimum-Time Maneuvers of Flexible Structures by Parameter Optimization," *Journal of Guidance, Control, and Dynamics*, 17(2):354-360 (1994).
55. Wie, B. and P. M. Barba. "Quaternion Feedback for Spacecraft Large Angle Maneuvers," *Journal of Guidance, Control, and Dynamics*, 8(3):360-365 (1985).
56. Wie, B. and J. Lu. "Feedback Control Logic for Spacecraft Eigenaxis Rotations Under Slew Rate and Control Constraints," *Journal of Guidance, Control, and Dynamics*, 18(6):1372-1379 (1995).
57. Wie, B., H. Weiss and A. Arapostathis. "Quaternion Feedback Regulator for Spacecraft Eigenaxis Rotations," *Journal of Guidance, Control, and Dynamics*, 12(3):375-380 (1989).

Vita

Kevin Ford, the son of Clayton and Barbara Ford and the youngest of six children, grew up in Montpelier, Indiana. He graduated from Blackford High School in 1978. During his teenage years, a book by Apollo Astronaut Michael Collins, *Carrying the Fire*, and the enthusiasm of his older brothers for aviation motivated him skyward. Kevin earned a Private Pilot certificate on his 17th birthday.

He attended the University of Notre Dame on an Air Force ROTC scholarship, majoring in Aerospace Engineering. In the summer of 1980, Kevin married the former Kelly Bennett, of Hartford City, Indiana (and also an alumnus of Blackford High School). He graduated from the University of Notre Dame and was commissioned a Second Lieutenant in the United States Air Force in May of 1982.

Kevin attended Air Force Undergraduate Pilot Training at Columbus Air Force Base in Mississippi. He then flew F-15 Eagles at Bitburg Air Base, West Germany, and Keflavik Naval Air Station, Iceland. He graduated from the United States Air Force Test Pilot School in 1990, and subsequently served as a Test Pilot in the F-16 Fighting Falcon at Eglin Air Force Base, Florida. During his flying tours, he earned a Master's Degree in International Relations from Troy State University, and another in Aerospace Engineering from the University of Florida.

In 1994, anticipating his first opportunity to fly a desk, Kevin applied for and was granted permission to attend the Air Force Institute of Technology in pursuit of a Doctorate. Though his background was primarily in aeronautics and flight operations, the needs of the Air Force dictated a major in Astronautical Engineering. Needs change, and Kevin has been assigned as an instructor at the Air Force Test Pilot School following his graduation in September of 1997.

Permanent address: 1102 N. Richmond
Hartford City, Indiana 47348

REPORT DOCUMENTATION PAGE

Form Approved
OMB No. 0704-0188

Public reporting burden for this collection of information is estimated to average 1 hour per response, including the time for reviewing instructions, searching existing data sources, gathering and maintaining the data needed, and completing and reviewing the collection of information. Send comments regarding this burden estimate or any other aspect of this collection of information, including suggestions for reducing this burden, to Washington Headquarters Services, Directorate for Information Operations and Reports, 1215 Jefferson Davis Highway, Suite 1204, Arlington, VA 22202-4302, and to the Office of Management and Budget, Paperwork Reduction Project (0704-0188), Washington, DC 20503.

1. AGENCY USE ONLY (Leave blank)	2. REPORT DATE 5 Sep 1997	3. REPORT TYPE AND DATES COVERED Doctoral Dissertation
----------------------------------	------------------------------	---

4. TITLE AND SUBTITLE Reorientations of Flexible Spacecraft Using Momentum Exchange Devices	5. FUNDING NUMBERS
--	--------------------

6. AUTHOR(S) Kevin A. Ford, Major, US Air Force
--

7. PERFORMING ORGANIZATION NAME(S) AND ADDRESS(ES) Air Force Institute of Technology School of Engineering 2950 P Street Wright-Patterson AFB, Ohio 45433-7765	8. PERFORMING ORGANIZATION REPORT NUMBER AFIT/DS/ENY/97-07
--	---

9. SPONSORING/MONITORING AGENCY NAME(S) AND ADDRESS(ES) Arje Nachman AFOSR/NM Bolling AFB, Washington, D. C.	10. SPONSORING/MONITORING AGENCY REPORT NUMBER
---	--

11. SUPPLEMENTARY NOTES

12a. DISTRIBUTION/AVAILABILITY STATEMENT Approved for Public Release; Distribution Unlimited	12b. DISTRIBUTION CODE A
---	---------------------------------

13. ABSTRACT (Maximum 200 words) We study rest-to-rest reorientations of flexible spacecraft using momentum exchange devices. A new and concise form of the equations of motion for a rigid body containing a cluster of gimballed momentum wheels is developed using the Euler-Newton approach. Special restrictions of the gimballed momentum wheel equations yield equations of motion for the momentum wheel cluster and the control moment gyroscope cluster. A mathematical model of a free spacecraft with Euler-Bernoulli appendages is developed. Using the assumed modes method, a complete set of equations is developed which describes the dynamics of a spacecraft with flexible appendages and gimballed momentum wheels. Special attention is paid to singularity problems in control moment gyro clusters. A control law based on the singular value decomposition is developed which avoids torque output commands in the nearly singular direction. The stationary platform maneuver, a maneuver along the set of equilibrium solutions of a zero angular velocity spacecraft, is extended to the control moment gyro cluster. The set of equilibria for a control moment gyro cluster is a unique surface in gimbal angle space. A control law which reorients the spacecraft while remaining close to this surface is developed using a Lyapunov method.
--

14. SUBJECT TERMS Reorientations, spacecraft, flexible, momentum exchange, momentum wheel, control moment gyro, CMG, gimballed momentum wheel, Euler-Bernoulli beam, rotational maneuver	15. NUMBER OF PAGES 147
	16. PRICE CODE

17. SECURITY CLASSIFICATION OF REPORT Unclassified	18. SECURITY CLASSIFICATION OF THIS PAGE Unclassified	19. SECURITY CLASSIFICATION OF ABSTRACT Unclassified	20. LIMITATION OF ABSTRACT Unlimited
---	--	---	---